Study on the Structure and Control of Novel Type of Magnetic Microrobotic Systems

by

Qiang Fu

A thesis submitted for the degree of Doctor of Philosophy
Graduate School of Engineering, Kagawa University

Abstract

Wireless microrobots controlled by the external magnetic field are used in a wide range of biomedical application. The wireless microrobots are both safe, reliable and can be carried deeply within the tissue of living organisms in the human body. They have many potential applications in the medical field. For example, the wireless capsule microrobot can be used to diagnose various diseases throughout the gastrointestinal tract. As the development of biology, many microrobots have been developed with biomimetic locomotion, such as crawling, walking, creeping, swimming, and so on. Most of them use traditional motor as an actuator to realize the control of the microrobot and the power is supplied by the cable. These microrobots are unsuitable for some small or narrow areas, because of their high power consumption, complex structure and limitations of cable. So an optimization design, flexible structure and continually power supply have been requested urgently. Although many biomimetic microrobots are developed in recent two decades, it is still difficult in developing a microrobot with compact structure, flexible locomotion and long-distance movement by power supply, because the three characteristics conflicts each other.

The medical safety, loading abilities and an effective propulsive performance are extremely important and challenging. Therefore, in this thesis, a multi-module magnetic actuated microrobotic system is proposed. Our proposed microrobotic system includes two parts, microrobots and

electromagnetic actuation (EMA) system. The microrobot composes of different module with multi-functional. It is comfortable and easy to swallow by patients, because it can realize the docking and releasing in various environments and has the flexible motion with wireless control. To increase the dynamic efficiency and adapt this electromagnetic actuation system to use in various working environments, a novel magnetically actuated hybrid mechanism is proposed. It has a hybrid locomotion scheme, consisting of two disparate magnetic actuation strategies: (1) conversion of synchronous rotation with a rotating field using a "spiral jet motion" to pull fluid through the center of the robot; (2) using a flexible tail to generate fish-like propulsion due to an oscillating magnetic field. With two motions, we confirmed that this microrobot has multi-DOFs locomotion, flexibility, and optimized for moving speed of the microrobot. And the hybrid motion can be controlled separately without any interference. The experimental results show that traditional linear-with-frequency controlled velocities can be generated with the spiral jet motion and that more a 2X increase in speed can be achieved using the flexible tail, although that mode of propulsion does not easily lend itself to simple analytical models. And then major part of EMA system which is 3 axes Helmholtz coils is analyzed, designed and evaluated performance, in order to realize flexible control the hybrid microrobot. Finally, the motion characteristics of hybrid microrobot are evaluated and the hybrid realized the multi-DOFs locomotion in pipe. Experimental results indicated the hybrid microrobot realize flexible motion in pipe by adjusting the magnetic field changing direction.

Acknowledgements

This dissertation is the result of 5 years study at Kagawa University. I would like to thank the people who have helped me.

First of foremost, I would like to express my sincere gratitude to my supervisor, Prof. Shuxiang Guo for his invaluable guidance, support and encouragement throughout my Ph.D. For improving my thesis, he gave me so many useful advices. I appreciate him not only for his guidance on my research, but also the great encouragement and help on my life.

I would like to give my best thanks to Prof. Hideyuki Hirata and Prof. Keisuke Suzuki for their warmly advisements on my research. I would like to express my thanks to Mr. Yamauchi who works with me in the same team. They gave me lots of help on my research and my life. Also, I wish to thank Dr. Muye Pang and Dr. Songyuan Zhang. They gave me lots of help about the software design. Most of all, they helped me a lot on my study when I got stuck on the study and showed me the way how to be an excellent researcher. I would like to acknowledge the efforts of all the laboratory members.

At last, I would like to thank my family because they provide strong spiritual and financial support to me.

Declaration

I hereby declare that this submission is my own work and that, to the best of my knowledge and belief, it contains no material previously published or written by another person nor material which to a substantial extent has been accepted for the award of any other degree or diploma of the university or other institute of higher learning, except where due acknowledgment has been made in the text.

Table of Contents

X

List of Figures

List of Tables

Chapter 1   Introduction

1.1 The background of research

The endoscope as a helpful tool for medical applications typically refers to inspect the interior of the body in medical procedures [1]-[20]. The first endoscope was developed by Philipp Bozzini in the 1806. The endoscope was made by Lichtleiter for examination of the interior of a hollow organ in the human body. In the 1960s, the first fiberoptic endoscope consisting of a bundle of flexible glass fibres was invented by Basil Hirschowitz and Larry Curtiss. It has the ability to coherently transmit an image and becomes a vital tool for diagnosing gastrointestinal (GI) diseases. There were physical limits to the image quality of a fibroscope. The electronic endoscope became more popular with the development of the electronic technology. Doctors can monitor intestinal image via the display and perform examination, rather than staring at eyepiece. Generally, these endoscopes are used to examine inside a large intestine. However, they brought much painful and traumatic due to being driven by a cable or tube. Especially, they are hard to carry deeply to some small or narrow areas within the tissue of living in human body.

To solve these problems, different kinds of medical microrobot have been developed [21]-[28]. In recent years, many kinds of microrobots have been developed to achieve various tasks due to technical advancements in manufacturing and further progress is expected in this field. The

microrobot is used in medicine to avoid unnecessary incisions during surgical operations. Some researchers have proposed a kind of capsule endoscope, which is swallowed by the patient to diagnose the intestinal organs of the human body, as shown in Figure 1.1. However, this kind of robot is uncontrollable due to involuntary muscle movements known as peristalsis [29]-[35]. To solve this problem, many microrobots have been developed with traditional motors and smart materials as actuators [36]-[40], as shown in Figure1.2. These microrobots look perfect in theory and design, but are more or less ineffective. There are diagnostic problems due to the cable or wire and it is very difficult to reach a position accurately or operate in a very narrow and deep space. Therefore, a new driving mode of the microrobot has urgently been demanded in medical applications.

Figure 1.1 Capsule endoscopy
(http://gi-chan.com/procedures-treatments/capsule-endoscopy/)
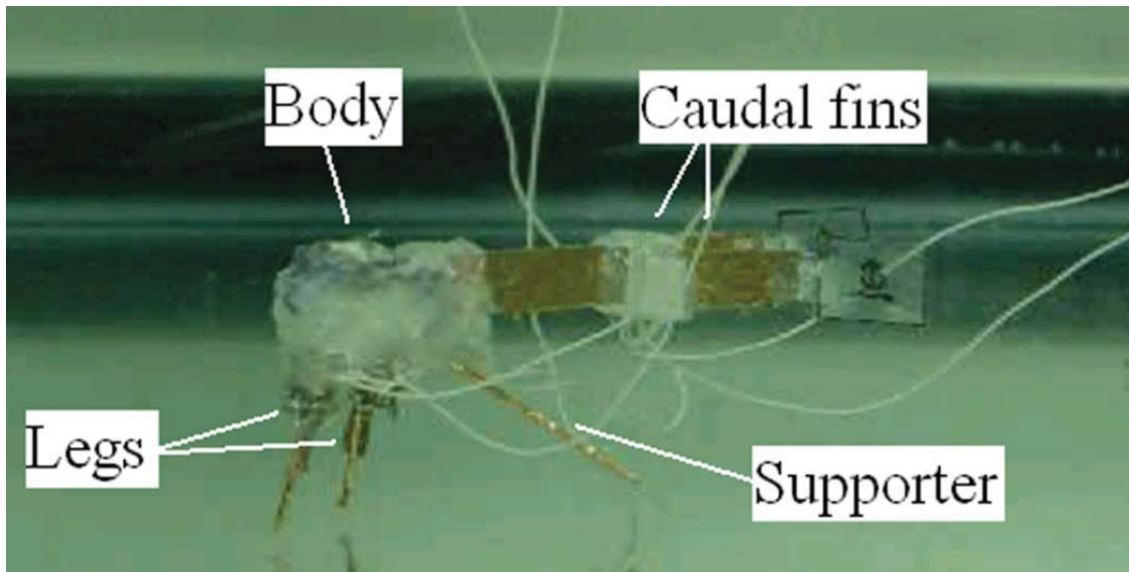
Figure 1.2 Swimming microrobot with ICPF

Recently, remote control of the magnetic actuated microrobot using a magnetic field has been popular and developed due to realize external wireless energy supply [41]-[46]. One of the microrobots is called a fish-like microrobot. It imitates the movement of a fish to produce a propulsive force with oscillatory motion or undulatory motion. The fish-like microrobot has one important limitation; it moves in only one direction inside a pipe. Therefore, another kind of proposed microrobot has been developed to solve this problem. This kind of microrobot can move with a spiral motion or a screw motion by using a bare screw propeller [47]-[56].

1.2 Electromagnetic actuation system

Motivated by controlling the magnetic microrobots, several magnetic robotic systems have been developed for controlling the microrobot in human body [57]-[61]. There are two main methods to control the magnetic actuated microrobot to realize the movement of the microrobot.
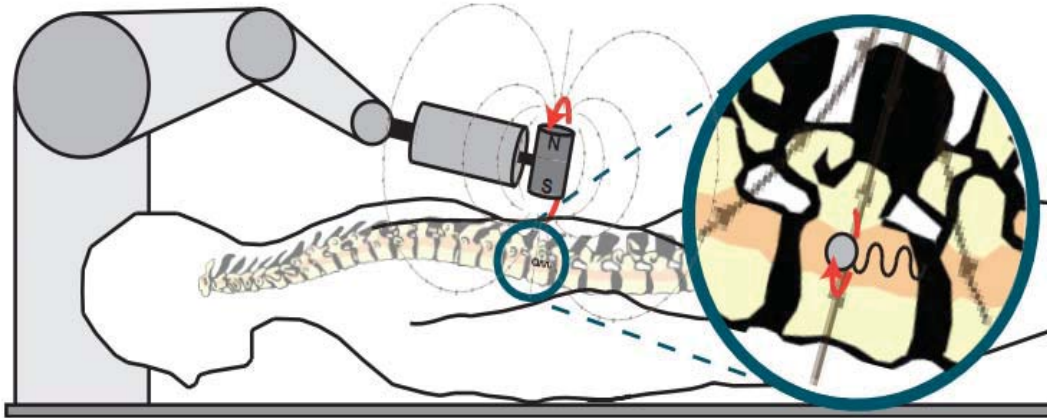
Figure 1.3 Rotating-permanent-magnet manipulator system
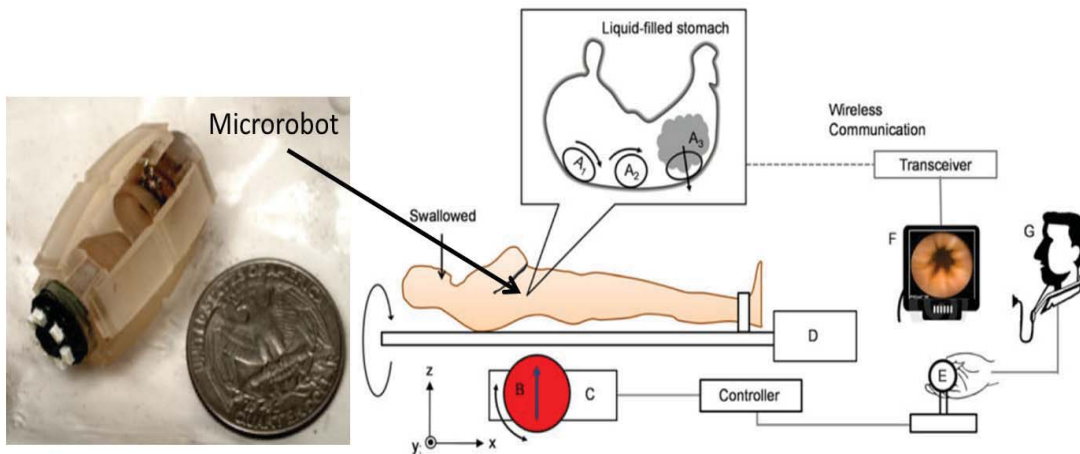
Figure 1.4 MASCE and the magnetic control system

Thomas W. R. proposed the use of non-uniform magnetic fields emanating from a single rotating-permanent-magnet (RPM) manipulator for the control of magnetic helical microrobots in 2010 [62]. It is shown in Figure 1.3. The RPM manipulator consists of a permanent magnet and a Maxon DC motor. The RPM manipulator was designed to have two different magnets: an axially magnetized cylindrical magnet 25.4mm in length and 25.4mm in diameter, and a diametrically magnetized cylindrical NdFeB magnet of the same dimensions.

Sehyuk Yim also proposed a magnetically actuated soft capsule

endoscope (MASCE) as a miniature mobile robot platform for diagnostic in medical applications in 2012 [63]. It is shown in Figure 1.4. Two internal permanent magnets and a large external magnet are used to control the robot. The proposed MASCE has three novel features. First, its outside body is made of soft elastomer-based compliant structures. Secondly, it can be actively deformed in the axial direction by using external magnetic actuation, which provides an extra degree of freedom that enables various advanced functions such as axial position control, drug releasing, drug injection, or biopsy. Finally, it navigates in three dimensions by rolling on the stomach surface as a new surface locomotion method inside the stomach.

The other method is that the microrobot is controlling by an electromagnet. Hyunchul Choi has been developed a stationary two-pair coil system to realize two-dimensional actuation of a microrobot as shown Figure 1.5 [64]. The EMA system consists of two pairs of stationary Helmholtz coils and Maxwell coils in the x-direction and y-direction. The microrobot is aligned to the desired direction by two pairs of Helmholtz coils and is propelled in the aligned direction by two pairs of Maxwell coils. But, the EMA system has the limitation of two-dimensional locomotion of the microrobot.
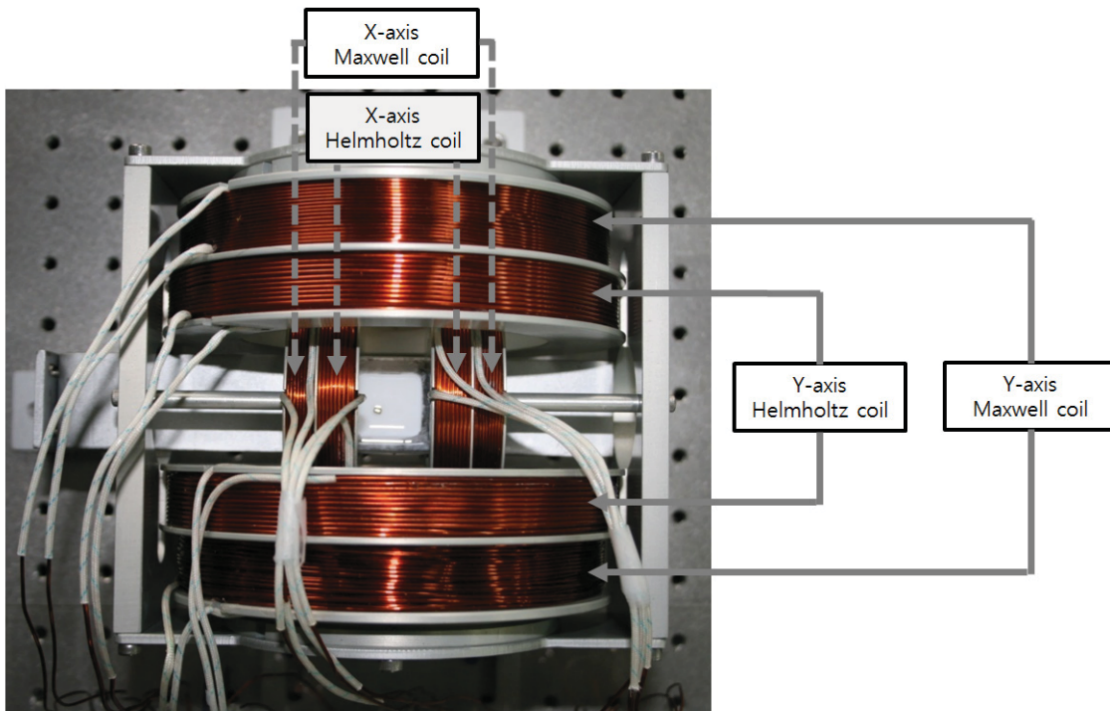
Figure 1.5 Electromagnetic actuation system

1.3 Motivation and research purpose
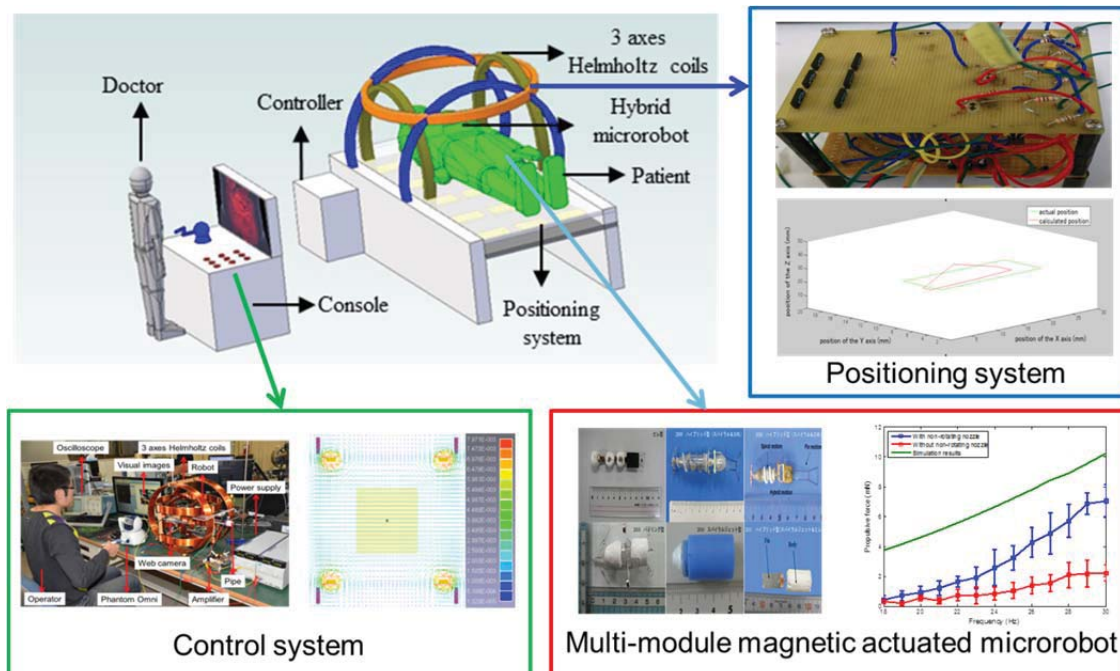
Figure 1.5 Project of a novel magnetic actuated microrobotic system

We have been proposed different kinds of microrobots [65]-[71].

However, further clinical application is needed in order to produce a robot that is capable of treating disease, diagnosing intestinal problems and conducting minimal invasive surgery. As well, the robot needs to be able to install actuating elements (e.g. drug delivery mechanism), a camera (e.g. endoscope) and sensing elements for achieving medical tasks. Therefore, medical safety, loading abilities and an effective propulsive performance is extremely important and challenging. There are several challenges in our research.

1) Robot body design for obtaining an effective propulsive performance on limited size or small size.

2) Method for controlling the multi-module magnetic microrobot in magnetic field and they are controlled separately without any interference.

3) Method for remote actuation and detecting position in human body in order to ensure the safety of patients.

Based on these requirements, I focus on developing a multi-module magnetic actuated microrobotic system for medical applications. The research purpose of this study can be summarized as follows:

1) Development and evaluation of a novel hybrid microrobot.

2) Physics modeling and analysis of the robot dynamics

3) Development and evaluation of a remote electromagnetic actuation (EMA) system for realizing the position control and posture control of the microrobot

1.4 Thesis contributions

In this thesis, a novel a multi-module magnetic actuated microrobotic system is proposed,

Contributions of this thesis are:

(1). Development of a novel multi-module magnetic actuated microrobotic system

The microrobot composes of different module with multi-functional. And the microrobots are comfortable and easy to swallow by patients, because it can realize the docking and releasing in various environments and has the flexible motion with wireless control.

(2) Design of a magnetically actuated hybrid microrobot

The magnetically actuated hybrid microrobot (MAHM) has two motion mechanisms. One is the spiral jet motion which can move by rotating the spiral propeller. The other is fin motion which can move by vibrating the fin. The MAHM can switch between the two motions to realize movement in various working environments. The spiral jet motion is used when the microrobot needs precision operation and stable movement. The fin motion is used when the high propulsive force is needed. Due to just only use one magnet inside the MAHM, two motions can be controlled separately without any interference.

(3) Development of a novel type of magnetic microrobotic system

Based on previous researches, a magnetic microrobotic system is developed to allow a doctor to remotely control a wireless capsule microrobot through a master device. This causes less pain to the patients

and there will be less tissue trauma. Thus reducing hospitalization time and enhancing recovery. On the master side, the doctor views a monitor which is produced by a CT-scan and operates the wireless microrobot to detect or treat the disease with an unknown and dynamic environment. The control instructions are transmitted to the slave side. On receiving instructions, the slave mechanisms control the wireless capsule microrobot. The monitor can also show the data calculated from the magnetic sensor array for obtaining the real-time position of the microrobot.

1.5 Structure of the thesis

Chapter 1. Introduction

Chapter 2. A Conceptual design of Multi-module Magnetic Microrobotic System

Chapter 3. A Novel Magnetic Actuated Microrobot with Screw Jet Motion

Chapter 4. A Magnetically Actuated Hybrid Microrobot

Chapter 5. Algorithm design of Multi-module Magnetic Actuated Microrobotic Systems

Chapter 6. Characteristic Evaluation of Multi-module Magnetic Actuated Microrobotic Systems

Chapter 7. Conclusion Remarks

Chapter 2   A Conceptual Design of Multi-module Magnetic Microrobotic System

2.1 Conceptual design of the multi-module Magnetic microrbotic system

Generally, the patients are placed on a liquid diet starting after lunch the day before the examination. And then, the patients should be drink the poly tetramethylene ether glycol 2000ml and water 500ml, 2~4 hours before examination. After all preparations, the microrobot is swallowed inside the digestive organs and can be manipulated [30], [72]. Conceptual diagram of the whole microrobotic control system is shown in Figure 2.1. The control system consists of a magnetically actuated hybrid microrobot, magnetic sensor array, three axes-Helmholtz coils, CT-Scan, monitor, and operation device (Phantom Omni device). Firstly, an intestinal image is generated by the CT scanner and the doctor views the intestinal image to confirm the area of a target in a monitor. Secondly, the doctor operates the Phantom Omni device to control the magnetically actuated hybrid microrobot to move to the target by using an external magnetic field. A 3 axes Helmholtz coils is used to generate the external rotational magnetic field. When the hybrid microrobot arrives at the target area, the operator controls the position and posture of the hybrid microrobot to detect or treat disease in an intestinal tract. Meanwhile, the monitor shows the real time position and position of the hybrid microrobot calculated from the

measurement data of magnetic sensor array. The magnetic sensor array is used to realize the close-loop control and ensure the hybrid microrobot to reach the target location. [71], [73]
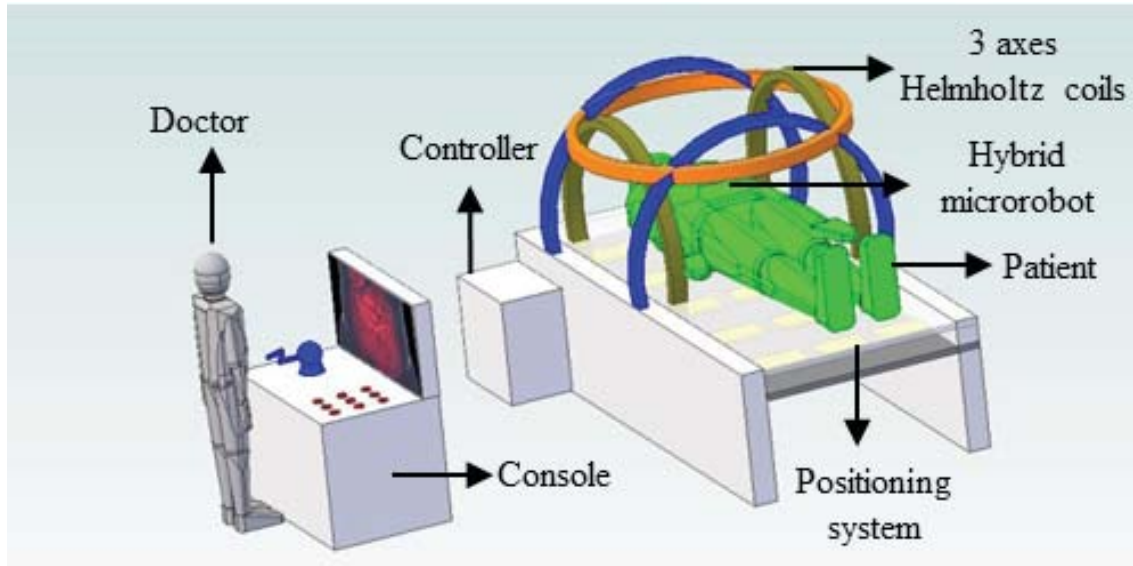
Figure 2.1 A Multi-module magnetic microrbotic system

2.2 Electromagnetic actuation system

2.2.1 Three axes Helmholtz coils design

To provide the magnetic torque to the microrobot, an EMA system which mainly consists of stationary 3 axes Helmholtz coils is proposed, as shown in Figure 2.2. It has a simple control method, because each Helmholtz coils is independent control. The 3 axes Helmholtz coils can produce a 3-D magnetic field vector in any direction and provide a magnetic torque for controlling the microrobot. Single-Helmholtz coil consists of two identical circular magnetic coils that are placed symmetrically one on each side of the experimental area along a common axis, and separated by the distance d equal to the radius r of the coil. Electrical current flows in the same direction in each coil.
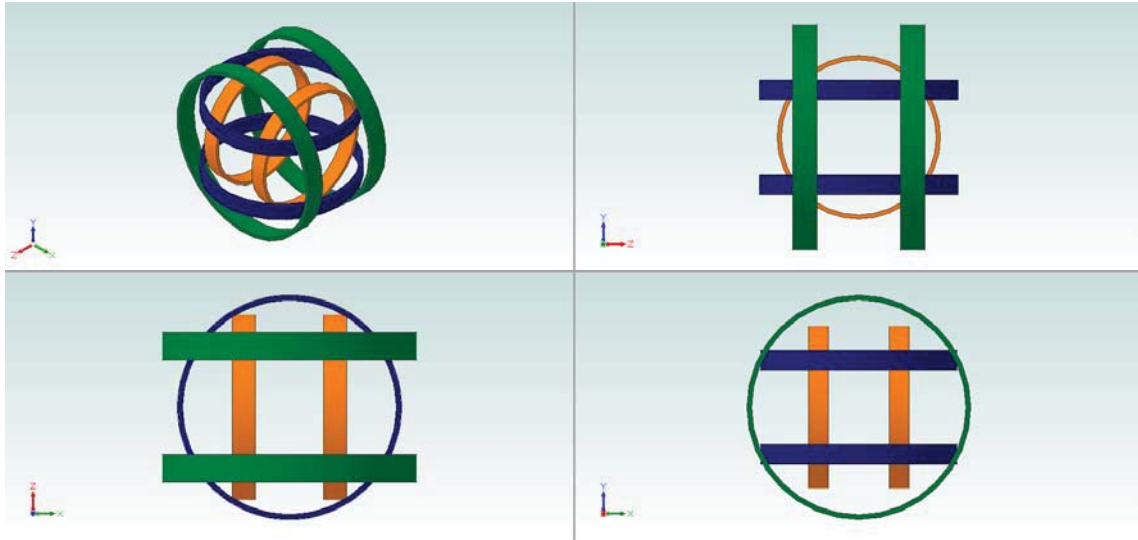
Figure 2.2 Structure of the 3 axes Helmholtz coils

Table 2.1 Specification of 3 axes Helmholtz coils

	Turns (n)	r (mm)	d (mm)	Resistance(Ω)	Material
x-axis coil	125	150	150	2.4	Cu
y-axis coil	150	175	175	3.3	Cu
z-axis coil	180	200	200	4.5	Cu

According to the Biot-Savart law, the magnetic flux density was generated by this coil. It is defined as following equation (2-1):

$$B(x) = \frac{in\mu_0 r^2}{2}\left\{\frac{1}{\left[r^2+(\frac{d}{2}-x)^2\right]^{\frac{3}{2}}}+\frac{1}{\left[r^2+(\frac{d}{2}+x)^2\right]^{\frac{3}{2}}}\right\} \qquad (2-1)$$

where, B= μ_0H is the magnetic flux density, at any point on the axis of the Helmholtz coils. μ_0 is the permeability of vacuum. n is the number of turns of coil. i is the current. r is the radius of the coil. x is the arbitrary

position from the center position of the pair coils. d is the distance between pair coils.

2.2.2 Characteristic evaluation of the three axes Helmholtz coils

Based on the electromagnetic theory, the magnetic flux density of the 3 axes Helmholtz coils is analyzed to realize control stable locomotion of the hybrid microrobot. For the characterization of the 3 axes Helmholtz coils, the magnetic flux density of Helmholtz coils was simulated with FEM method and experimentally measured with TESLA METER TM-501, as shown in Figure 2.3.

The simulation result of magnetic flux density with a constant current (1.5A) is shown in Figure 2.4. And then, the magnetic flux density measured with constant current and compared it with the simulation results, as shown in Figure 2.5. The different magnetic field direction is also simulated. Some simulation results are shown in Figure 2.6. The simulation results indicated the Helmholtz coils can generate a uniform magnetic field at the center of workspace, but it also generated a gradient magnetic field at the boundary of Helmholtz which can produce unintended consequences. In order to control the microrobot in the uniform magnetic field, the specification of 3 axes Helmholtz coils is designed, as shown in Table 2.1.

(a) TESLA METER TM-501
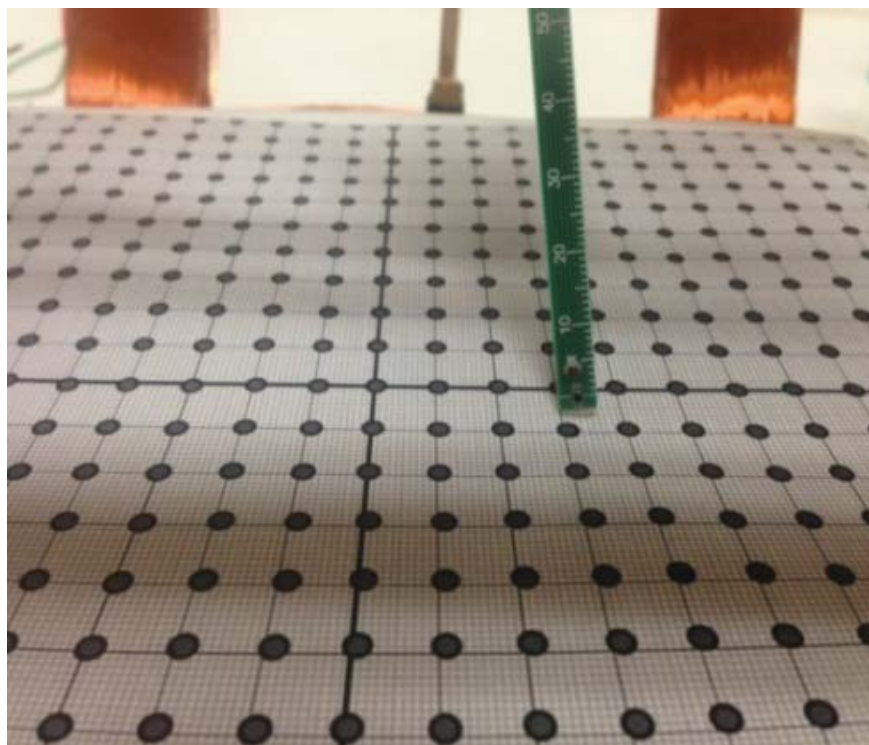
(b) Experiments

Figure 2.3 Measure the magnetic flux density
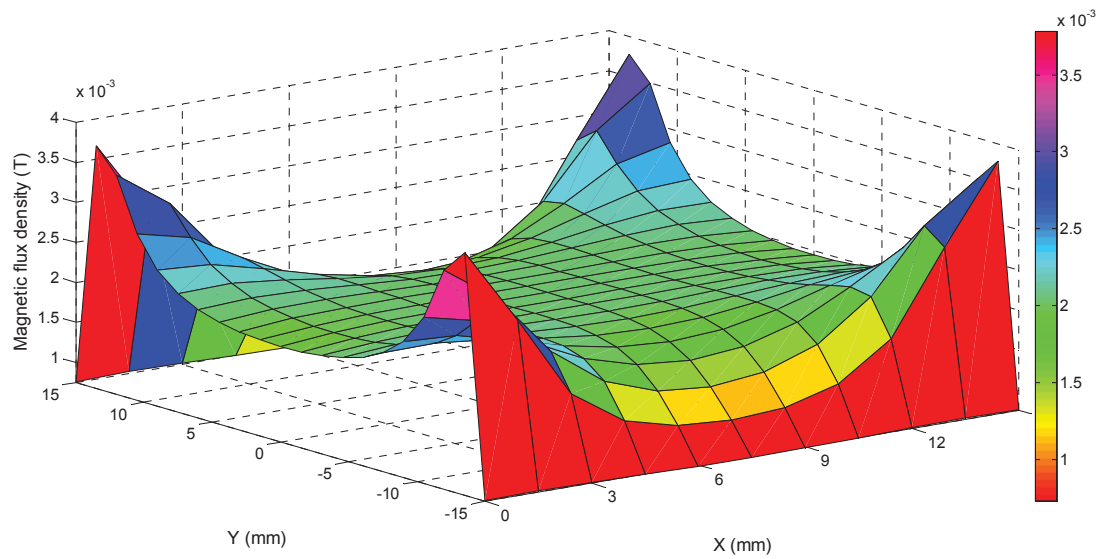
Figure 2.4 Simulation result of the magnetic flux density with constant

currents
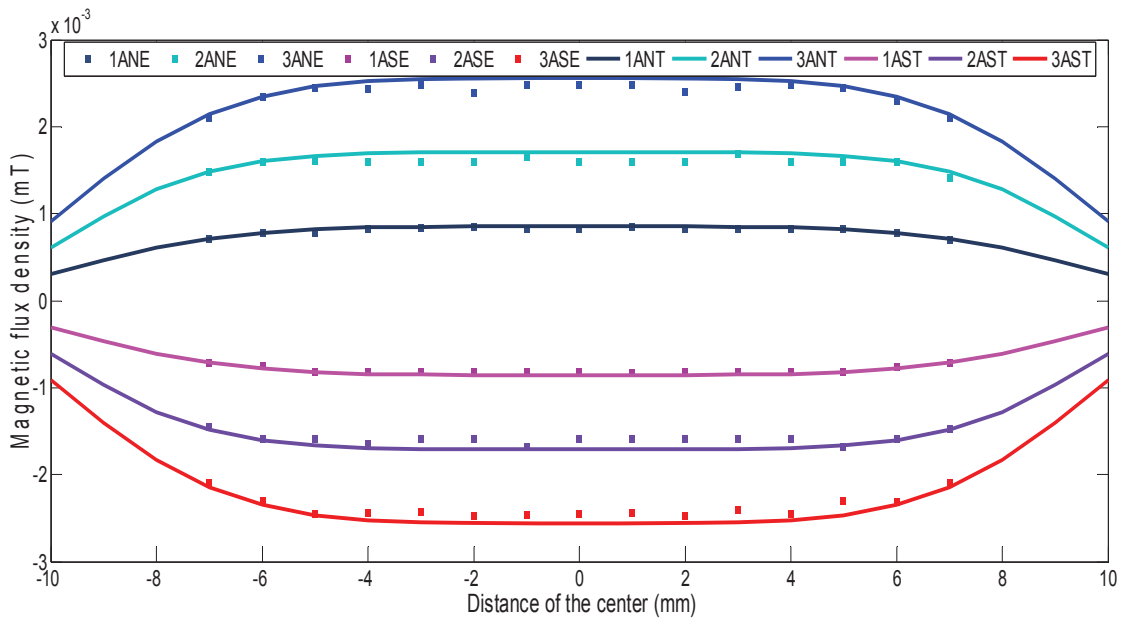
Figure 2.5 Compare magnetic flux density with different current.

N means north magnetic poles and S means south magnetic poles. T means

the theoretical value and E means the experimental value

(a) α, β ,γ=0^0 ,90^0 ,0^0
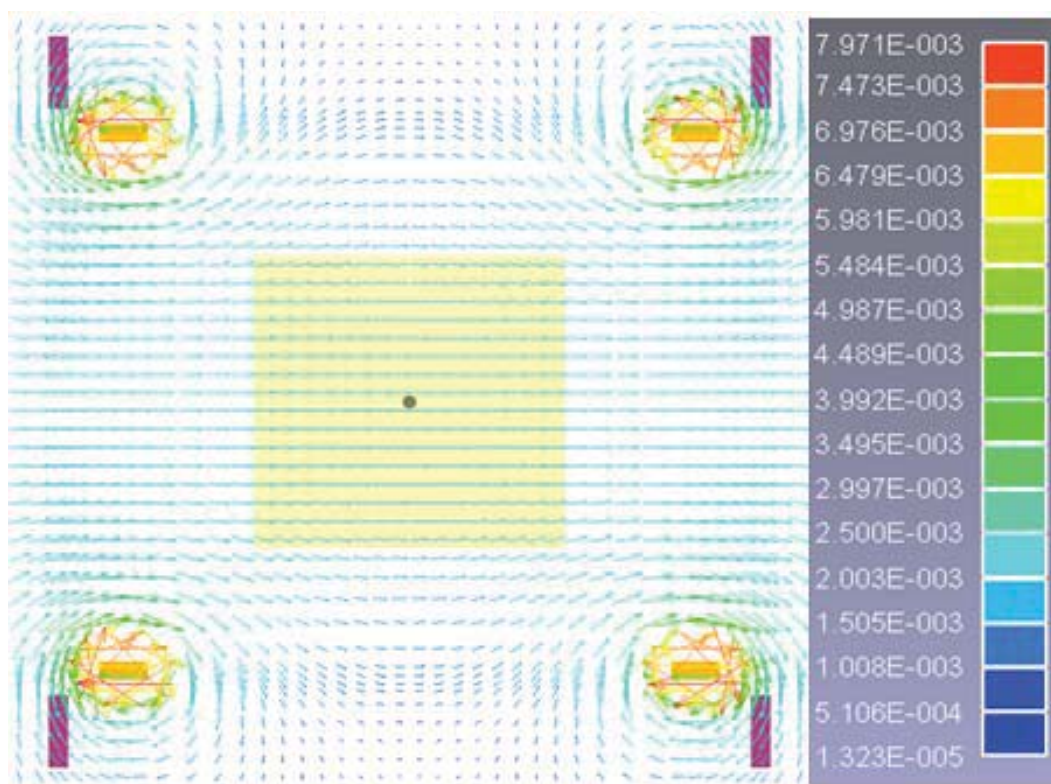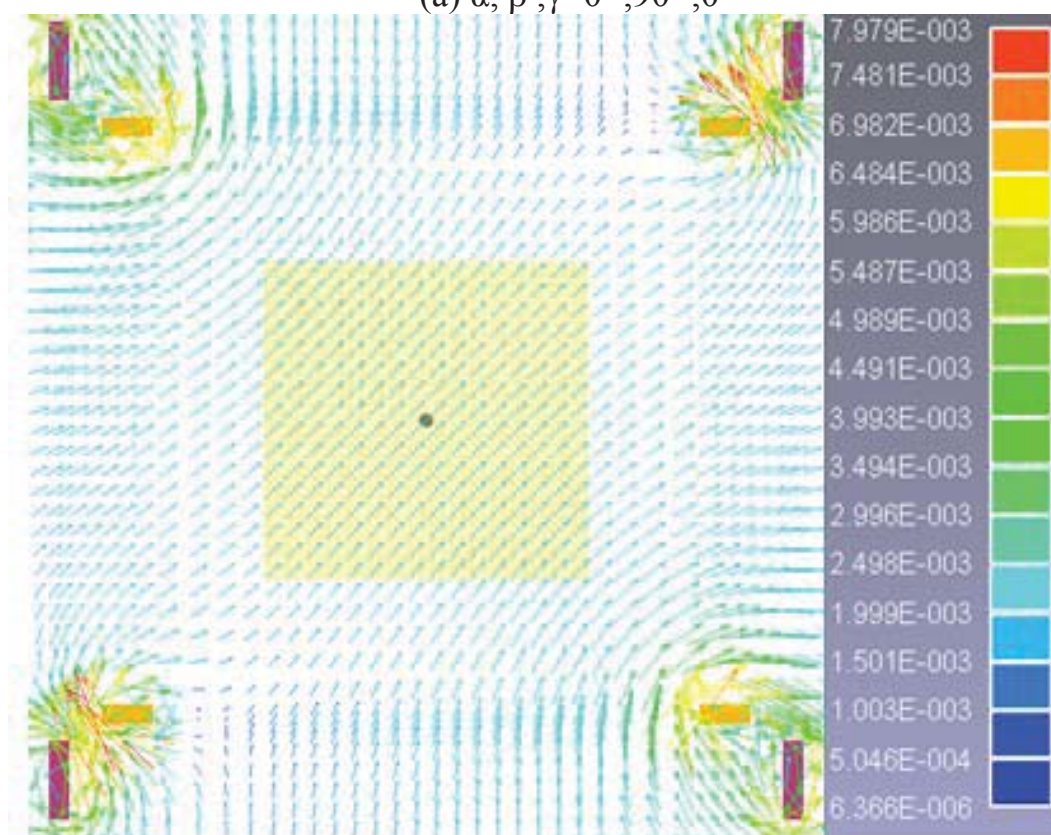
(b) α, β ,γ=45^0 ,45^0 ,0^0
Figure 2.6 Simulation of the magnetic direction (Unit is mT)

2.3 Positioning system

The monitoring of the microrobot in interesting region of human organ, e.g. gastrointestinal tract and blood vessels, is essential to guarantee the availability of the diagnosis, therapy and minimally invasive surgery. The 3-D ultrasound imaging, nuclear medicine imaging technology, fluorescence imaging and X-ray monitoring have been extensive in the clinical application [74]-[78]. However, these monitoring methods not only need the lager and expensive monitoring equipment, but also are harmful to the patient or doctor to a certain extent.

To obtain the positioning information of the microrobot, the magnetic sensor array composed six magnetic sensors is used to detect the intensity of magnetic field from magnet which is embedded inside the microrobot. Magnetic sensor array is placed at the under of microrobot to obtain the information of magnet.
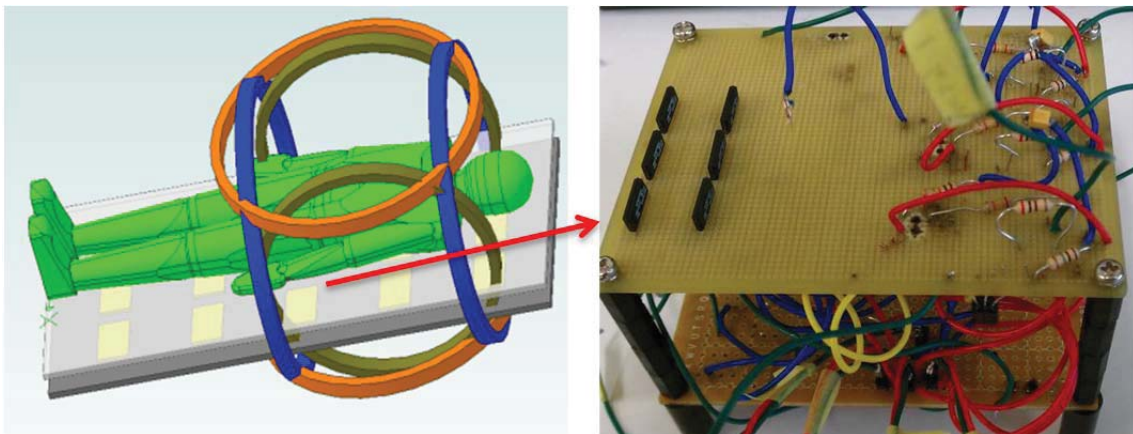
Figure 2.7 Positioning system with magnet sensor array

2.3.1 Analysis of the magnetic field
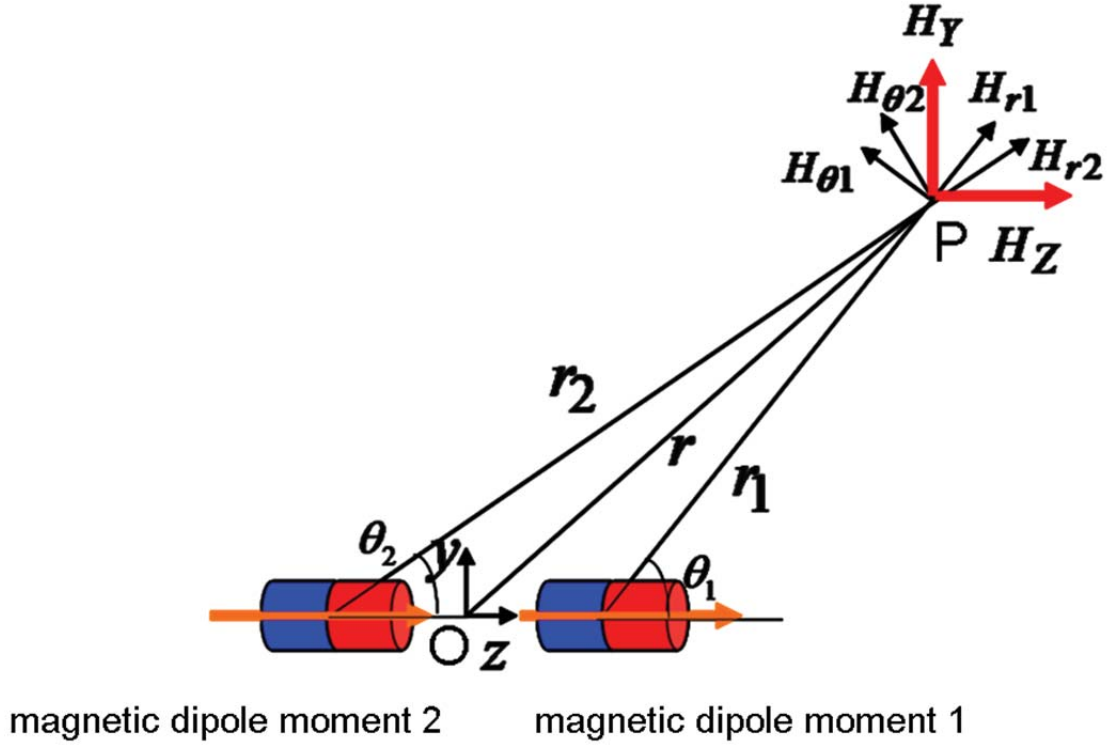
Figure 2.8 Magnetic dipole model

The magnetic flux density of the magnet inside microrobot is analyzed. The magnetic dipole model [79-84] is shown in Figure 2.8. The relationship between the distance and magnetic field as follows:

$$U = \frac{ml\cos\theta}{4\pi\mu_0 r^2} \tag{2-2}$$

$$H_r = -\frac{\partial U}{\partial r} = \frac{ml}{2\pi\mu_0 r^3}\cos\theta \tag{2-3}$$

$$H_\theta = -\frac{\partial U}{r\partial\theta} = \frac{ml}{4\pi\mu_0 r^3}\sin\theta \tag{2-4}$$

$$H_X = \frac{X}{\sqrt{X^2+Y^2}}(\frac{3ml}{4\pi\mu_0 r_1^3}\sin\theta_1\cos\theta_1 + \frac{3ml}{4\pi\mu_0 r_2^3}\sin\theta_2\cos\theta_2) \tag{2-5}$$

$$H_Y = \frac{Y}{\sqrt{X^2+Y^2}}(\frac{3ml}{4\pi\mu_0 r_1^3}\sin\theta_1\cos\theta_1 + \frac{3ml}{4\pi\mu_0 r_2^3}\sin\theta_2\cos\theta_2) \tag{2-6}$$

$$H_Z = \frac{ml}{4\pi\mu_0 r_1^3}(2\cos^2\theta_1 - \sin^2\theta_1) + \frac{ml}{4\pi\mu_0 r_2^3}(2\cos^2\theta_2 - \sin^2\theta_2) \qquad (2\text{-}7)$$

Where U is the magnetic potential, m is the magnetic moment, l is the distance between the magnetic poles, r is the distance between measurement position and magnet, θ is the angle between measurement position and magnet. μ_0 is the permeability of vacuum. L is the half length between two magnetic potentials of the magnet. H_r is intensity of magnetic field in r direction, and H_θ is intensity of magnetic field in θ direction.

2.3.2 Simulation results

We analyzed the magnetic field. Figure 2.9 and Figure 2.10 shows the simulation results. This result indicated that the magnet having multi magnetic potentials is higher magnetic field area than one magnetic potential type.

We used a magnetic sensor array (HMC1021Z by Honey Well, as shown in Figure 2.12) to obtain the position parameter of the microrobot, which is used to calculate the real position of our microrobot by least square method. The mean error is 6.09mm, as shown in Figure 2.13.
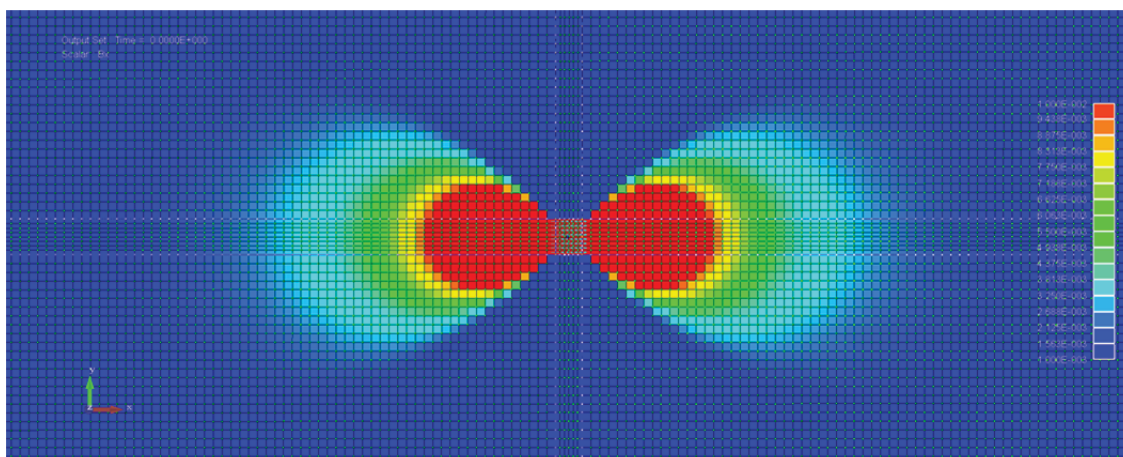
Figure 2.9 Analytical results of one magnet
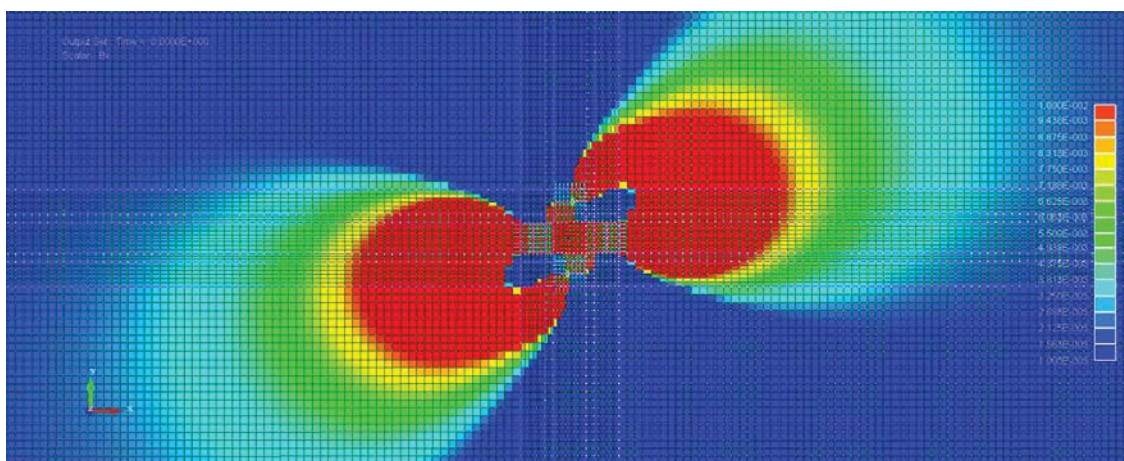
Figure 2.10 Analytical results of four magnets
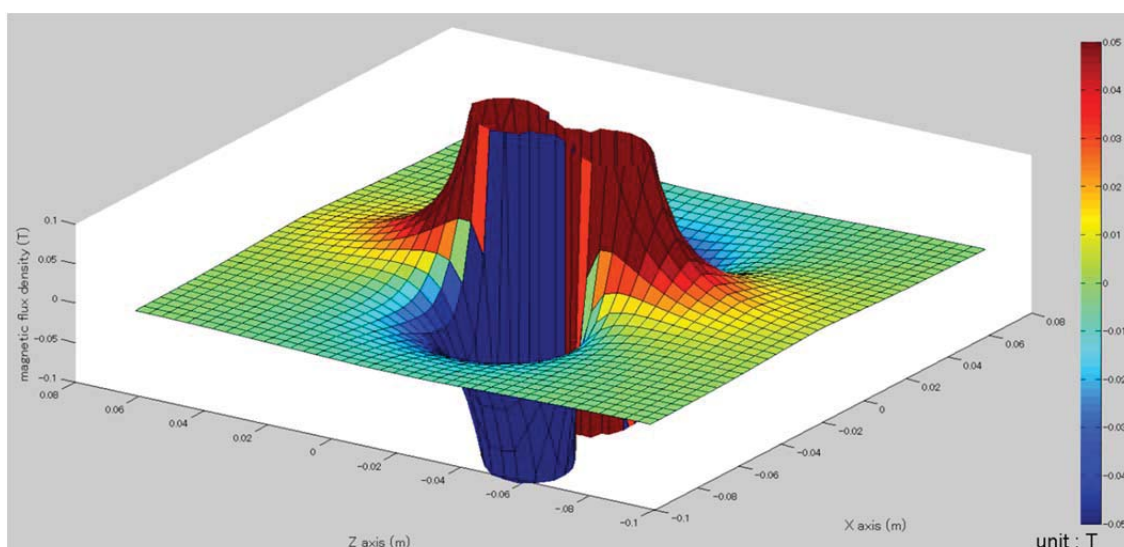
Figure 2.11 Analytical results of O-ring type magnets
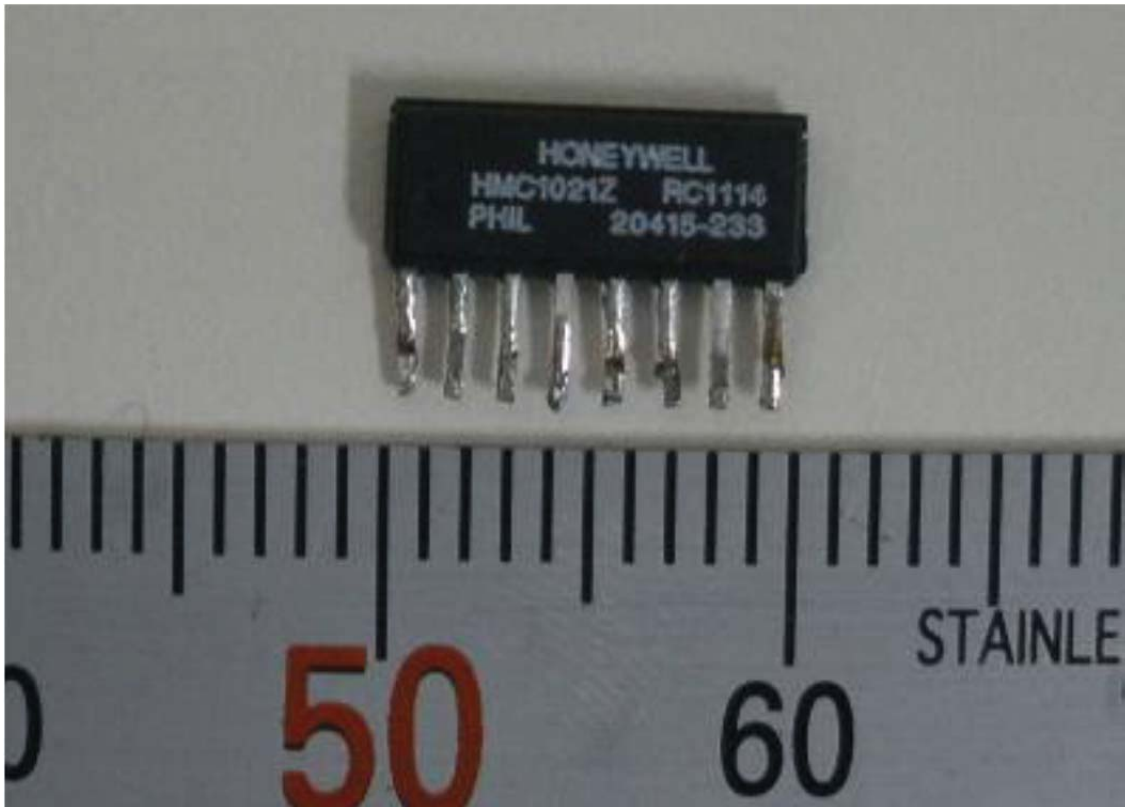
Figure 2.12 High sensitive magnetic field sensor
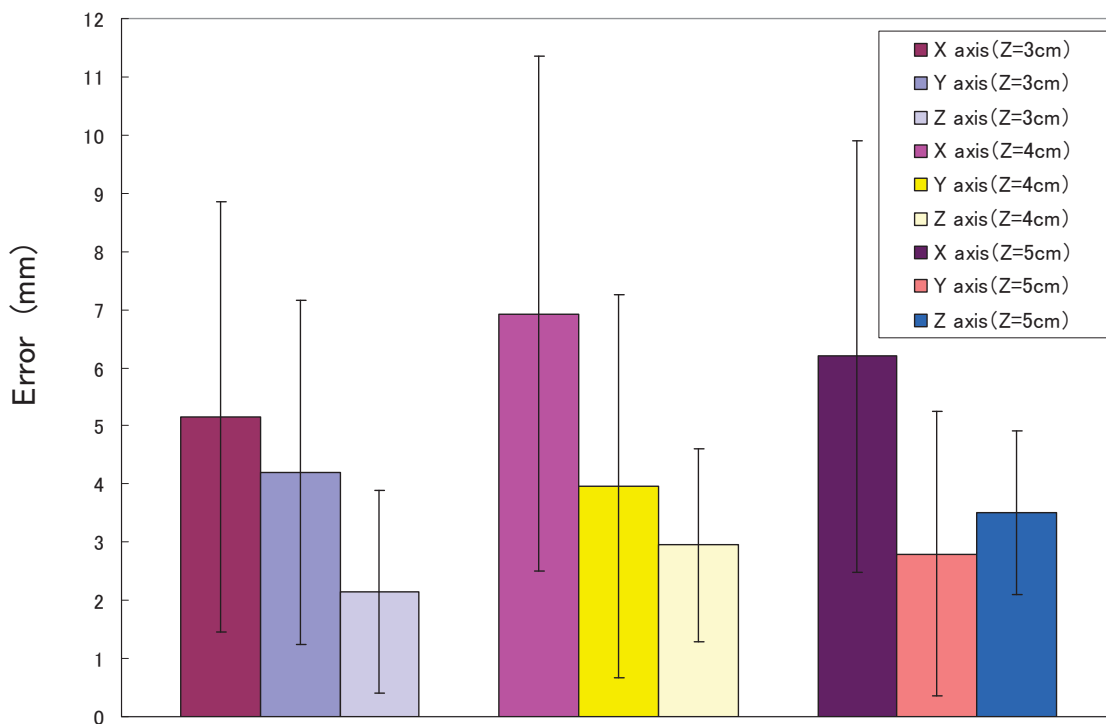
Figure 2.13 Experimental results of the position detection
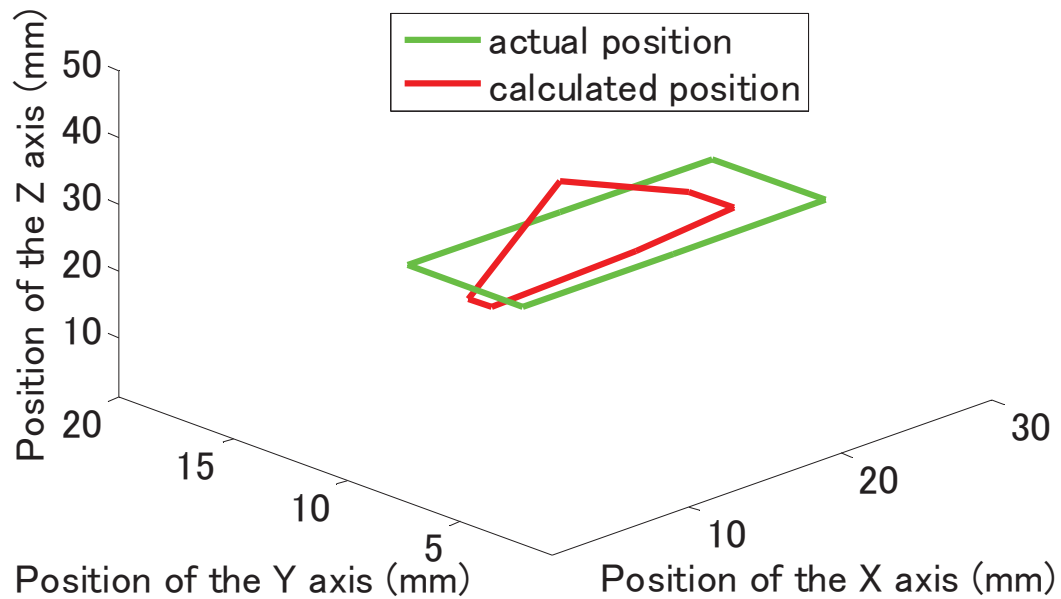
Figure 2.14 Errors of the trajectory

2.3.3 Evaluated error of the trajectory

The least square method is used to detection the position and posture of the wireless microrobot in human body. We compared the errors of the trajectory between calculated position and actual positions of the magnet using the positioning system. That result is shown in Figure 2.14. Green line is the trajectory of the magnet, and red line is the trajectory of the calculated result.

2.4 Summary

In this chapter, we proposed a multi-module magnetic actuated microrobotic system. It consists of an electromagnetic actuation (EMA) system, which is used to generate a magnetic field with any direction in the work spaces, and a positioning system, which is used to detect the position of the microrobot. We used our proposed control system to manipulate the

microrobot to realize the flexible motion. We can realize the remote control and local control using our proposed control system.

The 3 axes Helmholtz coils have been proposed. The Helmholtz coils are made for controlling the wireless microrobot and proving the energy for the wireless microrobot.

Firstly, in order to have enough inner space to accommodate a human subject in the medical application, the shape and the performance of the Helmholtz coils is analyzed.

Secondly, the 3 axes Helmholtz coils are fabricated to generate a rotational magnetic field which can be used to realize control the wireless microrobot in 3D space.

Thirdly, the magnetic flux density is measured with a constant current and compared the experimental results with the simulation results. And the magnetic flux density is also measured with different current and compared the experimental results with the simulation results. The experimental results are coincided with the theoretically analysis. The results prove that the designed 3 axes Helmholtz coils are effective.

Through the above analysis, the 3 Helmholtz coils are possible to generate the uniformed magnetic field in 3D space to realize the 3DOFs locomotion of the wireless microrobot in human body

Chapter 3   A Novel Magnetic Actuated Microrobot with Screw Jet Motion

3.1 Magnetic actuated microrobot with screw motion

3.1.1 Structure of magnetic screw type microrobot

During diagnosis and surgery, some factors such as, length of microrobot and diameter of microrobot, need be taken into account. Due to the overall limited size of microrobots, there is insufficient space for modules such as a camera module, a battery module, and a transmit/receive module. In addition, to accomplish medical tasks, a microrobot should be controlled by doctors. Therefore, a flexible, controllable, and wireless power supply is important for microrobots. To solve the above problems, we developed a self-propelled screw microrobot manipulated by 3-axis Helmholtz coils, which generate an external orthogonally rotating magnetic field. The conceptual design of the magnetic spiral microrobot is shown in Figure 3.1. The magnetic screw microrobot is composed of a screw outer shell based on the Archimedes screw structure [86-88] and an O-ring magnet as an actuator. The Archimedes screw structure provides a propulsive force while the microrobot rotates using an external magnetic field. Due to the energy provided by the external magnetic field, the microrobot can work for a long time in the human body to accomplish medical tasks. In addition, 50% of the inner space is used to support tools for diagnosis. The prototype of the magnetic spiral microrobot is shown in

Figure 3.1(d). The spiral outer shell is made of polythene plastic and is connected to the O-ring magnet by a strong adhesive. The specifications are given in Table 3.1.
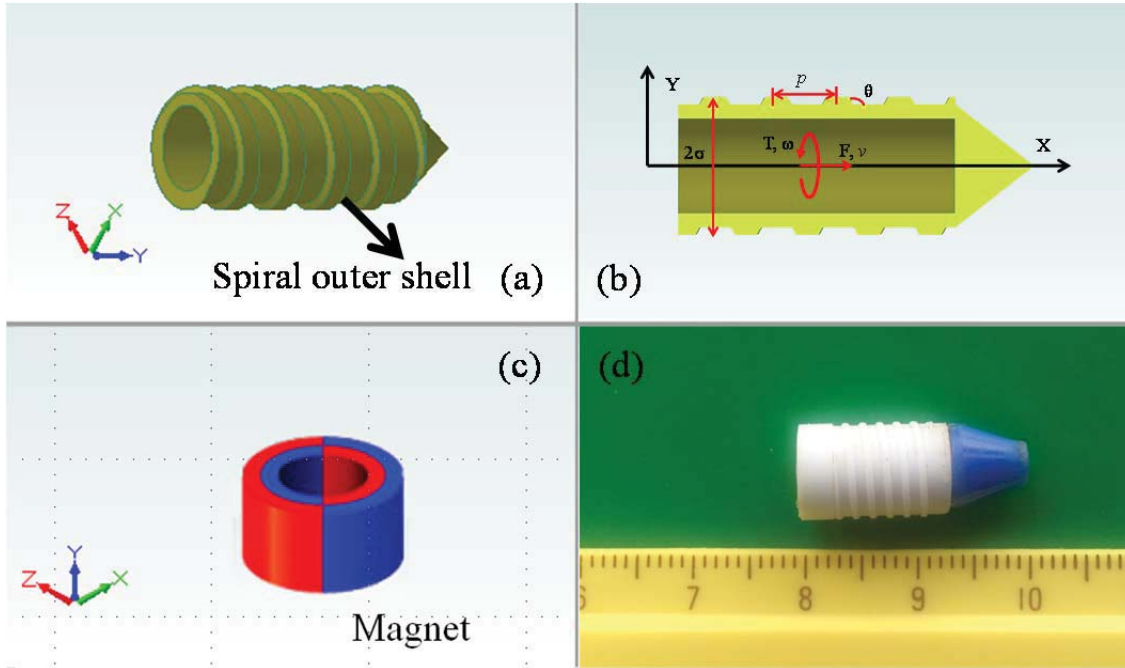
Figure 3.1 Concept of the proposed magnetic screw type microrobot (a) Structure and (b) model of magnetic screw type microrobot. (c) O-ring magnet. (d) Prototype of magnetic screw type microrobot

Table 3.1 Specifications of magnetic screw type microrobot

Length of microrobot	20 mm
Radius of microrobot	8 mm
Weight of microrobot	2.306 g
Magnetization direction	Radial
Radius of magnet	6 mm
Weight of the microrobot	1.036 g
Material of body	Polythene

3.1.2 Propulsion force on magnetic spiral microrobot

The propulsive force of a magnetic spiral microrobot is along the central axis. In a low-Reynolds-number regime, the total applied nonfluidic torque and force are linearly related to the axial speed and angular speed with the parameters defined in Figure 3.1(b). The following symmetric propulsion matrix equation [89]-[92] is used to describe the propulsive force and torque of the magnetic spiral microrobot:

$$\begin{bmatrix} F \\ T \end{bmatrix} = \begin{bmatrix} a & b \\ c & d \end{bmatrix} \begin{bmatrix} v \\ \varpi \end{bmatrix} \tag{3-1}$$

where F is the non-fluidic applied force, T is the non-fluidic applied torque, v is the axial speed, and ω is the angular speed.

We assume that the microrobot moves in water that has a constant density. k_1 and k_2, which are the viscous drag coefficients for the magnetic spiral microrobot along and perpendicular to the axis, respectively, are constant. These two parameters are a theoretical maximum value that is related to parameters such as the radius of the microrobot, number of turns of the microrobot, and pitch of the microrobot [89], [90]. From the symmetric propulsion matrix, the speed of the microrobot is a function of the geometric parameters, are given by:

$$\left.\begin{aligned} a &= 6.2n\sigma\left(\frac{k_1\cos^2\theta + k_2\sin^2\theta}{\sin\theta}\right) \\ b &= 6.2n\sigma\left(k_1 - k_2\right)\cos\theta \\ c &= b \\ d &= 6.2n\sigma\left(\frac{k_2\cos^2\theta + k_1\sin^2\theta}{\sin\theta}\right) \end{aligned}\right\} \tag{3-2}$$

where k_1 and k_2 are the constants defined above and n is the number of

turns of the microrobot.

3.1.3 Fluid drag force on magnetic spiral microrobot

The total drag force depends on the Reynolds number and the shape of the magnetic spiral microrobot. In a pipe, the Reynolds number is generally defined as:

$$Re = \frac{\rho v d}{\mu} \tag{3-3}$$

The total drag force can be expressed as:

$$F_D = C_D \frac{1}{2} \rho v^2 S + \mu_f N \tag{3-4}$$

where ρ is the density of the fluid, v is the speed of the microrobot, d is the diameter of the microrobot, μ is the coefficient of kinematic viscosity, S is the maximum cross area that is vertical to the flow of fluid, C_D is the resistance coefficient, μ_f is the coefficient of friction, and N is the normal force between the microrobot and the surface of the pipe.

3.1.4 Evaluation performance of the magnetic microrobot with screw motion

To achieve wireless real-time control of the microrobot, a microrobotic control system is proposed [92]. It includes a data acquisition board (USB-4716, Advantech, China), a DC power supply, a control unit, 3-axis Helmholtz coils, an oscilloscope, a Phantom Omni device (SensAble), a web camera, a pipe, and a personal computer. The microrobot was placed in a transparent pipe (inner diameter: 26 mm; thickness: 3 mm) filled with water. The control signals were applied to the 3-axis Helmholtz coils in order to obtain a rotating magnetic field via the

data acquisition board and control unit. The magnetic flux density and the magnetic field frequency were adjusted using the Phantom Omni device. The web camera was used to monitor the inside of the pipe. During experiments, the Phantom Omni device was used to control the position and posture of the microrobot with the help of a display. The display showed data used for obtaining the real-time position of the robot. The oscilloscope showed the magnetic flux density changing frequency.

The bi-directional relationship between the magnetic flux density changing frequency and the speed was investigated. The results, shown in Figure 3.2(a), show that in the frequency range of 0 to 15 Hz, the microrobot can rotate continuously, synchronized with the rotating magnetic fields, and generate enough propulsion to overcome the resistance of fluids. In the frequency range of 15 to 20 Hz, the microrobot can no longer rotate continuously. The frequency of 15 Hz is called a step-out frequency. The step-out frequency is related to the microrobot's weight, magnetic torque, and any other loads. This frequency is well understood for magnetic spiral microrobots in uniform magnetic fields and is discussed in our previous research [92]. The experimental results indicate a linear relation between magnetic field changing frequencies and speed in the range of 0 to 15 Hz. At 15 Hz, the maximum speed is 11.8 mm/s in the horizontal direction and 3.64 mm/s in the vertical direction. Figure 3.2(b) shows the relationship between the rotational frequency and the speed of the magnetic spiral microrobot in the vertical direction. This disparity of the experimental result between the Figure 3.2(a) and Figure 3.2(b) is due

to the extra force needed to overcome gravity. Figure 3.3 shows a video sequence of forward/backward motion controlled by the Phantom Omni device in a pipe. Figure 3.4 shows the variable speed motion controlled by the Phantom Omni device in the pipe.

(a)

(b)
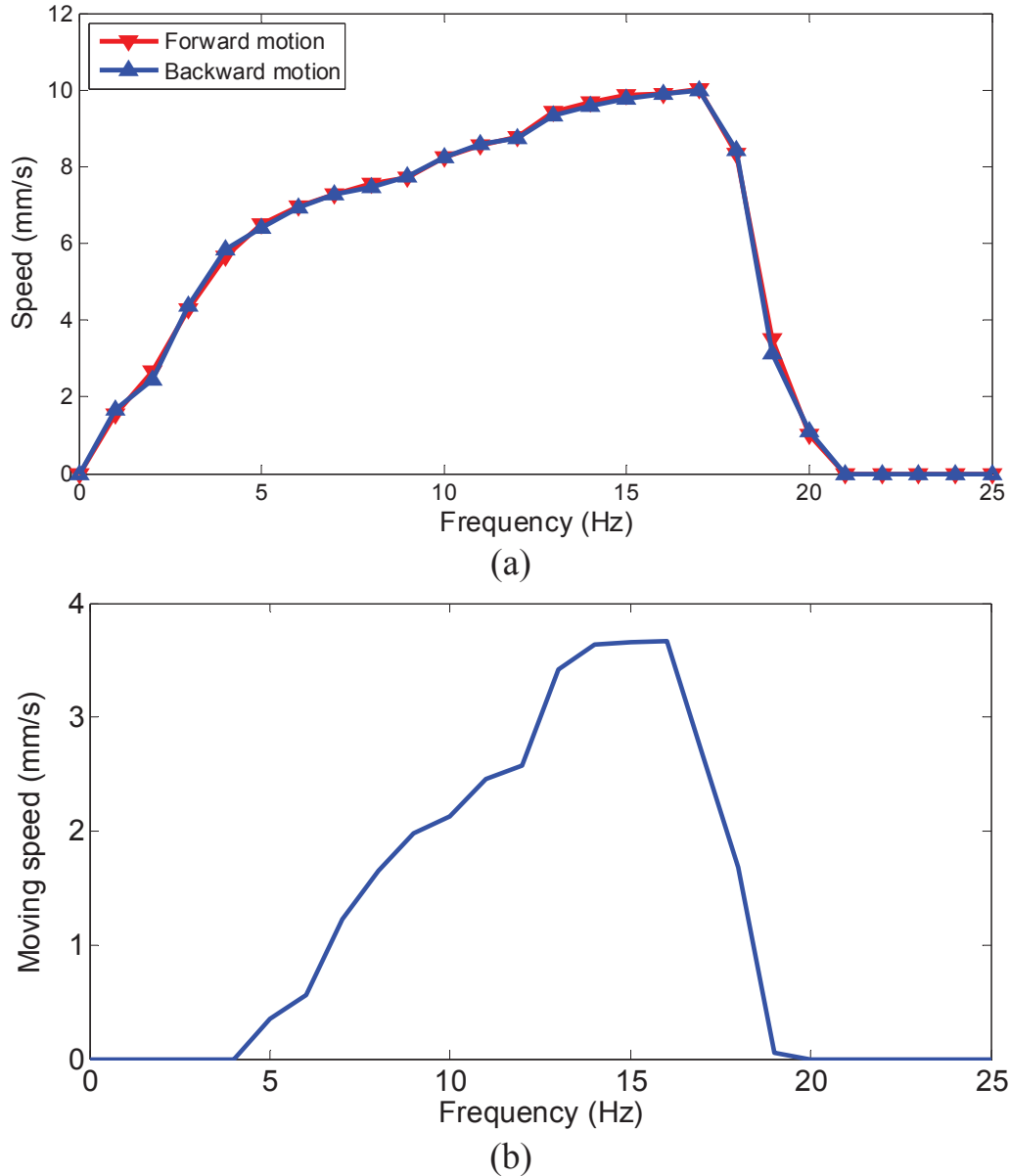
Figure 3.2 (a) Bi-directional relationship between magnetic flux density changing frequency and speed. (b) Relationship between magnetic flux density changing frequency and speed in vertical direction.
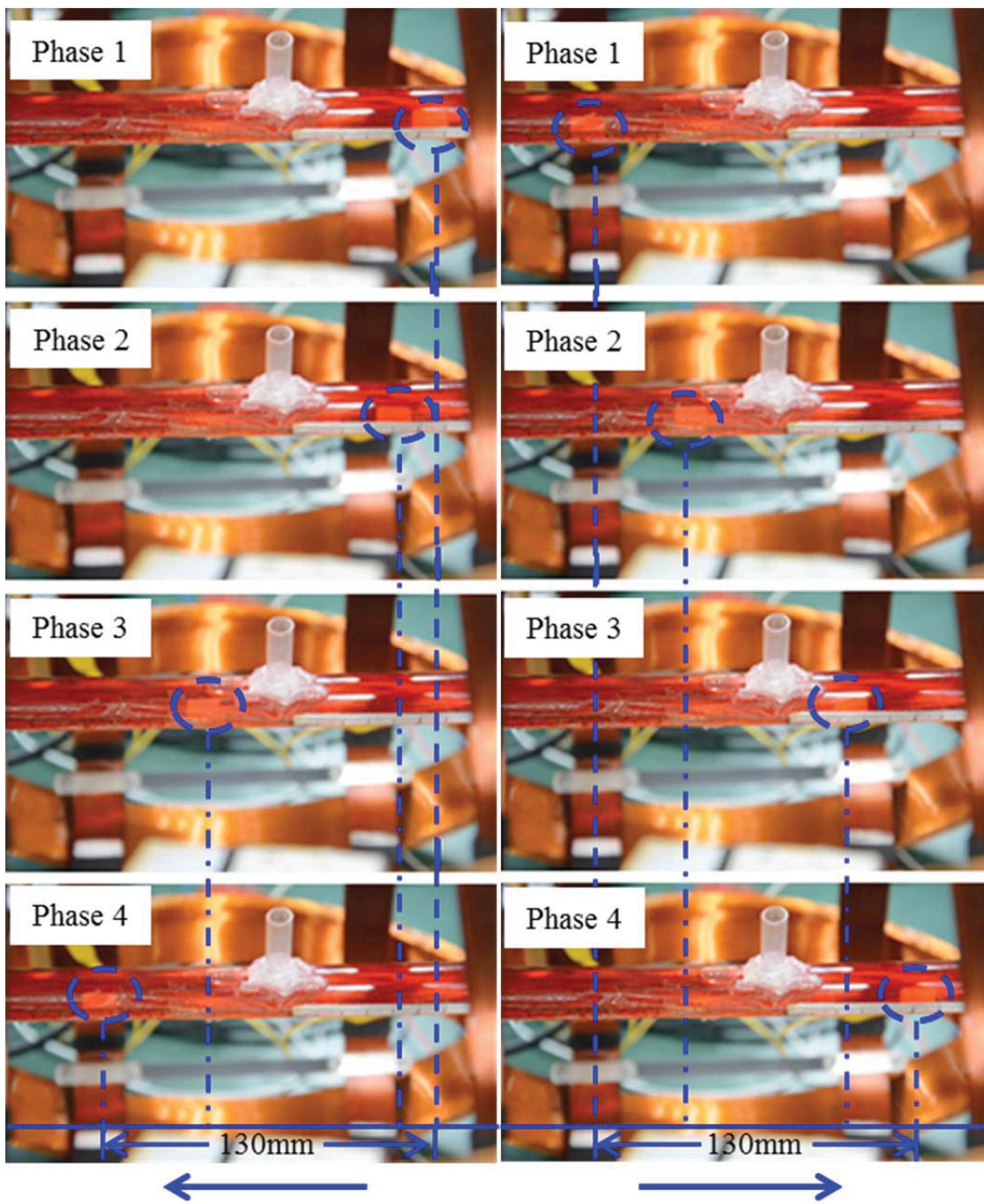
(a)Forward motion   (b) Backward motion

Figure 3.3 Movement of the microrobot controlled by Phantom Omni
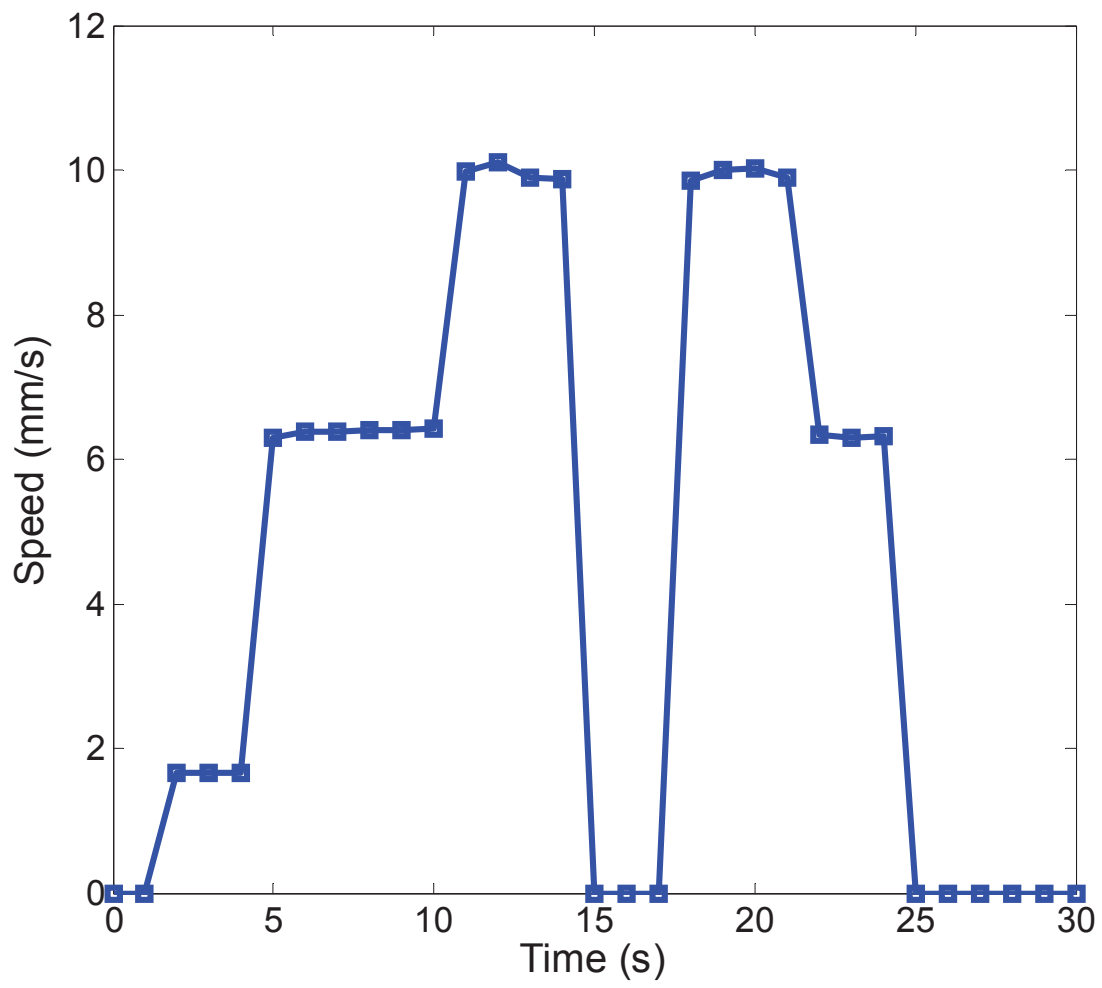
Figure 3.4 Experimental results of variable motion

3.2 Magnetic actuated microrobot with screw jet motion

3.2.1 Structure of magnetic screw jet type microrobot

Several spiral or screw types of microrobots have recently been developed for achieving various functions. However, their propulsive mechanisms are comprised of a bare propeller, which leads to a low propulsive force. Thus, we proposed a novel propulsive mechanism for a magnetic actuated microrobot to increase the efficiency of the propulsive force. Figure 3.5 illustrates our proposed microrobot, which moves using a propulsion arrangement called a shrouded propeller. A shrouded propeller is a bare propeller fitted with a non-rotating nozzle, which is used to improve the efficiency of the propeller, especially on propellers with a limited diameter. The non-rotating nozzle connects to the propeller with an axis and bearing. When the propeller rotates to accompany the magnetic actuator, the shrouded propeller pushes the fluid backward generating a reaction force, which creates a forward motion, also called a spiral jet motion. In respect to hydrodynamics, the shrouded propeller produces a larger propulsive force than the bare propeller. For medicine, the shrouded propeller type of microrobot can reduce the damage caused to the intestinal wall due to the non-rotating nozzle thereby reducing pain for patients.
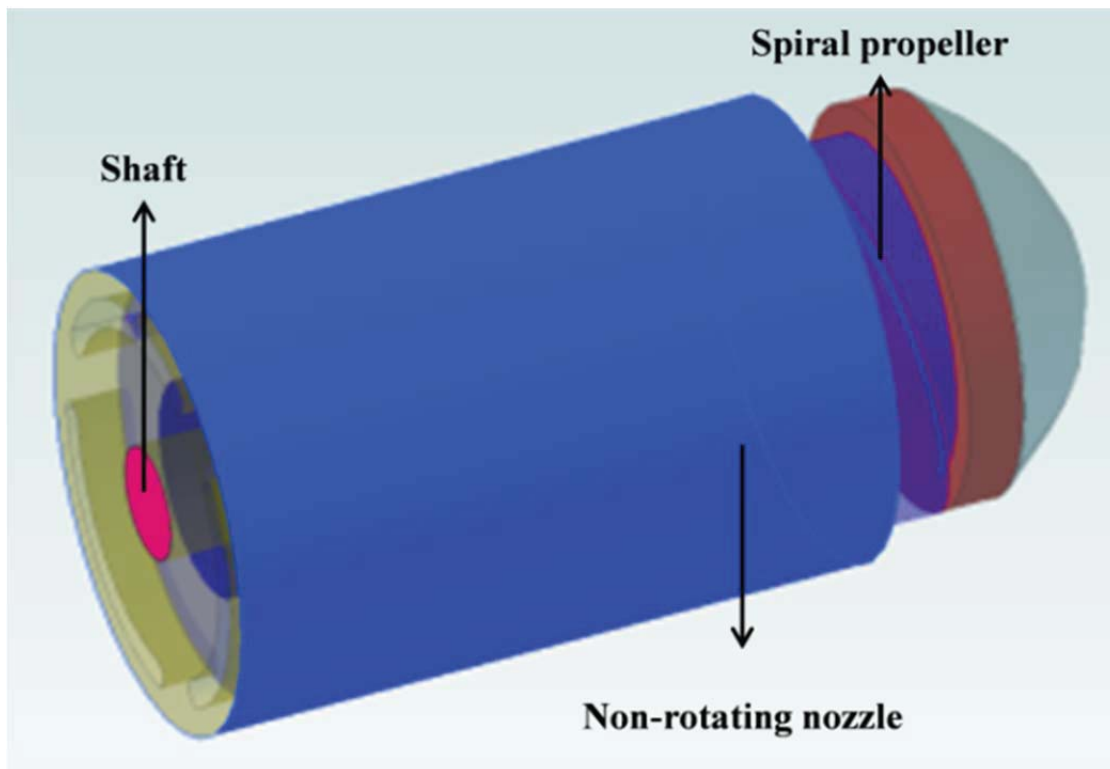
(a) Overall view
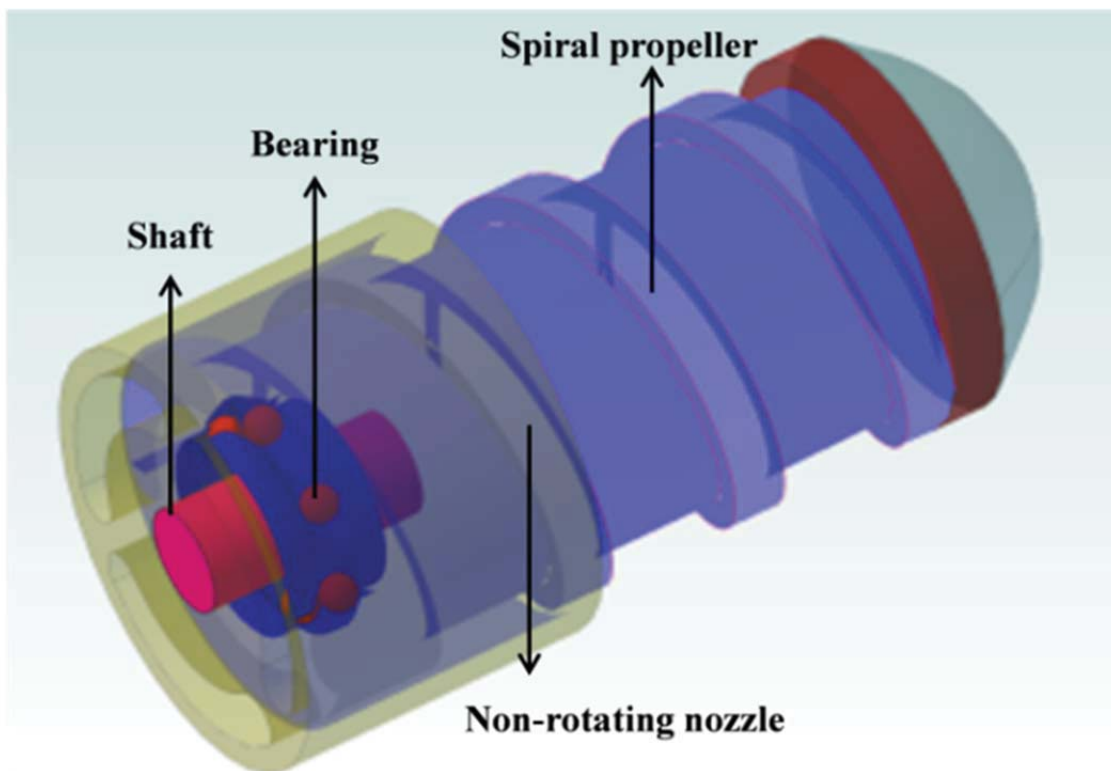
(b) Perspective view

Figure 3.5 Conceptual design of the microrobot with shrouded propeller

3.2.2 Modeling of the magnetic actuated microrobot with screw jet motion
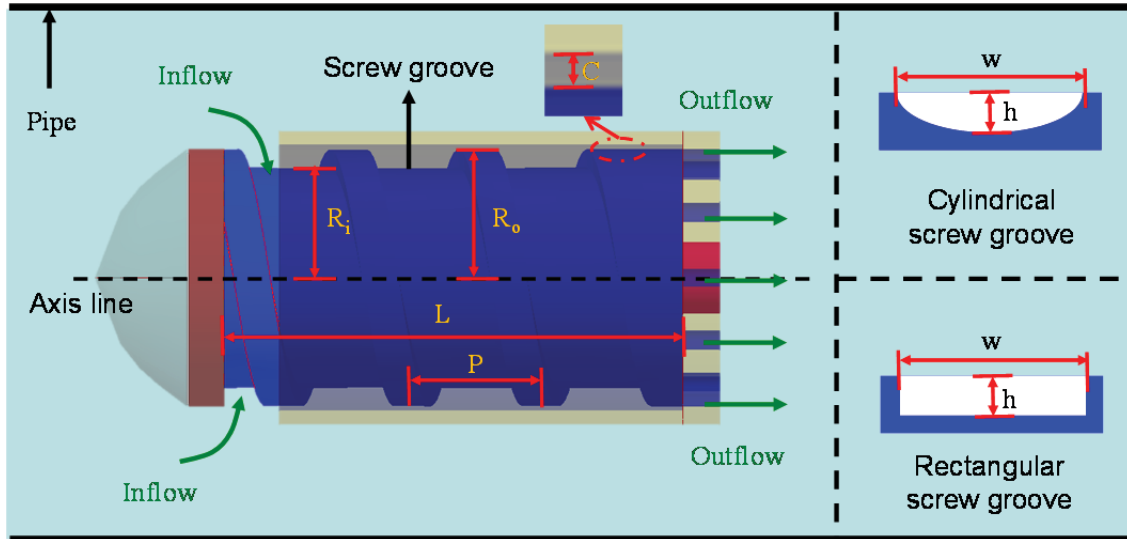
Figure 3.6 Propulsive force model

Figure 3.6 shows the propulsive force model of the shrouded propeller. When the microrobot moves inside the pipe, which is completely filled by the liquid, the liquid enters one end of the microrobot and leaves the other end of the microrobot at the same time. Since the liquid is incompressible, the volume of liquid through any perpendicular plane in any interval of time must be the same everywhere in the microrobot. Consider the inflow area and outflow area of the microrobot whose cross-sectional area are inflow area A_1 and outflow area A_2. The volume of liquid passing through the inflow area is equal to the volume of liquid passing through the outflow area for unit time, to give equation (3-5)

$$Q = A_1 V_1 = A_2 V_2 \tag{3-5}$$

where, Q is the flow of spiral jet motion, V_1 is the inflow velocity of the area A_1 and V_2 is the outflow velocity of the area A_2.

The propulsive force is defined by equation (3-6)

$$F_p = \rho Q v_2 = \rho Q \times \frac{Q}{A_2} = \rho \frac{Q^2}{A_2} \tag{3-6}$$

where, F_p is the propulsive force, ρ is the density of liquid.

The propulsive performance of a hydrodynamic shrouded propeller is determined, to a large extent, by the flow of fluid Q. The Q is usually determined by two parameters: external parameters and internal parameters. The external parameters usually include the length of the microrobot L, and the interval between the spiral propeller and non-rotating nozzle C [93]. In this paper, these external parameters are taken as fixed. The following internal parameters (e.g. Q_{cyc}, n, ω) should be considered in order to obtain a high propulsive force. Q_{cyc} means the flow of one cycle of the screw depends on the outer radius R_O and inner radius R_i, as shown in Figure. 3.4. n is the screw numbers which is equal to L/P, where P is the pitch of one screw. While the rotational speed is N, the propulsive force is defined by equations (3-7)

$$F_p = \rho \frac{(Q_{cyc}N)^2}{A_2} \tag{3-7}$$

If the angle of the angular speed of the microrobot is ω, we have:

$$F_p = \frac{\rho}{4} \frac{Q_{cyc}^2 \omega^2}{\pi^2 A_2} \tag{3-8}$$

According to the above discussion, we designed two types of screw grooves, a cylindrical screw groove and a rectangular screw groove, with different parameters Q_{cyc} to evaluate the performance of the microrobot. Here, we assumed the dimensions to be R_o=6.5mm for the outer radius, R_i=5.5mm for the inner radius, and L=30mm for the length respectively. If

the microrobot generated a propulsive force F_p=10mN, the cylindrical screw groove type with h=1mm and w=2mm needed a rotational speed of N=130rad/s, whereas, the rectangular screw groove type with h=1mm and w=2mm, needed a rotational speed of N=102rad/s. It meant that the rectangular screw groove type microrobot needs a lower rotational speed than the cylindrical screw groove type microrobot in order to generate the same propulsive force. In other words, the rectangular screw groove type microrobot generated a larger propulsive force than the cylindrical screw groove type microrobot at the same rotational speed. The simulation results with different parameters are shown in Figure 3.6. This model would also allow the prediction of swimming performance as the overall dimensions scale down.
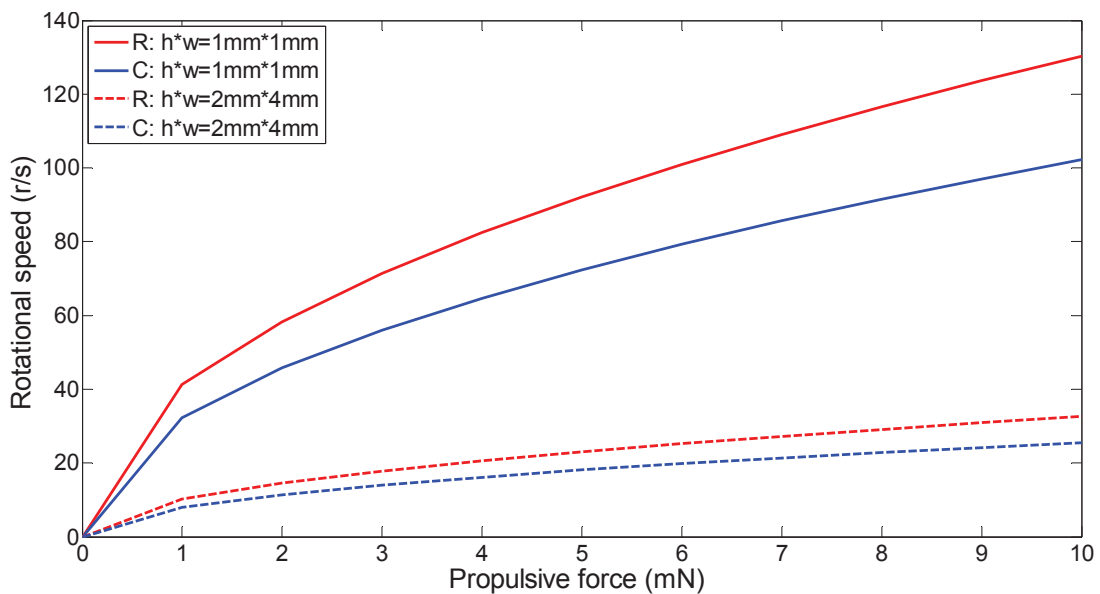
Figure 3.7 Simulation results with different parameters

R means rectangular screw groove, C means cylindrical screw groove

(a) Prototype of magnetic actuated microrobot with screw jet motion

(b) A bare propeller and a non-rotating nozzle

Figure 3.8 Prototype of the magnetic microrobot with screw jet motion.

3.2.3 Fabrication of the magnetic screw type microrobot

The magnetic actuated microrobot with a shrouded propeller was assembled to text its performance. The prototype of the electromagnetic actuated microrobot and the permanent magnet actuated microrobot are shown in Figure 3.8 (a). The bare spiral propeller and a non-rotating nozzle are made of polystyrene. Both the bare spiral propeller and the non-rotating nozzle are made of polystyrene. The diameter of the propeller is 12mm and the length is 30mm. The non-rotating nozzle is a hollow cylinder with a diameter of 14mm and a length of 27mm. To reduce the weight of the microrobot, we used an O-ring type magnet (Φ9.5mm*Φ5mm*4mm) instead of the four permanent magnets, as shown in Figure 3.8 (c).

3.2.4 Evaluation performance of the magnetic microrobot with screw jet motion

A measured system of rotational speed was set up to measure the rotational speed of the magnetic actuated microrobot [94, 95].The experiments were repeated over ten times. The rotational speed was measured, as shown in Figure 3.9. The rotational speed of the permanent magnet actuated microrobot was adjusted by changing the frequency of the external magnetic field until the maximum rotational speed was obtained.
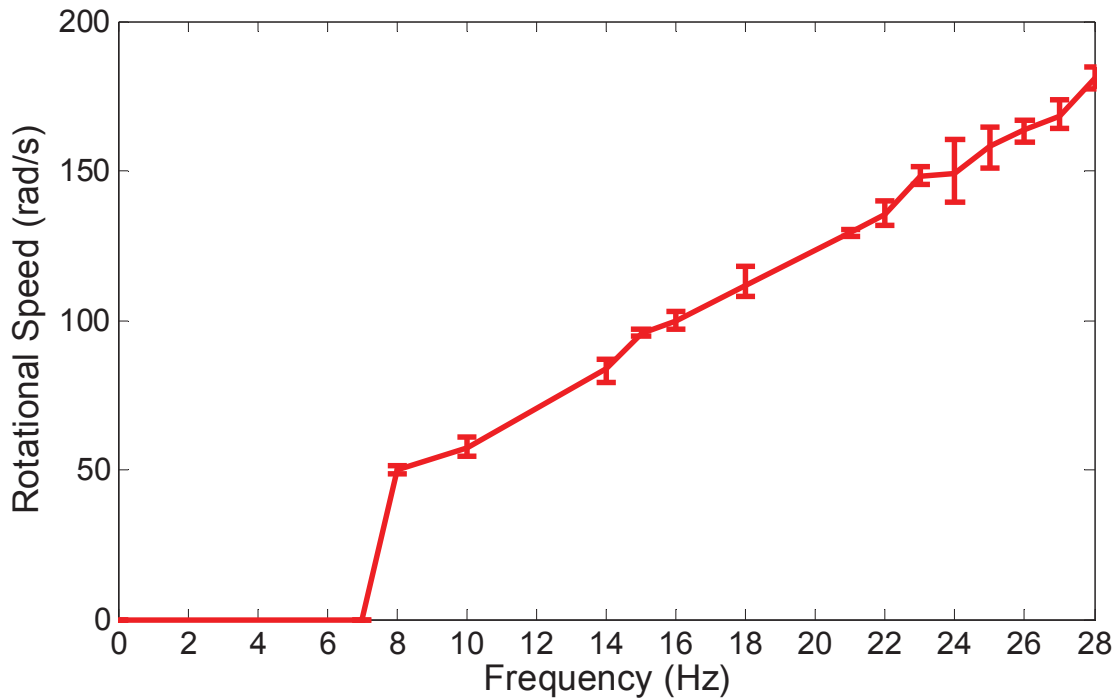
Figure 3.9 Measurement results of the rotational speed of the magnetic actuated microrobot.

3.3 Compared the propulsive force of the screw type microrobot with screw jet type microrobot

The measured experimental system was used to measure the propulsive force of the magnetic actuated microrobot in the water. Measured experiments of the propulsive force are divided to two steps. Firstly, a calibration test is necessary to confirm the deformation of the copper beam in order to maintain an effective deformation range and calculate the calibration of the relationship between the propulsive force and the bending displacement of the copper beam. Secondly, the rotational speed of the magnetic actuated microrobot is controlled by adjusting the frequency of the electric current. The displacement of the copper beam

was obtained using a laser displacement sensor (KEYENCE LB-1000), and the propulsive force of the magnetic actuated microrobot was calculated.

The measured result of the propulsive force is shown in Figure 3.10. The experimental results indicated that the propulsive force of the magnetic actuated microrobot with a non-rotating nozzle was larger than the magnetic actuated microrobot without a non-rotation nozzle with the same condition. Loss of some energy is converted into thermal energy due to external force, such as, the drag force of the water and viscous drag. The growth rates of the propulsive force are shown in Figure 3.11. From the experimental results, we know that the shrouded propeller mechanism has the capability to increase the performance of the propulsive force and is given by:

$$\eta = \frac{V_2 - V_1}{V_1} \times 100\% \tag{3-9}$$

where, η is growth rates of the propulsive force, V_1 is the speed of microrobot without a non-rotating nozzle and V_2 is the speed of microrobot with non-rotating nozzle.
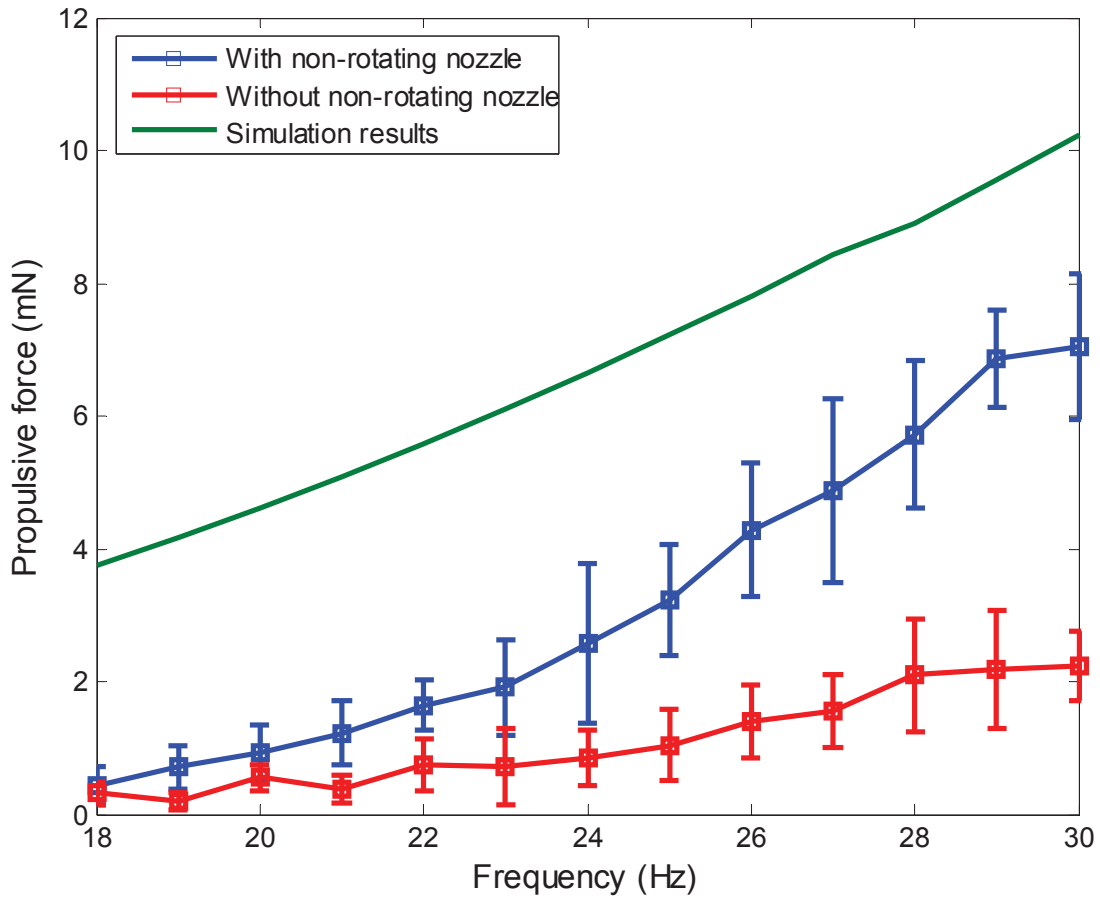
Figure 3.10 Measured results of the propulsive force
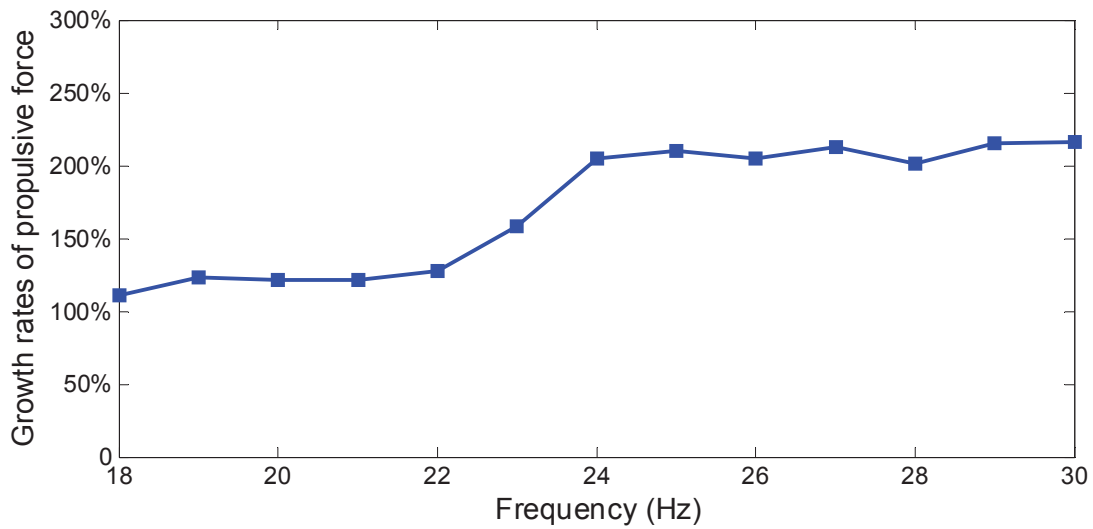
Figure 3.11 Growth rates of propulsive force

3.4 Summary

In general, a medical microrobot, which consists of a control module, power module, communicating module and a function module, is used to treat disease, diagnose intestinal problems and conduct minimal invasive surgery for clinical applications. Flexible locomotion is a key factor for the medical microrobot, which can represent the performance of microrobots. According to the controllability of the movement mechanism, medical microrobots can be split into two types: a passive locomotion type and an active locomotion type. The passive locomotion type medical microrobot has been applied in clinical diagnosis, such as M2A, PillCam®SB, and Norika3®. But their movement direction is only a single forward motion because their movement depends on intestinal peristalsis. Some active locomotion type microrobot can achieve a backward motion or a stop motion in the intestine, but their movement area is limited due to cables. Nevertheless, the screw type microrobot perhaps leads to less damage to the intestinal wall, thereby reducing the pain felt by patients. Based on the above performance comparisons, the shrouded propeller type microrobot is becoming the future development trend for medical microrobots by means of their comprehensive advantages, flexibilities and safety.

44

.

Chapter 4   A Magnetically Actuated Hybrid Microrobot

4.1 Concept of the magnetically actuated hybrid microrobot

The conceptual design of magnetic actuated hybrid microrobot (MAHM) with compact and efficient structure is illustrated in Figure 4.1. The Archimedes screw structure (screw propeller) is fixed inside the microrobot. An O-ring type permanent magnet is assembled at the front end of the tube. A bearing is assembled at the back end of the tube. Inner ring of bearing connects to the tube and outer ring of bearing is fastened inside the body. The fin is connected to the back end of the propeller with a bearing and a shaft.

The magnetic actuated hybrid microrobot that uses a hybrid locomotion scheme, consisting of two disparate magnetic actuation strategies: (1) conversion of synchronous rotation with a rotating magnetic field using a screw jet motion to pull fluid through the center of the robot; (2) using a flexible tail to generate fish-like propulsion due to an oscillating magnetic field. The MAHM can change switch between the two motions to realize movement in multiple various working environments. The spiral jet motion is used when the microrobot needs precision operation and stable movement. The fin motion is used when the high propulsive force is needed. The magnetic actuated hybrid microrobot has the most relevant features.

1) The magnetic actuated hybrid microrobot has just only one magnetic actuator, O-ring type magnet, to achieve its hybrid motion, screw jet motion and flexible fin motion.

2) Two motions can be controlled separately without any interference. It can obtain rapid responsive than the microrobot in.

3) The fin can improve the dynamic characteristic and reduce the shake which caused by the axial traction force at the spiral jet motion.

The prototype of the magnetic actuated hybrid microrobot is shown in Figure 4.2. The hybrid microrobot has been improved to realize the light structure, stable motion and high propulsive force. The screw propeller is fixed on the center axis of the body. The diameter is 5mm. An o-ring type neodymium magnet is used as an actuator to reduce the weight of the body. The specification of hybrid microrobot is given in Table I.

Table 4.1 Specification of hybrid microrobot

Magnetically actuated hybrid microrobot			
Length	Diameter	Weight	Material
52 mm	14 mm	3.56 g	Polystyrene
O-ring type magnet			
Outer diameter	Internal diameter	Height	Material
9.5 mm	5.1 mm	1.5 mm	Neodymium
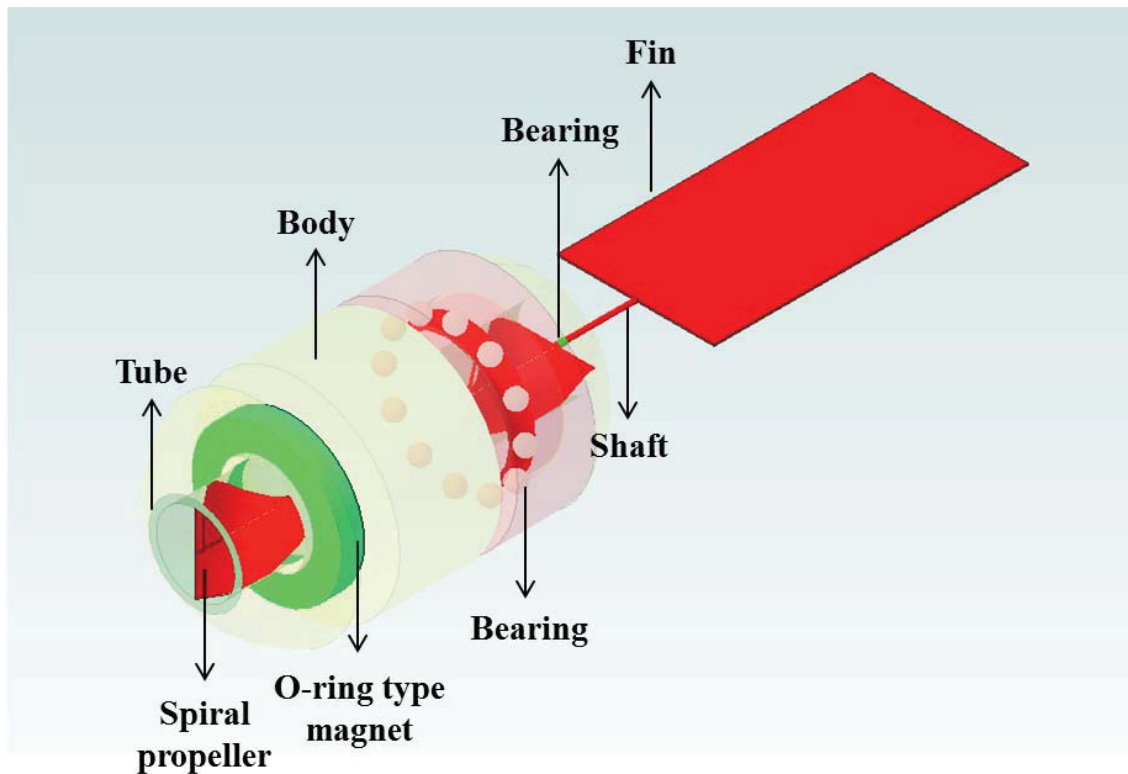
(a) Overall view of the robot
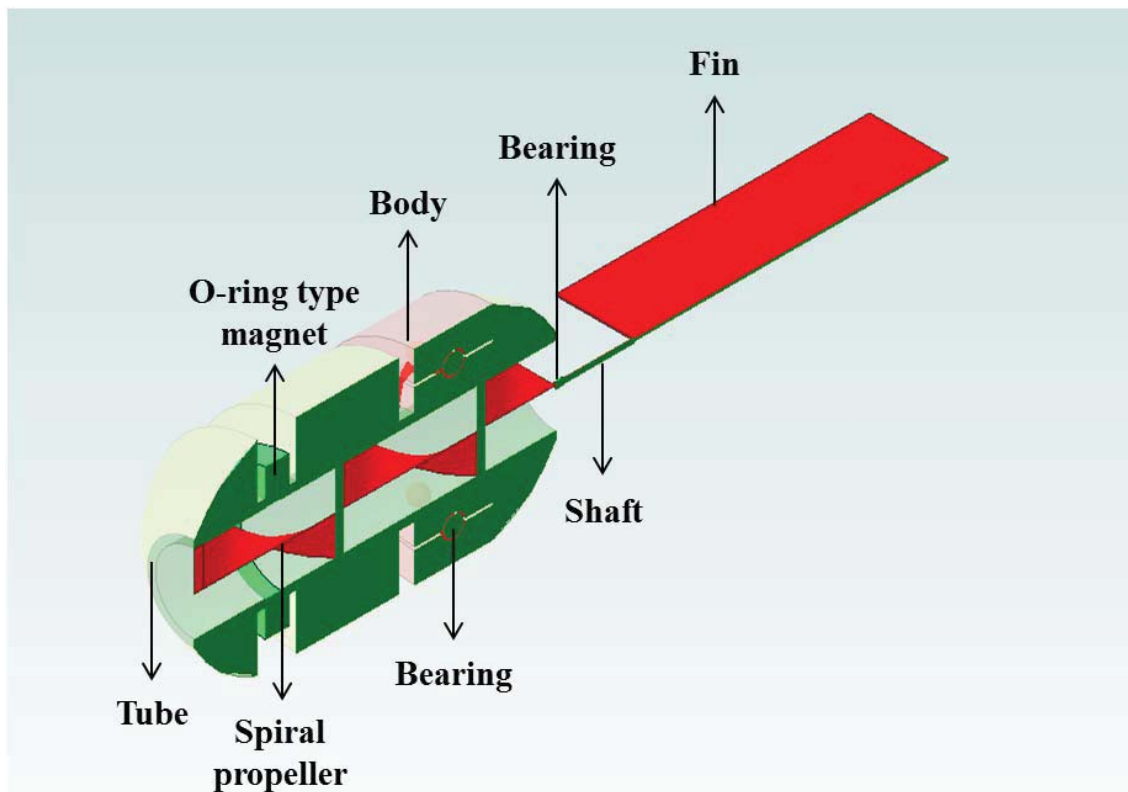
(b) Cross section

Figure 4.1 Conceptual design of magnetically actuated hybrid microrobot

Figure 4.2 Prototype of the magnetic actuated hybrid microrobot

4.2 Movement Mechanism

Based on the magnetic theory, rotation of the microrobot in an external magnetic field requires at least a pair of forces in opposite directions, and a torsional moment should be generated. The microrobot is rotated due to an embedded inner O-ring type magnetic with radial magnetization, and the axial propulsive force is generated by pushing the fluid backward to obtain the forward motion due to the reaction force. Figure 4.3 shows the principle of screw jet motion according to changes in rotational direction of the magnetic field. Figure 4.4 shows the principle of fin motion according to changing the alternate magnetic field.
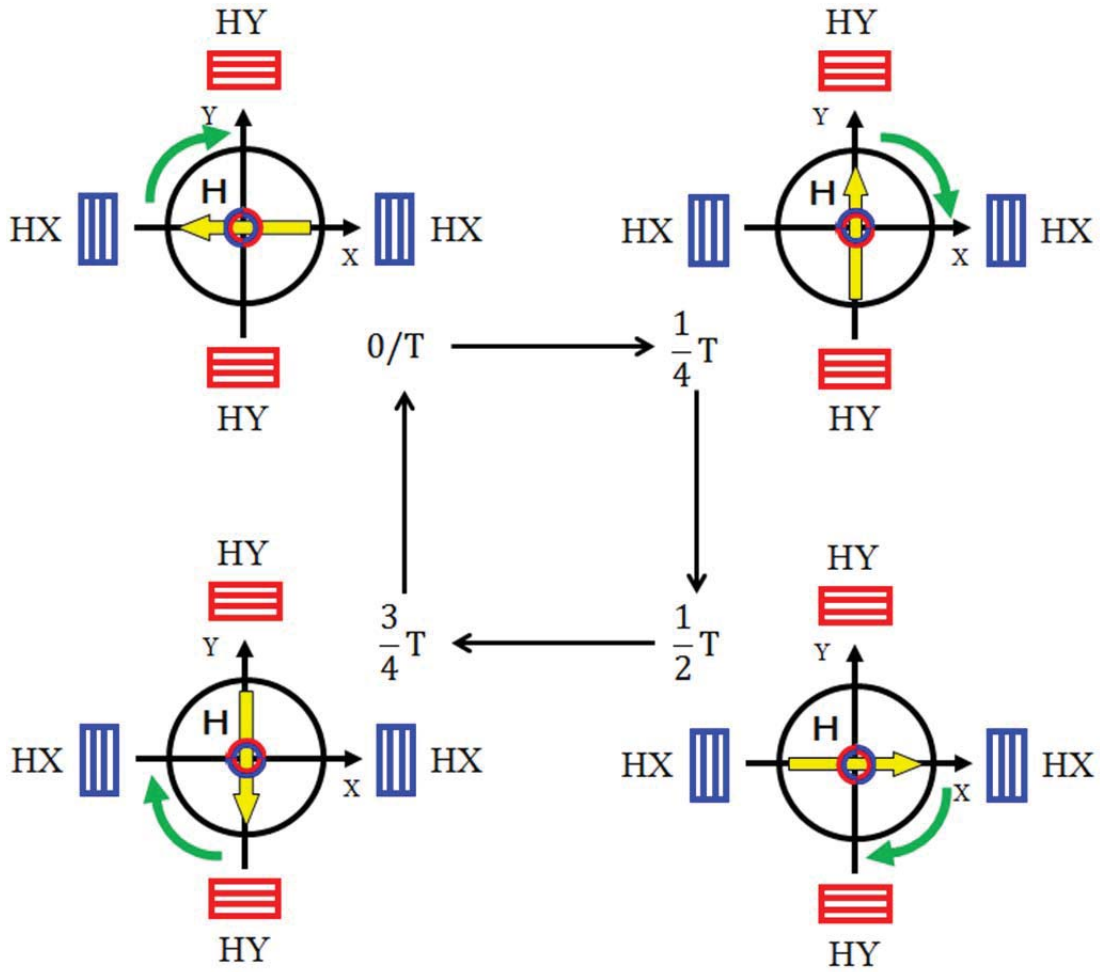
Figure 4.3 Movement mechanism of screw jet motion
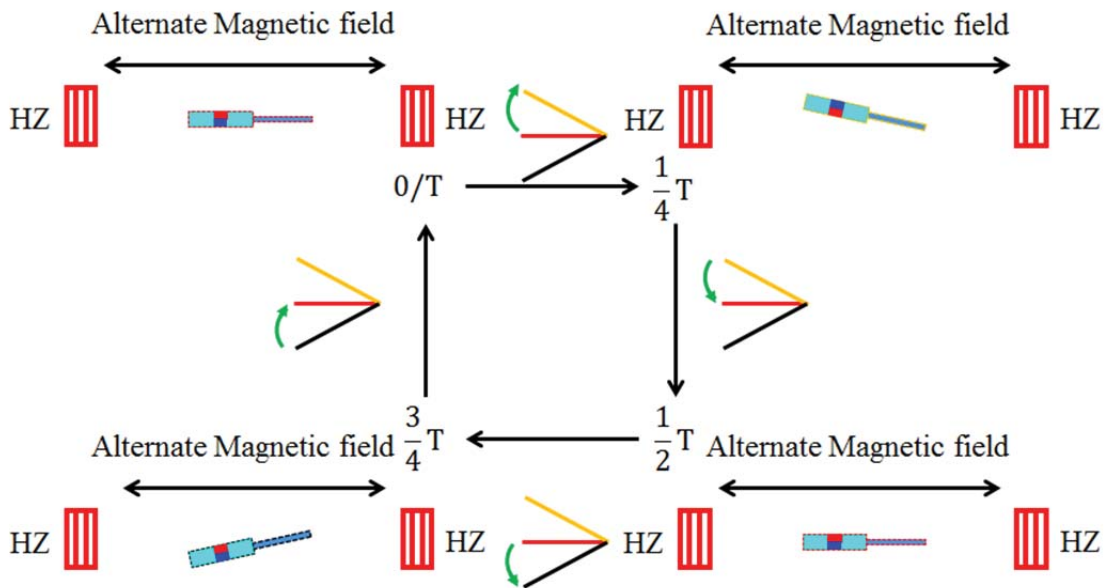
Figure 4.4 Movement mechanism of fin motion
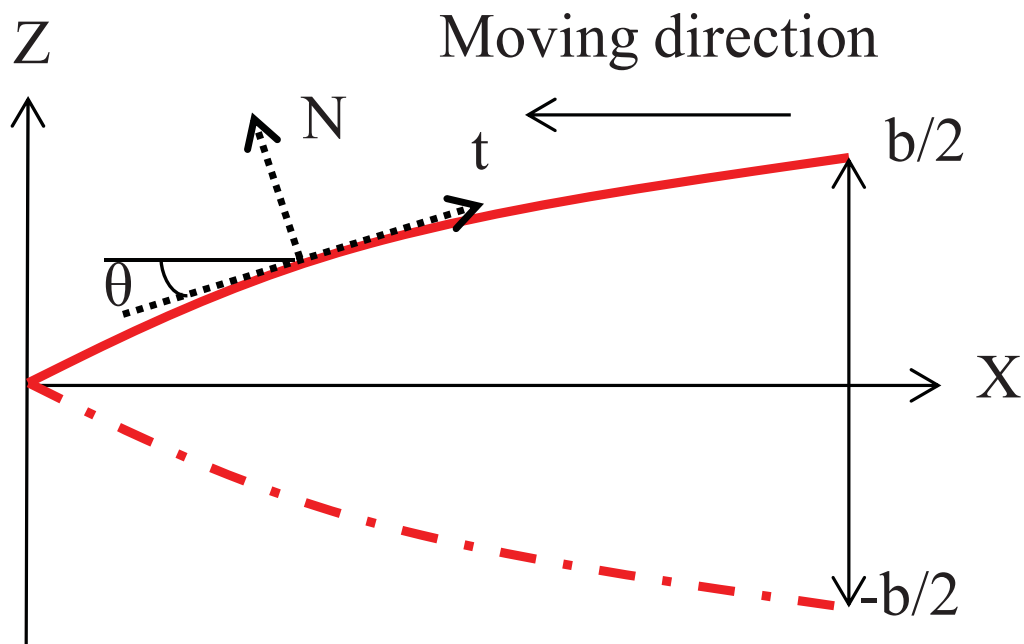
(a) X-Z plane
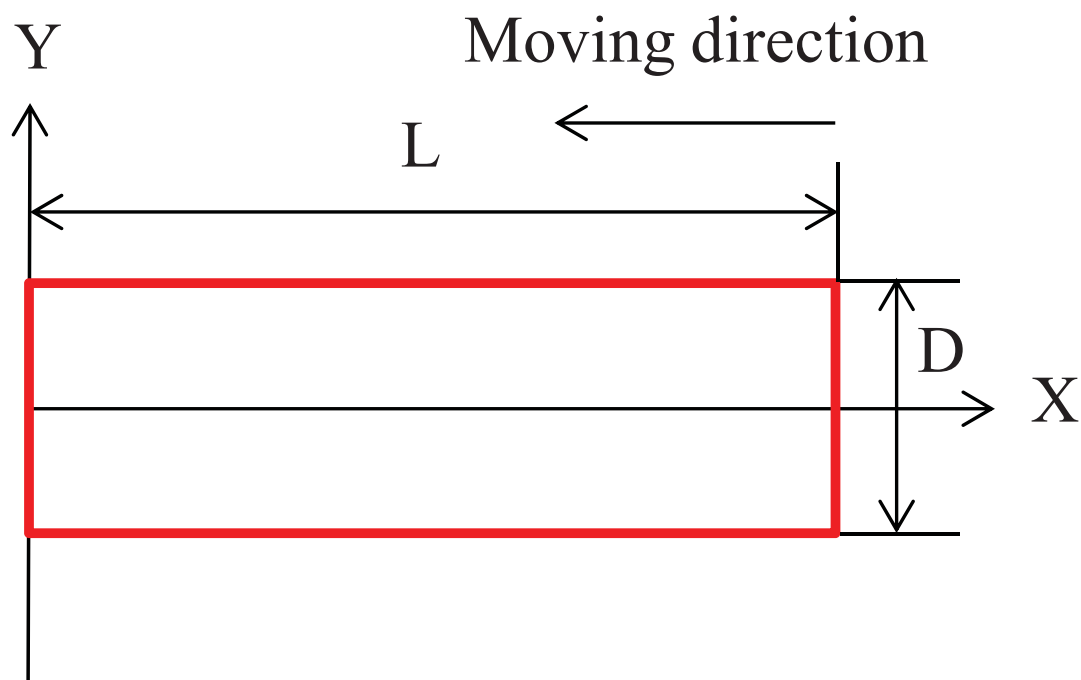
(b) X-Y plane

Figure 4.5 Model of tail with fin motion

4.3 Modeling

4.3.1 The model of fin motion

According to Vortex Peg Hypothesis, the fish uses tail or fin to propel itself forward by thrusting its body against the seemingly fixed vortices and utilizing their rotational energy [96-99]. The placement and direction of these vortices indicate that the wake structure generated by the fin takes the form of a series of parallel waves or a reverse Karman vortex street which is indicative of thrust generation. The velocity field induced by this wake structure expels a jet of water in the downstream direction, propelling the fin forward to conserve momentum. Then, thrust of fish-like robot generated by the added mass and vortices methods combine to yield the total propulsive force. In previous study, we have discussed that the undulatory motion of the tail which can obtain good performances is better than the oscillatory motion. Therefore, the undulatory motion is used to generate the thrust for the microrobot. A model of the tail with fin motion is shown in Figure 4.5. The total propulsive force (F_{fin}) of fin motion and total normal force (N) are indicated in (4-1) - (4.3).

$$F_{Fin} = \int_{\frac{-b}{2}}^{\frac{b}{2}} t \, dy = \int_{\frac{-b}{2}}^{\frac{b}{2}} (L\sin\alpha - D\cos\alpha) \, dy \qquad (4\text{-}1)$$

$$N = \int_{\frac{-b}{2}}^{\frac{b}{2}} n \, dy = \int_{\frac{-b}{2}}^{\frac{b}{2}} (L\cos\alpha + D\sin\alpha) \, dy \qquad (4\text{-}2)$$

The induced flow angle (α) is

$$\alpha = \tan^{-1}(\frac{V_x}{V_z}) \qquad (4\text{-}3)$$

where, t is propulsive force. n is normal force. V_x is velocity of the x direction and V_z is velocity of the z direction.

The power is calculated, as follows (4-4):

$$P = \int_{\frac{-b}{2}}^{\frac{b}{2}} \{[h_c \cos(2\pi f t)]'(L\cos\alpha + D\sin\alpha) - m[\theta_c \cos(2\pi f t + \varphi_\theta)]'\}dy \quad (4\text{-}4)$$

where, θ_c is the amplitude of feathering movement. h_c is the amplitude of heaving motion. ϕ_θ is phase difference of feathering movement. f is oscillating frequency.

The mechanical efficiency η is calculated by (4-5):

$$\eta = \frac{F_{Fin}V}{P} = \frac{C_T}{C_P} \quad (4\text{-}5)$$

where, C_T is propulsive coefficient and C_P is power coefficient.

4.3.2 The model of screw jet motion

The propulsive force model of the screw jet motion is shown in Figure 4.6. The microrobot is rotated due to an embedded inner O-ring type magnetic with radial magnetization, and the axial propulsive force is generated by pushing the fluid backward to obtain the forward motion due to the reaction force. According to the fluid mechanics, screw jet propulsive mechanism is analyzed. The velocity of the outflow is given by (4-6).

$$v = \frac{Q}{A_1} \quad (4\text{-}6)$$

Flow for the spiral jet motion is calculated by (4-7).

$$Q = a \cdot b \cdot \sqrt{p^2 + (2\pi r)^2} \cdot \Omega \quad (4\text{-}7)$$

The propulsive force of the spiral jet motion is obtained indicated in (4-8):

$$F_{screw} = \rho \cdot A_2 \cdot v_2^2 - \frac{1}{2} \cdot C_D \cdot \rho \cdot A \cdot v_2^2 \quad (4\text{-}8)$$

where, F_{screw} is the propulsive force of the microrobot. v_1 is velocity of the inflow. v_2 is velocity of the outflow. Q is the flow for the spiral jet motion. a is the height of the spiral ditch and b is the width of the spiral ditch. p is the pitch of the spiral, and r is the radius of the robot's width. Ω is the speed of revolution. A is the cross section of the body. A_1 is the cross section of the inflow. A_2 is the cross section of the outflow. The simulation results are shown in Figure 4.7.
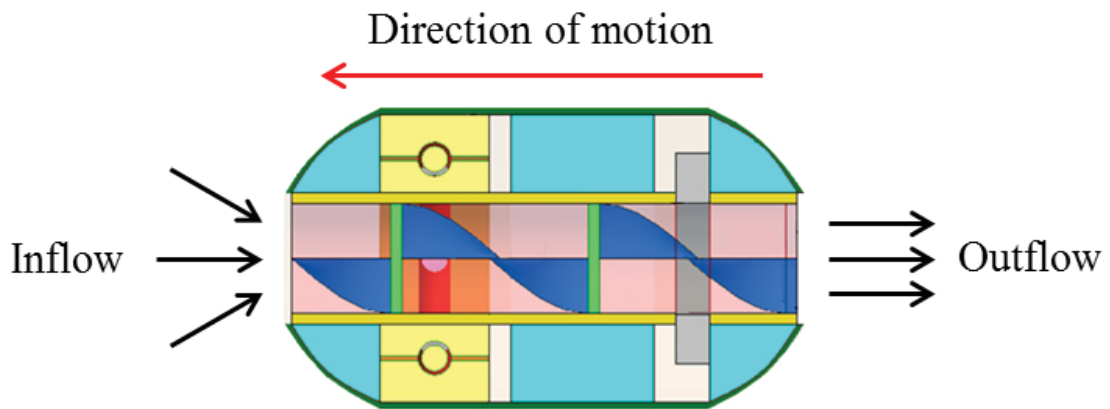
Figure 4.6 Model of body with screw jet motion
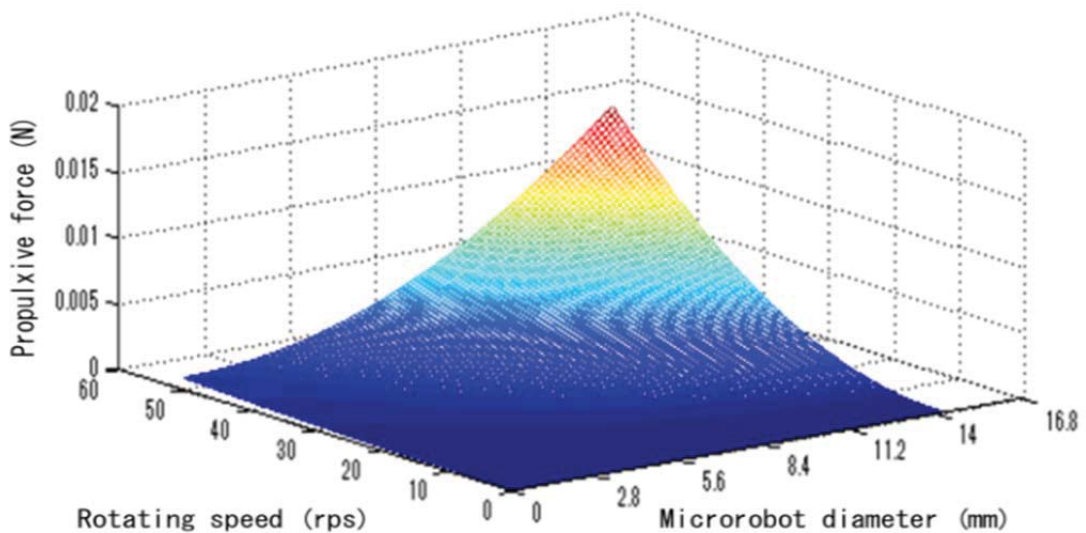
Figure 4.7 Simulation results of propulsive force

4.3.3 Dynamic model of the microrobot
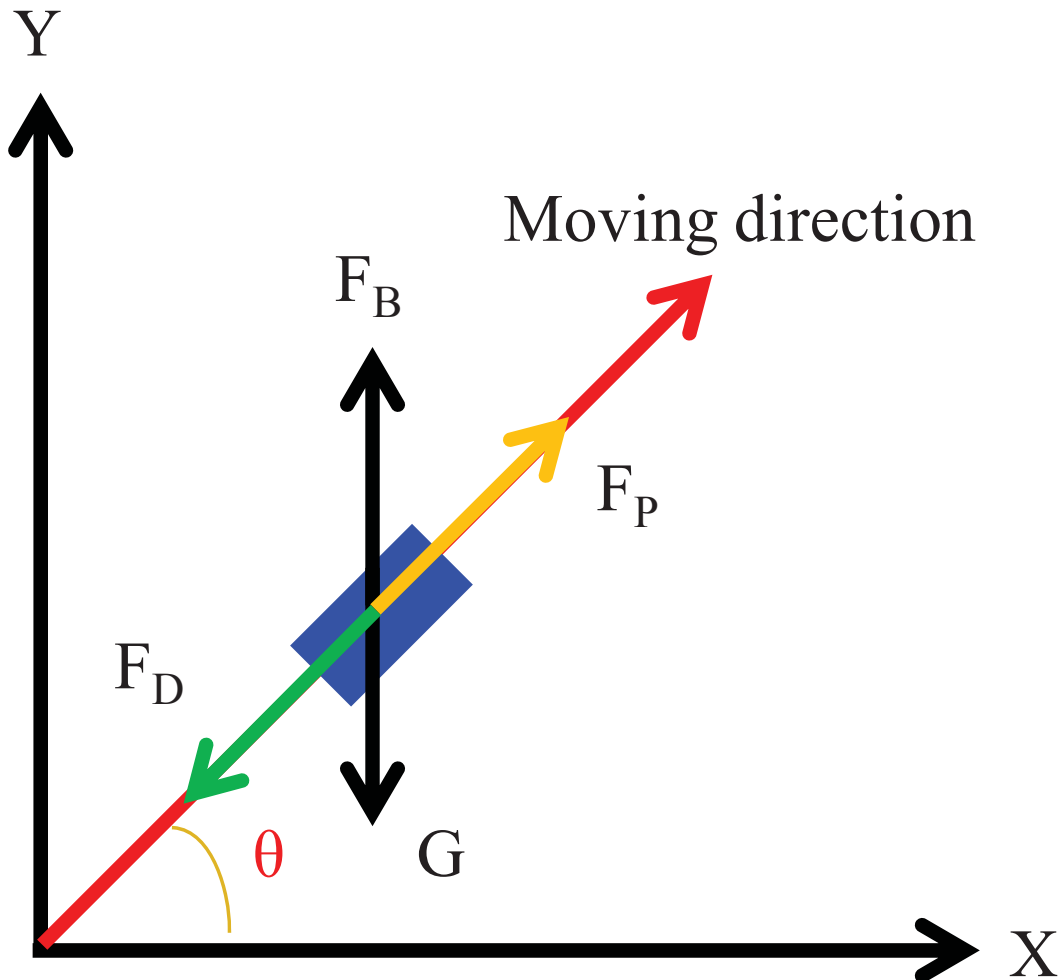
Figure 4.8 Dynamic model of the microrobot

Figure 4.8 shows the dynamic model which is used to analyze the screw jet motion of the microrobot in fluid. While the microrobot moves in the fluid, the distribution of force on the microrobot is simplified including propulsive force, hydraulic resistance, buoyancy and gravity force. According the Newton second law, the equation of the motion of the microrobot in indicated in equation (4-9):
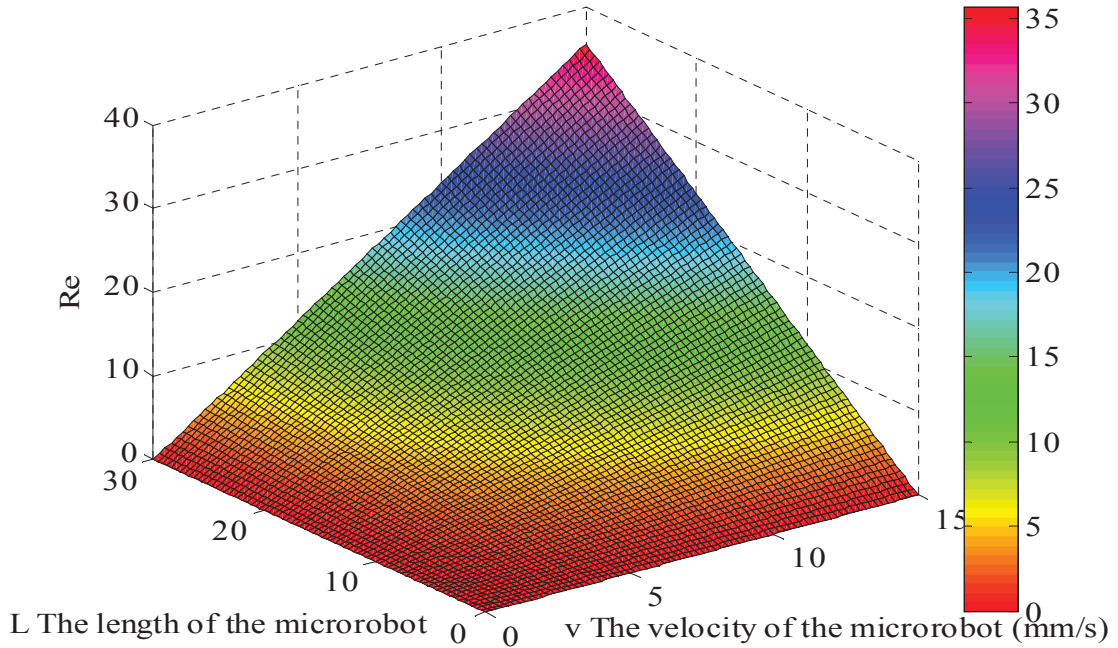
Figure 4.9 Re (water)

$$F_P - F_D \pm F_B \sin\theta \mp G\sin\theta + m\frac{dv}{dt} = 0 \tag{4-9}$$

where, F_B is buoyancy, resistance, G is gravity force, m is the mass of microrobot, v is moving speed of the microrobot.

The hydraulic resistance is calculated by equation (4-10)

$$F_D = C_D A \frac{\rho v^2}{2} \tag{4-10}$$

where, F_P is the propulsive force, F_D is hydraulic resistance.

In order to calculate the resistance of the robot, the equation (3-13) is used to calculate the Reynolds number (Re). Here, the velocity is v(m/s), the length is L(m), the coefficient of kinematic viscosity is u(m²/s). The Figure 4.9 and the Figure 4.10 show the Re in water and oil.

$$Re = \frac{\rho v L}{u} \tag{4-11}$$
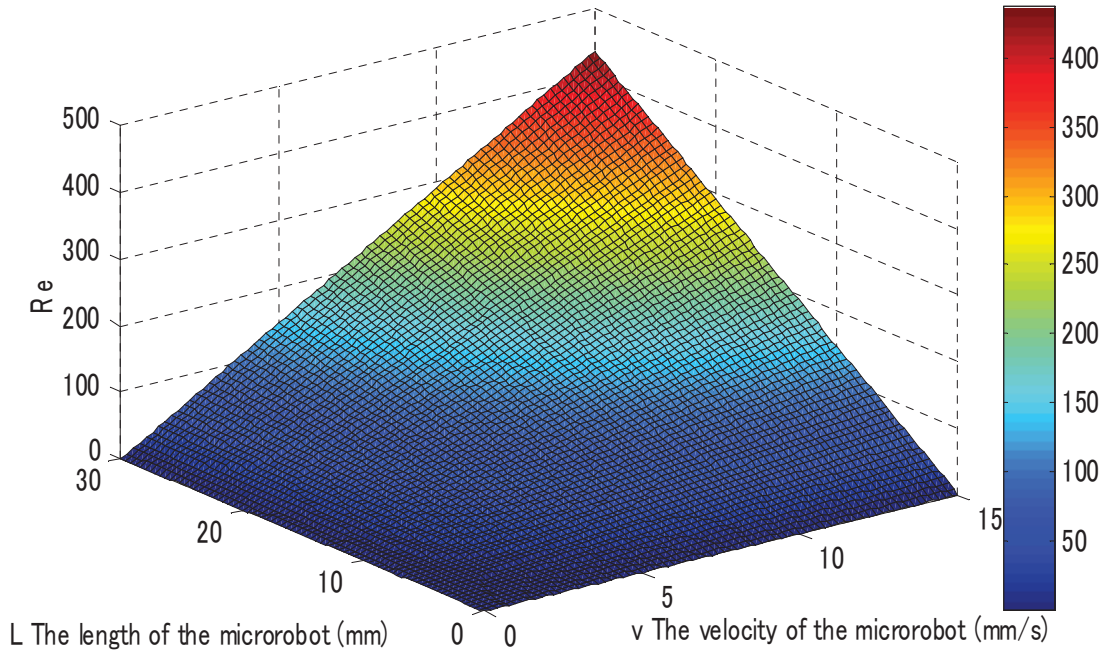
Figure 4.10 Re (oil)

4.4 Experiments and results

4.4.1 Evaluation performance of the fin motion

The resonance frequency of the fin motion is confirmed by equations (4-12) (4-13) and (4-14). Assuming the beam deflection for the transverse vibration, the transverse vibration of fin is calculated by equation (4-12). The conditional expression by using fixed end is shown in equation (4-13).

$$EI\frac{\partial^4 y}{\partial x^4}+\rho A\frac{\partial^2 y}{\partial t^2}=0 \tag{4-12}$$

$$1+\cos\beta\cdot\cosh\beta=0 \tag{4-13}$$

The resonance frequency (f) of the fin can be calculated as follows (4-14):

$$f=\frac{\beta}{2\pi}\frac{1}{L^2}\sqrt{\frac{EI}{\rho A}} \tag{4-14}$$

56
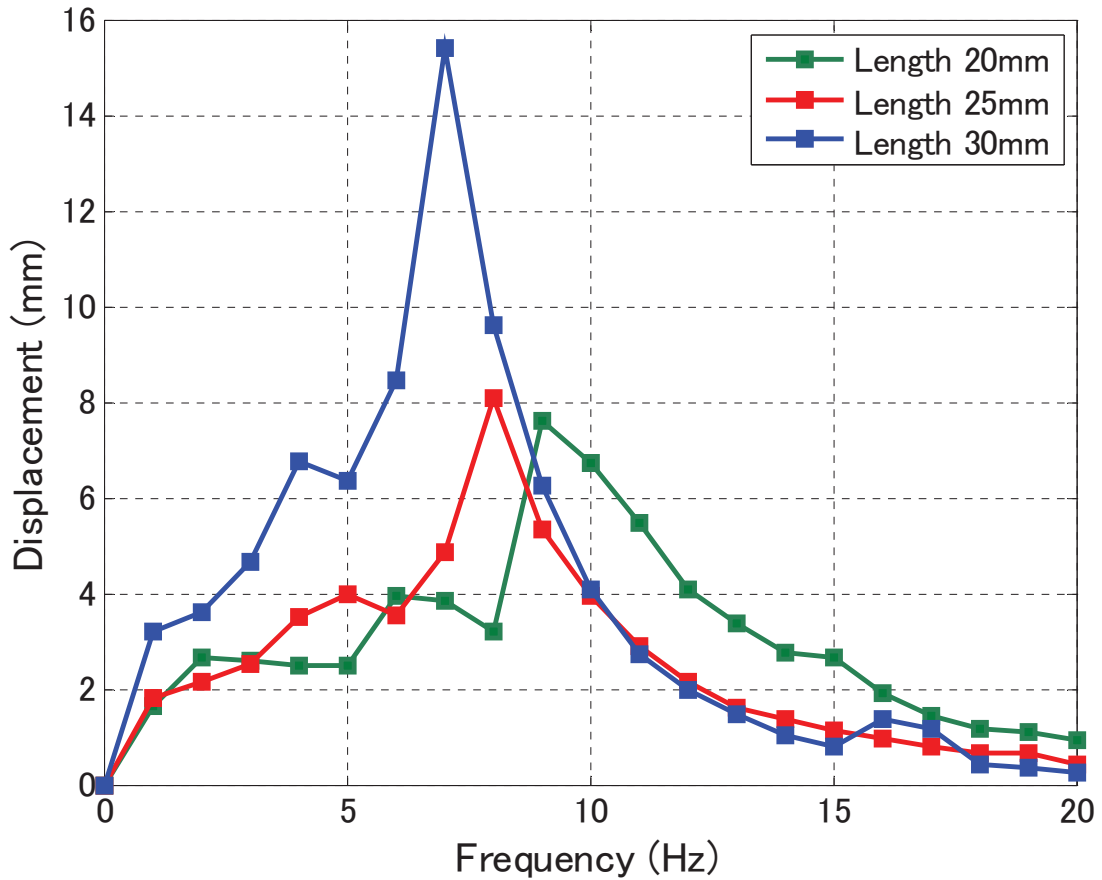
Figure 4.11 Relationship between frequency and displacement of fin with different length

The relationship between resonance frequency and displacement of fin is measured with measurement system. Figure 4.11 shows the experimental results that the maximum displacement of the fin with the same width and the different length is measured. The resonance frequency is from 0 Hz to 20 Hz. And maximum displacement was obtained at 7 Hz.
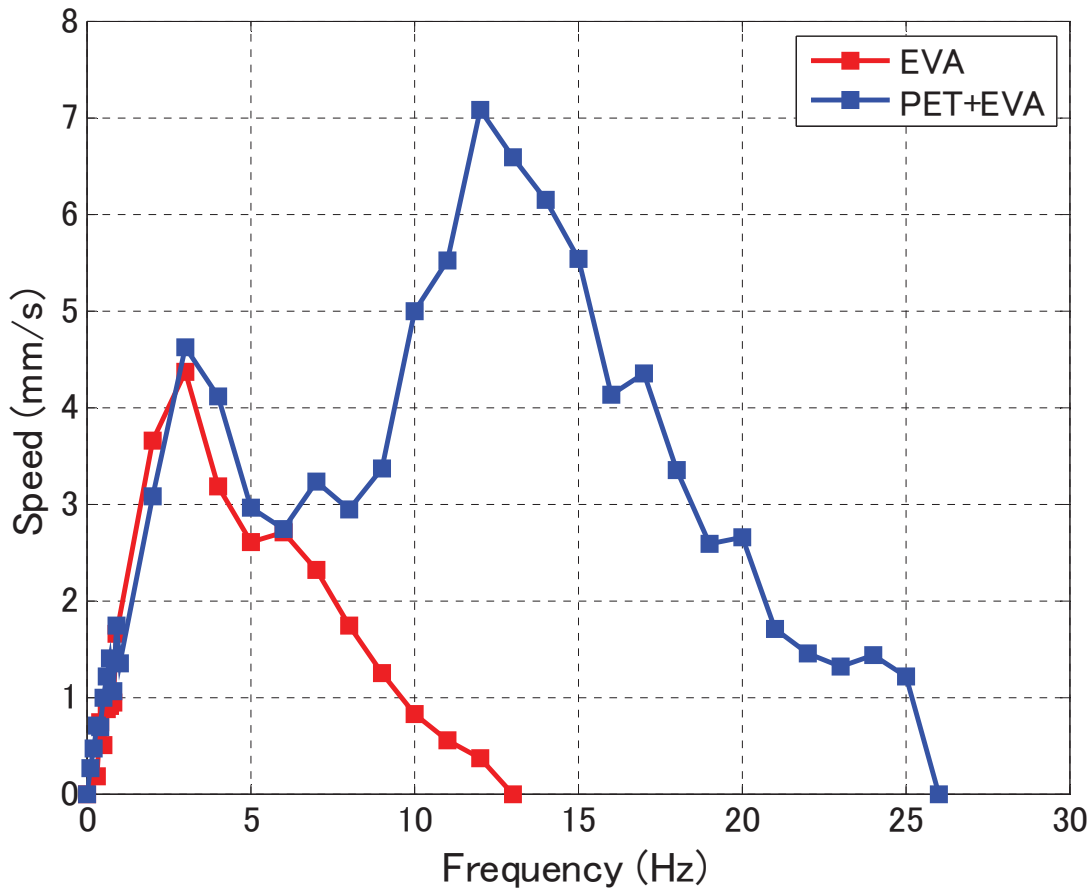
Figure 4.12 Relationship between frequency and moving speed with

different materials

Figure 4.12 shows the experimental results that the performance of the fin motion with different materials. One is the fin which is made of polyethylene terephthalate (PET). The other is the fin which is made of ethylene-vinyl acetate (EVA) and PET. The size is constant which is 20mm*10mm*0.1mm. It indicated the fin which is composed by PET and EVA obtained higher moving speed and wider frequency than the fin which is made by PET. Because the former is softer than the latter, the former one can realize the higher moving speed with the undulatory motion better. Therefore, the former is utilized for the microrobot in our research.
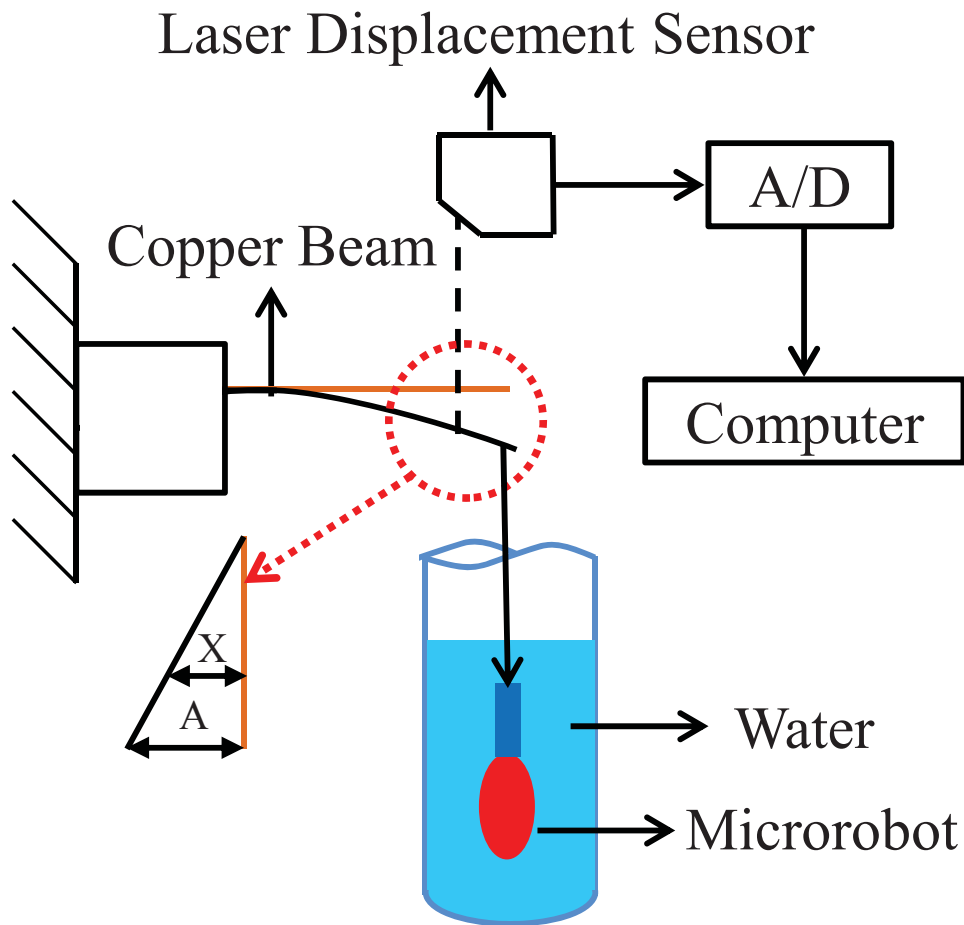
Figure 4.13 Measurement system of the propulsive force

4.4.2 Evaluation performance of the screw jet motion

The propulsive forces for various frequencies were measured using a measurement setup which mainly consists of a laser displacement sensor and a copper beam and electric balance, as shown in Figure 4.13. The copper beam was soft enough to bend under the propulsive force and the propulsive force is evaluated by the electric balance. The displacement of copper beam and propulsive force are able to be considered as right triangle. According to the measurement of displacement (x) and the force (F), a calibration calculation of relationship between the propulsive force the bending displacement of the copper beam is obtained.
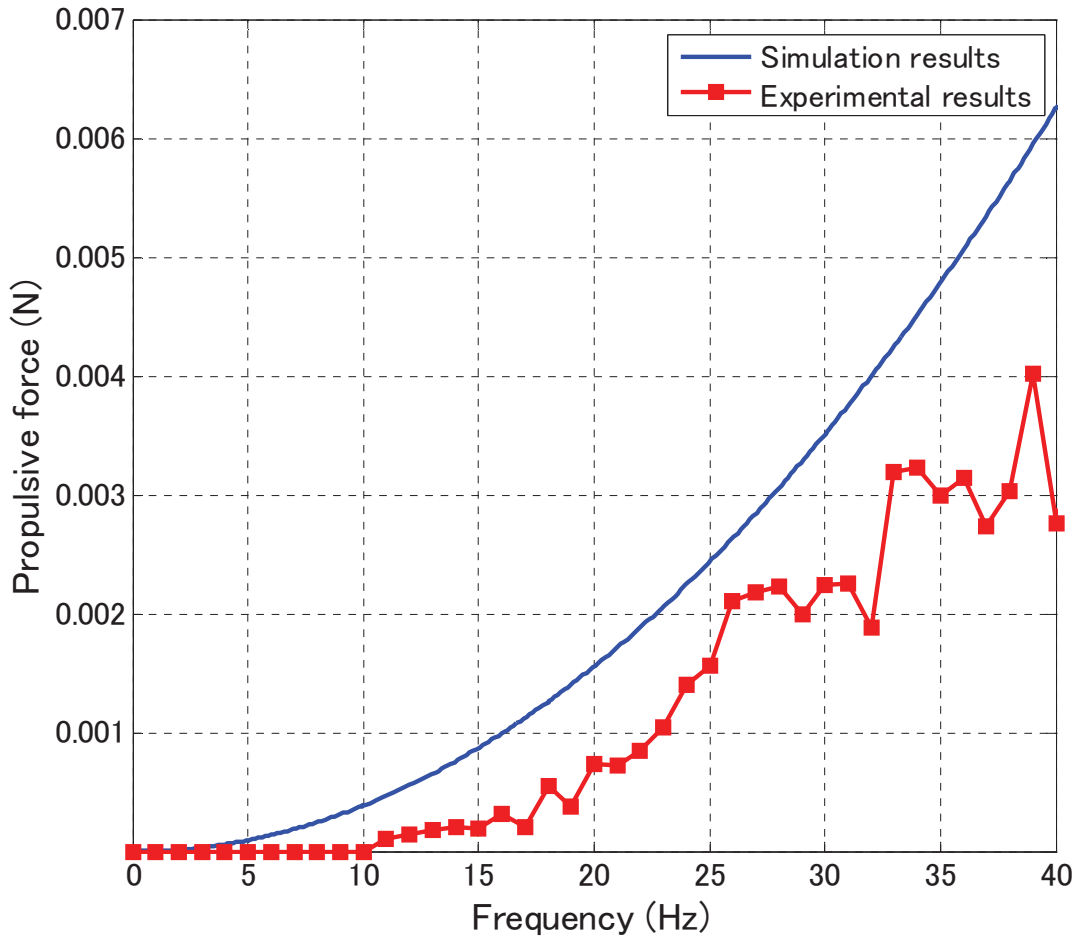
Figure 4.14 Measurement results of the propulsive force

During the testing experiment of the propulsive force, the microrobot was placed in the pipe which was filled the water. And then, by adjusting the frequency of input electric currents to control the rotating speed of the body, the displacement of the copper beam was obtained by the laser sensor. At last, the calibration calculation equation is used to calculate the propulsive force. Measurement results of mean propulsive force are shown in Figure 4.14. In experiment condition, the experimental results are smaller than the simulation results due to drag force of the water. This tendency is similar to the simulation results.

4.6 Summary

In this chapter, a novel type of magnetically actuated hybrid microrobot (MAHM) based on a rotational magnetic field is proposed. The hybrid microrobot with screw jet motion and fin motion has a small scale with a wireless power supply, can be propelled by low voltage, and has a quick response. And also the hybrid microrobot can work for a long time in human. It can convert its two motions (screw jet motion and fin motion) through the proposed structure of the microrobot with rotational magnetic field, so that it realizes the movement in the different environment. The body of the microrobot with a screw jet motion can obtain a stable motion and high propulsive force. The fin motion can improve the dynamic characteristic and reduce the shake which caused by the axial propulsive force of the screw jet motion. Screw jet motion and fin motion can be controlled separated without any interference, due to the hybrid microrobot has only use one actuator to realize the screw jet motion and fin motion.

Chapter 5　　Algorithm Design of Magnetic Actuated Microrobotic Systems

5.1 Algorithm design of microrobotic systems

When the rotational direction of the magnetic field is clockwise (CW), the microrobot moves forwardly motion. When the rotational direction of the magnetic field is counter-clockwise (CCW), the microrobot can realize moves backwardly motion, as shown in Figure 5.1. When an alternate magnetic field parallel to the direction of advance is applied, movement due to an impelling force arising from a permanent magnet rotates and vibrates the connected fin, as shown in Figure 5.2. When the plane of the rotational magnetic field is CCW, the microrobot can turn left at a branch point. When the plane of the rotational magnetic field is CW, the microrobot can turn right at a branch point, as shown in Figure 5.3. Therefore, the velocity of the hybrid microrobot can be controlled by adjusting the rotational magnetic field changing frequency. And adjusting the direction of the magnetic field in the any plane, the microrobot can realize the forward motion and backward motion in the perpendicular to the rotational magnetic field.
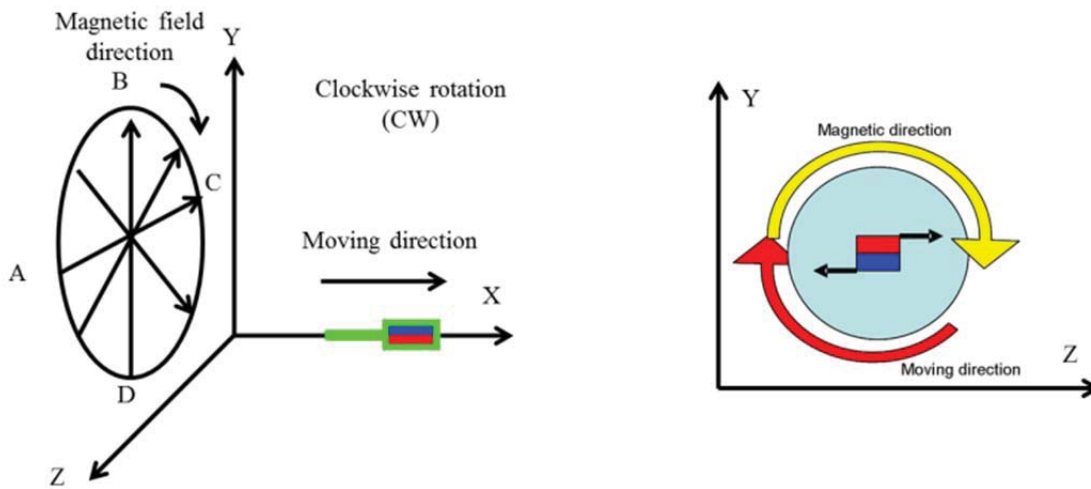
Figure 5.1 Hybrid microrobot with screw jet motion
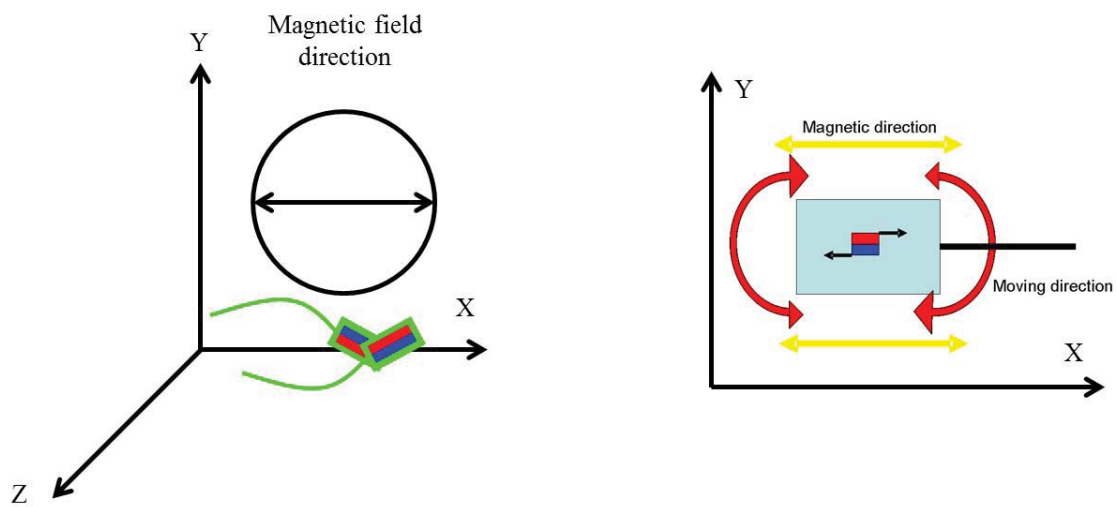
Figure 5.2 Hybrid microrobot with fin motion
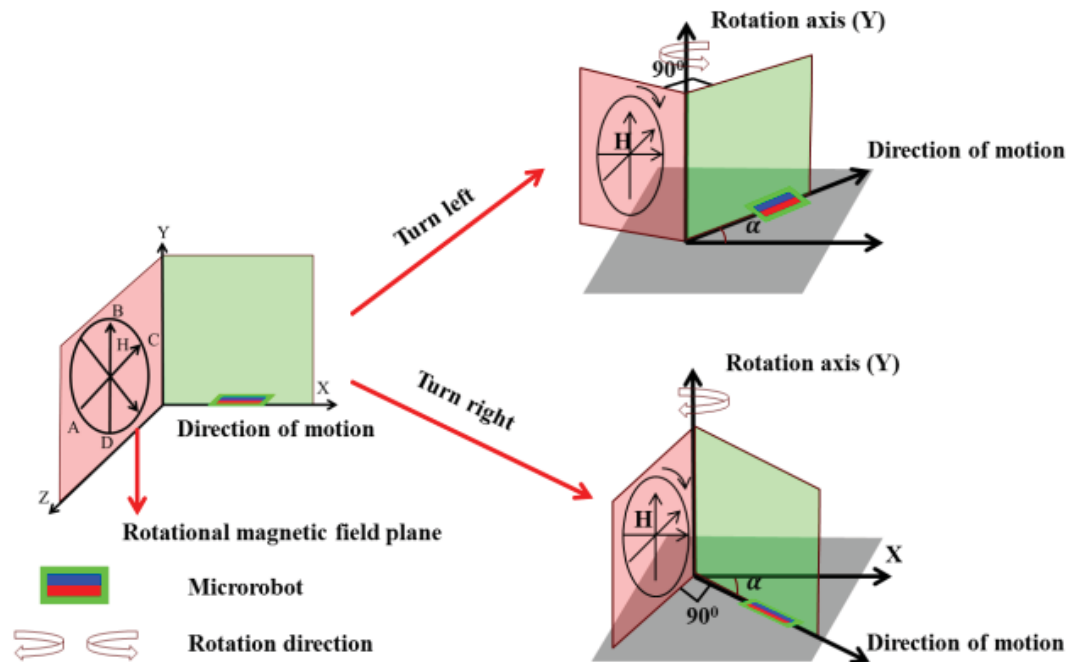
Figure 5.3 Rotational movement

5.2 Magnetic modeling

The magnetic fields are produced by currents and calculated from Ampere's Law or the Biot-Savart Law and characterized by magnetic flux density B measured in Tesla. But when the generated fields pass through magnetic materials which themselves contribute internal magnetic fields, ambiguities can arise about what part of the field comes from the external currents and what comes from the material itself. It has been common practice to define another magnetic field quantity, usually called the "magnetic field strength" designated by H. It can be defined by equation (5-1):

$$H = \frac{B}{\mu_0} - M \qquad (5\text{-}1)$$

They have the value of unambiguously designating the driving magnetic influence from external currents in a material, independent of the

material's magnetic response. The relationship for B can be written in the equivalent form (5-2):

$$B = \mu_0(H + M) \tag{5-2}$$

H and M will have the same units, amperes/meter. To further distinguish B from H, B is sometimes called the magnetic flux density or the magnetic induction. The quantity M in these relationships is called the magnetization of the material. Another commonly used form for the relationship between B and H are shown equations (5-3) and (5-4):

$$B = \mu_m H \tag{5-3}$$

$$\mu = \mu_m = K_m \mu_0 \tag{5-4}$$

where, μ_0 is permeability of vacuum and K_m the relative permeability of the material. If the material does not respond to the external magnetic field by producing any magnetization, then $K_m = 1$. Another commonly used magnetic quantity is the magnetic susceptibility which specifies how much the relative permeability differs from one.

The magnetic field applies a magnetic torque for the microrobot to produce the propulsive force [100-101]. The magnetic force F_M and magnetic torque T_M acting on the O-ring magnet in the external magnetic field of the 3 axes Helmholtz coils is given by the equations (5-5) and (5-6):

$$F_M = \mu_0 V (M \bullet \nabla) H \times \sin \alpha \tag{5-5}$$

$$T_M = \mu_0 V M \times H \times \sin \alpha \tag{5-6}$$

where, M is the average magnetization of the internal magnet and V is the volume of the internal magnet. H is magnetic field intensity. α is the angle of between M and H.

The direction of the magnetic is always aligned along the axial directions. It can also happen that the anisotropy direction itself is not aligned with the correct axis of the magnet. Based on the magnetic theory, the 3 axes Helmholtz coils are used to generate the orthogonally rotating magnetic field. The Figure 5.4(a) shows that the orthogonally rotating magnetic is generated in the Y-Z plane when the current is flowing in the Helmholtz coil pairs. The Helmholtz coil Y generates the magnetic field in the Y axes and the Helmholtz coil Z generates the magnetic field in the Z axes. Figure 5.4(b) shows the current of the Helmholtz coil pairs, the directions of current with a 90° phase difference. Through changing the frequency of input current, the rotational speed of the magnet in the microrobot is changed. The magnet is fixed on the microrobot. So the microrobot is driven by the 3 axes Helmholtz coils. The forward and backward motion can be realized by changing the direction of current. By changing the value of the current, the direction of the wireless capsule microrobot can be turned in the three dimensional space.
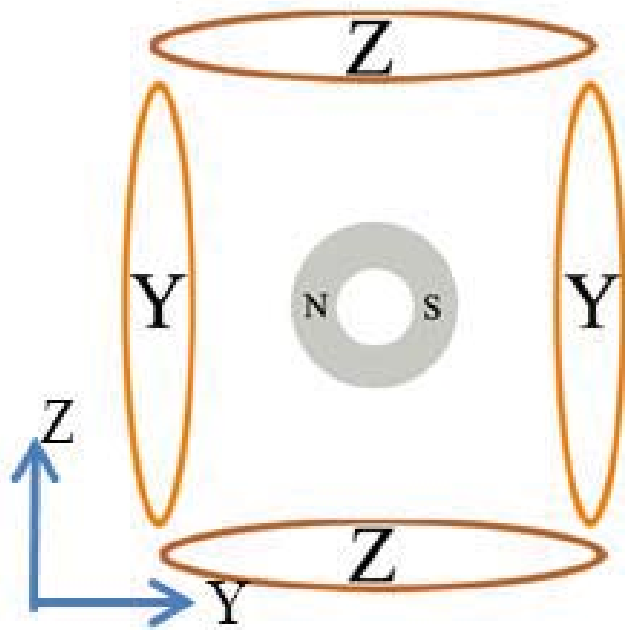
(a) Y-Z Helmholtz coil
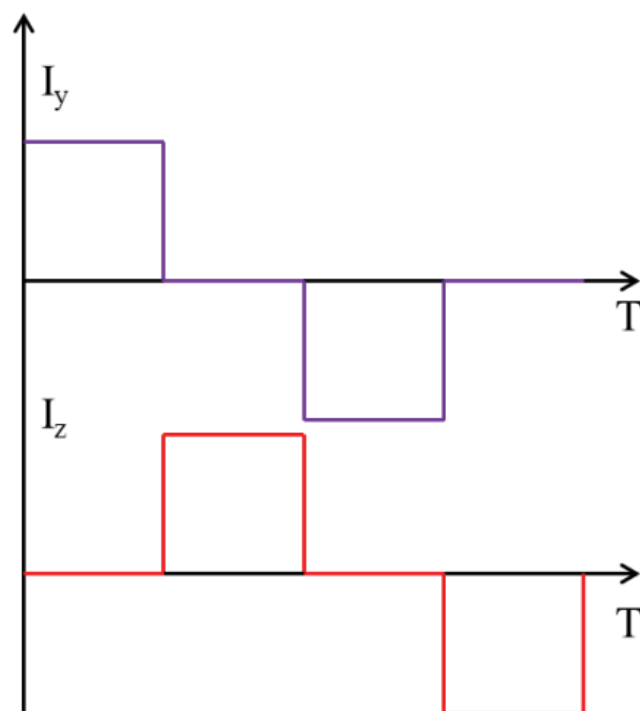
(b) The current of the coil

Figure 5.4 Principle of the orthogonally rotating magnetic
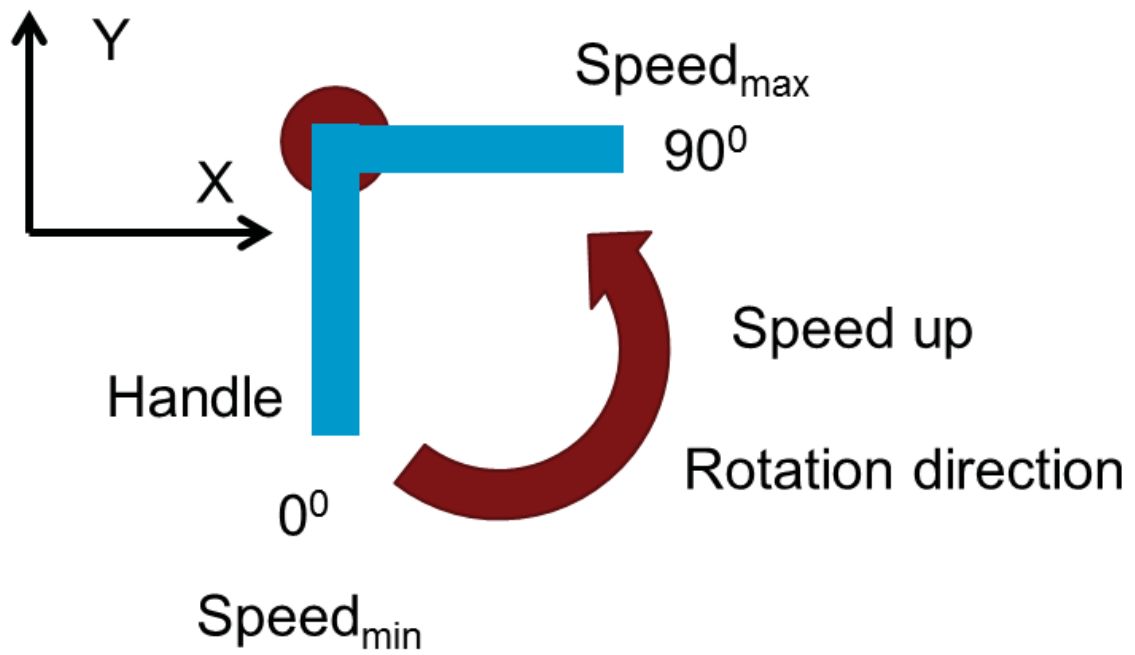
(a) Speed up
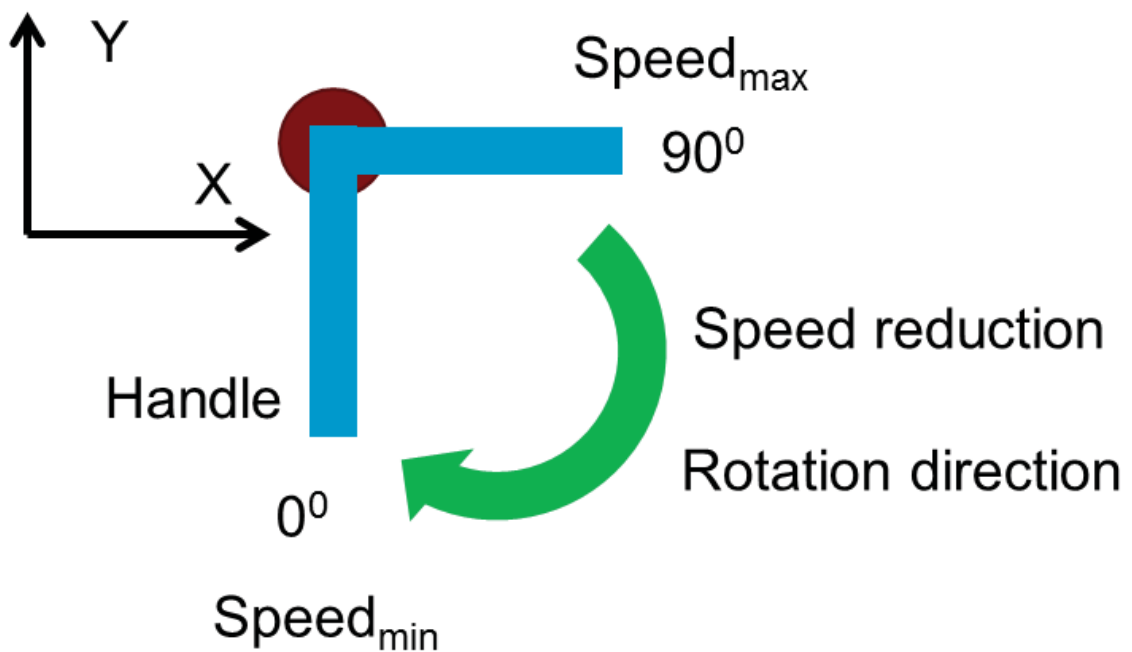
(b) Speed reduction

Figure 5.5 Principle of speed control with Phantom Omni

5.3 Principle of speed control with Phantom Omni

Figure 5.5 shows the principle of speed control of the wireless microrobot according to changes in rotating direction of handle of the Phantom Omni. An angle of Y axis is 0 degree, the wireless microrobot can obtain a $speed_{min}$ and an angle of y axis is 90 degree, the wireless microrobot can obtain a $speed_{max}$. When the rotational direction of the handle is counter-clockwise (CCW), the wireless microrobot can realize speed up, as shown Figure 5.5(a). When the rotational direction of the handle is clockwise (CW), the wireless microrobot can realize speed reduction, as shown Figure 5.5(b). By adjusting the rotational direction of the handle, the wireless microrobot can realize speed up and speed reduction.

As the equipment of the experiment, the wireless microrobot moved a transparent pipe which is 26mm inner diameter, 3mm thickness filled with water. The operator controls the handle of the Phantom Omni to rotate. And the Helmholtz coils can produce a frequency of the magnetic flux density to control the wireless microrobot in the pipe. The oscilloscope shows the magnetic flux density changing frequency. The rotational angle is from 0^0 to 90^0, which can be generated the frequency from 0Hz to 17Hz. The relationships are shown in Figure 5.6 and Figure 5.7. The equation (5-7) shows the relationship between the frequency of the magnetic flux density and the rotational angle degree of the handle.

$$f = \frac{17}{90} \times C \qquad (5\text{-}7)$$

where, f is the frequency of the magnetic flux density. C is the rotational angle of the handle.
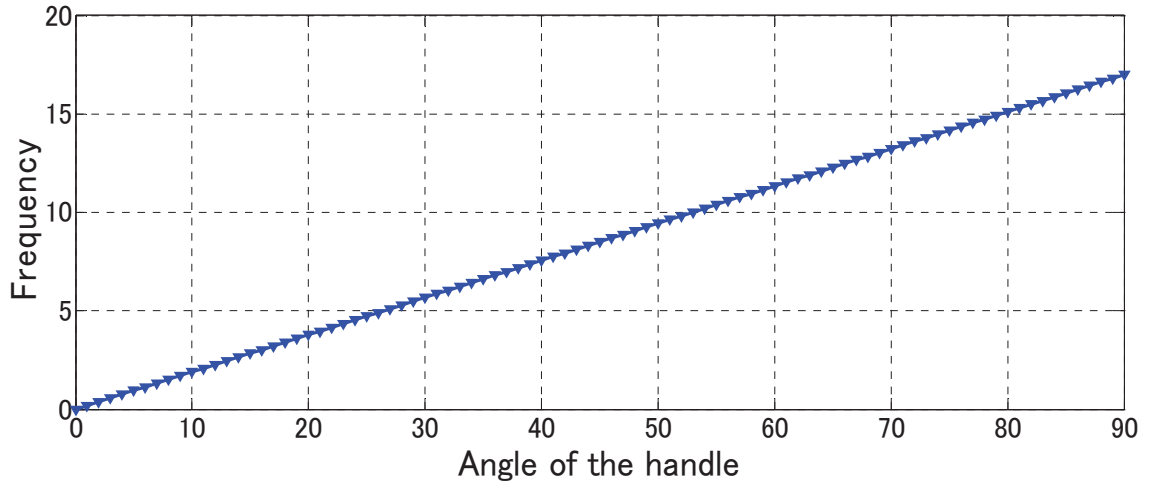
Figure 5.6 Relationship between angle of the handle and frequency
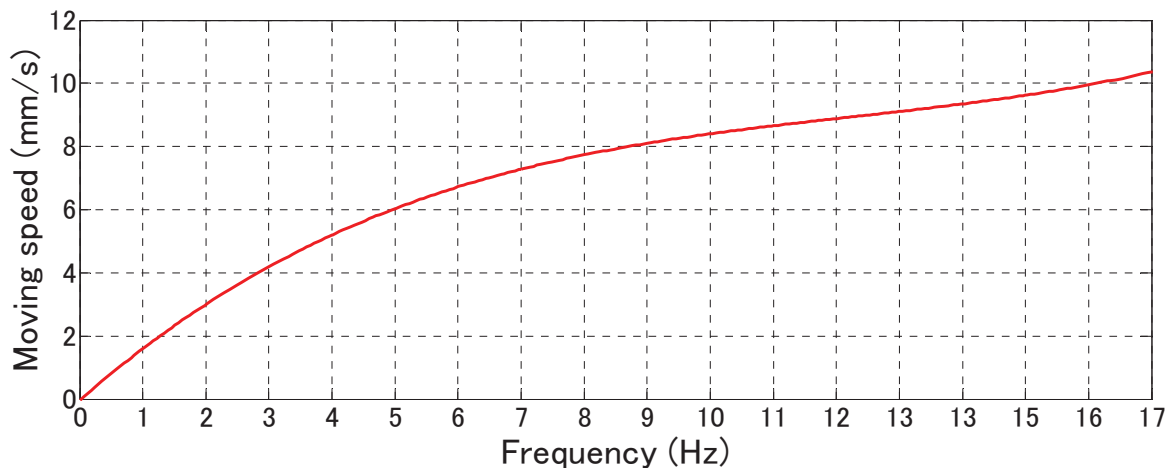
Figure 5.7 Relationship between frequency and the theoretical value of speed

Figure 5.8 shows the algorithm design of the microrobotic system. 3 axes Helmholtz coils generate a uniform magnetic field to provide the magnetic force and magnetic torque for the hybrid microrobot. The 3 axes Helmholtz coils is very simple control, because each axial coil generates the magnetic field in only one direction. Therefore, the 3 axes Helmholtz

71

coils can generate a magnetic field vector in any direction. The hybrid microrobot rotated by the uniform magnetic fields at the center of the workspace. According to the Biot-Savart law, the 3-D magnetic field vector for circular current is combined and defined by the (5-8):

$$
\begin{cases}
B_x(t) = a_x \dfrac{r_x}{n_x} I_x \cos(\omega t) \cos \alpha \\[2mm]
B_y(t) = a_y \dfrac{r_y}{n_y} I_y \cos(\omega t) \cos \beta \\[2mm]
B_z(t) = a_z \dfrac{r_z}{n_z} I_z \cos(\omega t) \cos \gamma
\end{cases}
\qquad (5\text{-}8)
$$

where, $B_x(t)$, $B_y(t)$ and $B_z(t)$ denote the magnetic flux density of x-axis, y-axis and z-axis. α, β and γ denote an angle between the magnetic flux density and x-axis, y-axis, z-axis. a_x, a_y and a_z are a constant.
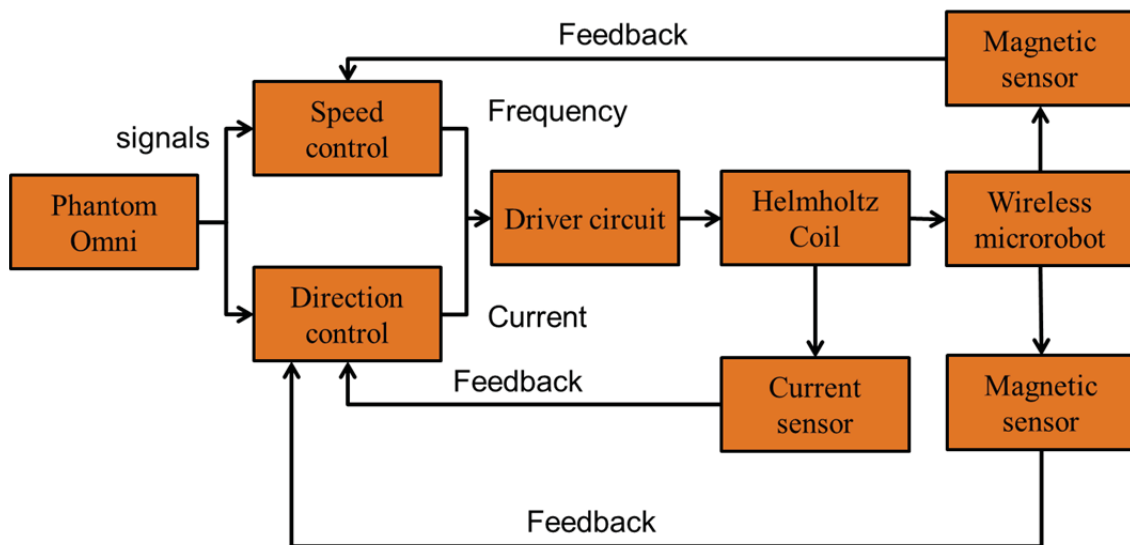
Figure 5.8 Algorithm design of the microrobotic system

(a) Control platform
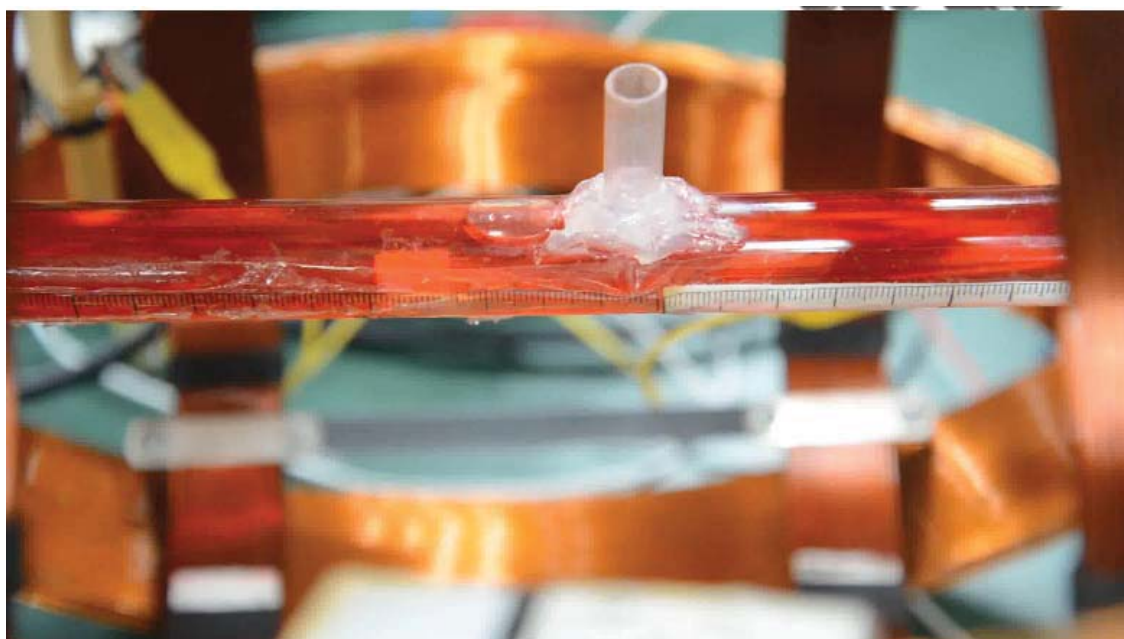
(b) Microrobot

Figure 5.9 Experiments with Phantom Omni

The wireless microrobot realized variable speed motion in horizontal plane as show in Figure 5.9. By adjusting the rotational angle of the handle from 0 degree to 90 degree, the wireless microrobot achieves accelerated motion. By adjusting the rotational angle of the handle from 90 degree to 0 degree, the wireless microrobot can achieve speed reduction motion when the rotational angle for the handle is 0 degrees, the microrobot achieves stop motion in the pipe. The Figure shows the experiment with Phantom Omni.
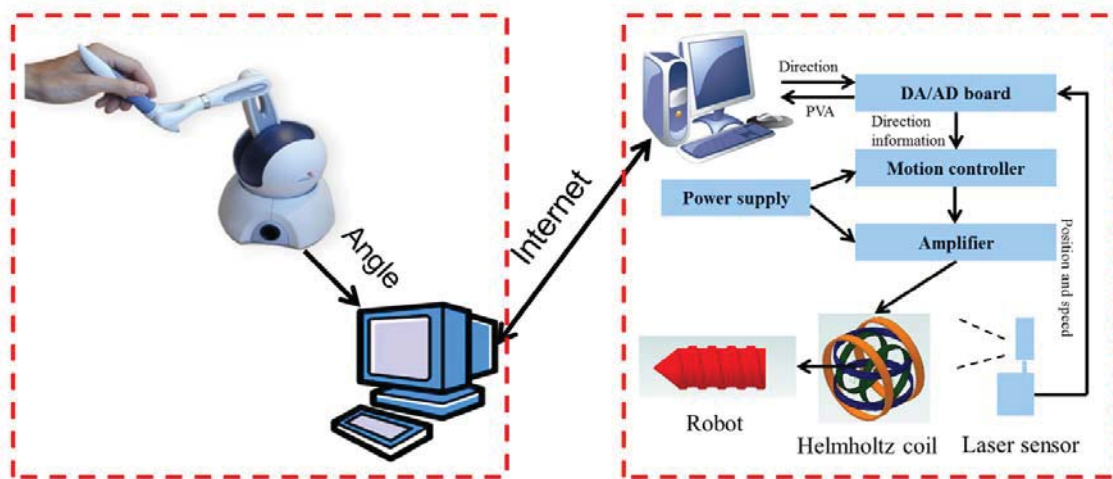
Figure 5.10 Algorithm design of remote control

5.4 Evaluation performance

5.4.1 Remote control

The Figure 5.10 shows the principle of tele-operation control system with Phantom Omni. It includes master side and slave side. In the master side, Phantom Omni is used to generate the drive signals of the 3 axes Helmholtz coils to transmit the slave side through the network. In the slave side, the 3 axes Helmholtz coils can generate a rotation magnetic field,

which control the wireless microrobot to move in the pipe. The operator takes the visual images from web camera to control the motion of the wireless capsule microrobot in the pipe. The oscillosope shows the magnetic flux density changing frequency.

Figure 5.11 shows the experimental setup of the tele-operation control system. As the equipment of the experiment, the wireless microrobot moved a transparent pipe which is 26mm inner diameter, 3mm thickness filled with water. The operator controls the handle of the Phantom Omni to rotate in master side. And the operator takes the visual images from web camera to control the motion of the wireless capsule microrobot of slave side. In the slave side, the Helmholtz system can produce a frequency of the magnetic flux density to control the wireless microrobot in the pipe. The oscilloscope shows the magnetic flux density changing frequency. The wireless microrobot realized the tele-operation control with the Phantom Omni in horizontal plane.
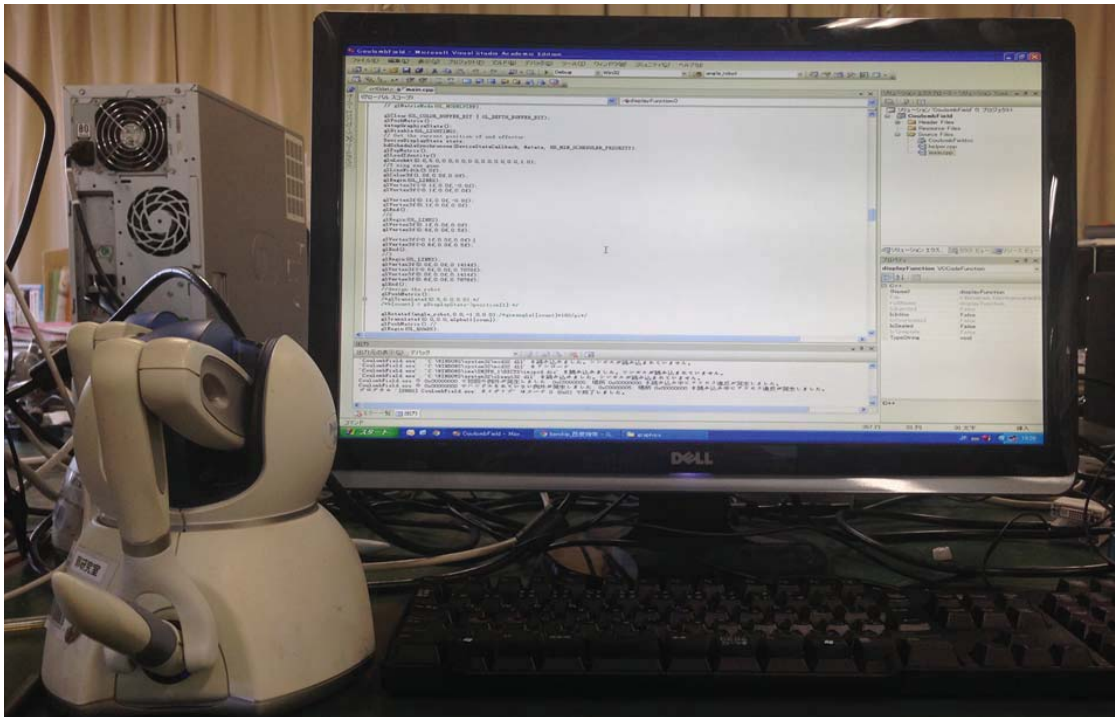
(a) Master side
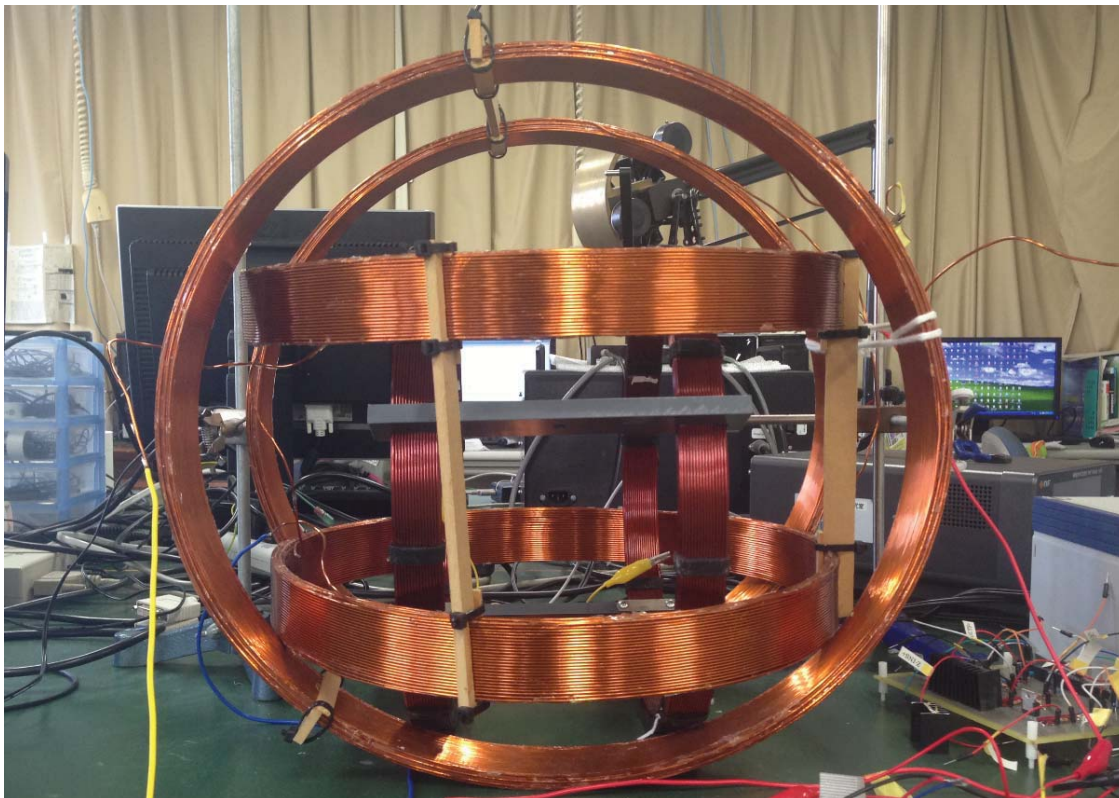
(b) Slave side

Figure 5.11 Remote control

5.4.2 Results

The experimental results are shown in Figure 5.12. During the experiments, we adjusted the magnetic flux density changing frequency via the user interface from 0 to 20 Hz. We measured the speed of the microrobot with each step 1 Hz. The experimental results indicated the relationship between the magnetic flux density changing frequencies is linear before 15 Hz. After the 15 Hz the microrobot did not move in the pipe because the microrobot can no longer rotate continuously in synchronous with the rotational magnetic fields above 15 Hz. According the experimental results, we designed a composite experiment, forward-stop-back motion in the pipe, as shown in Figure 5.13.
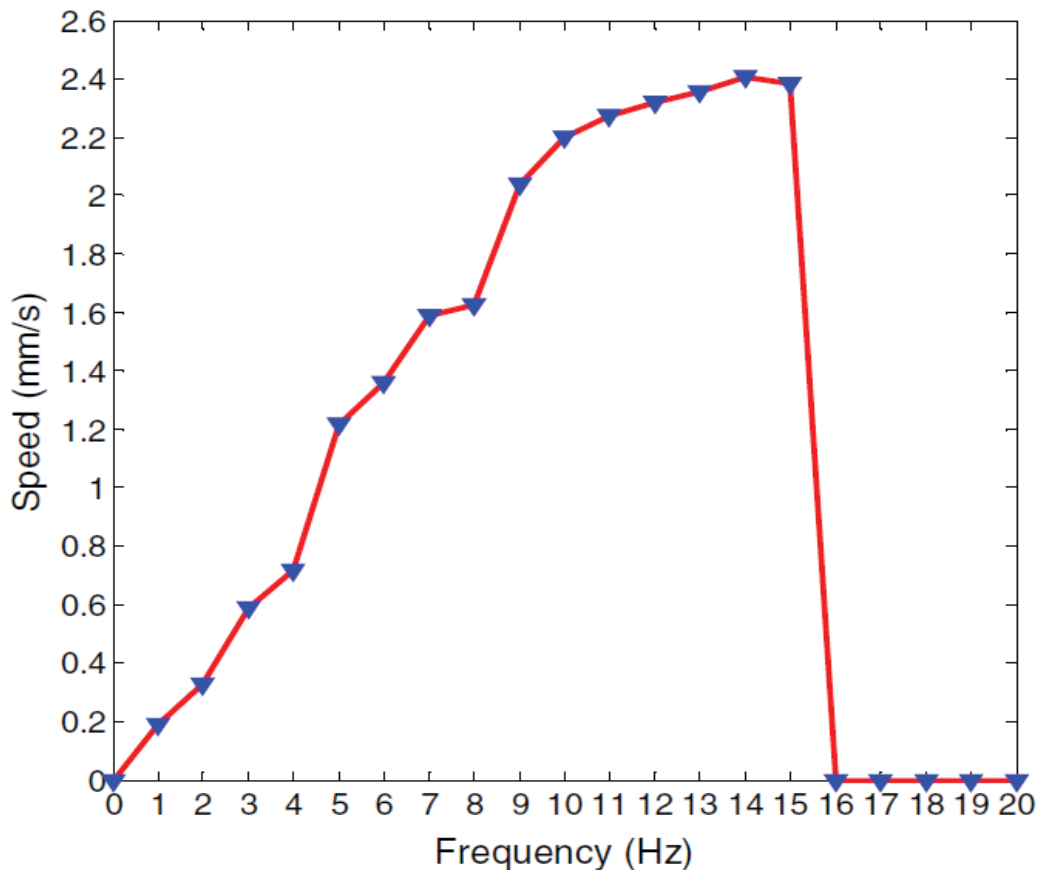
Figure 5.12 Relationship between the frequency and speed
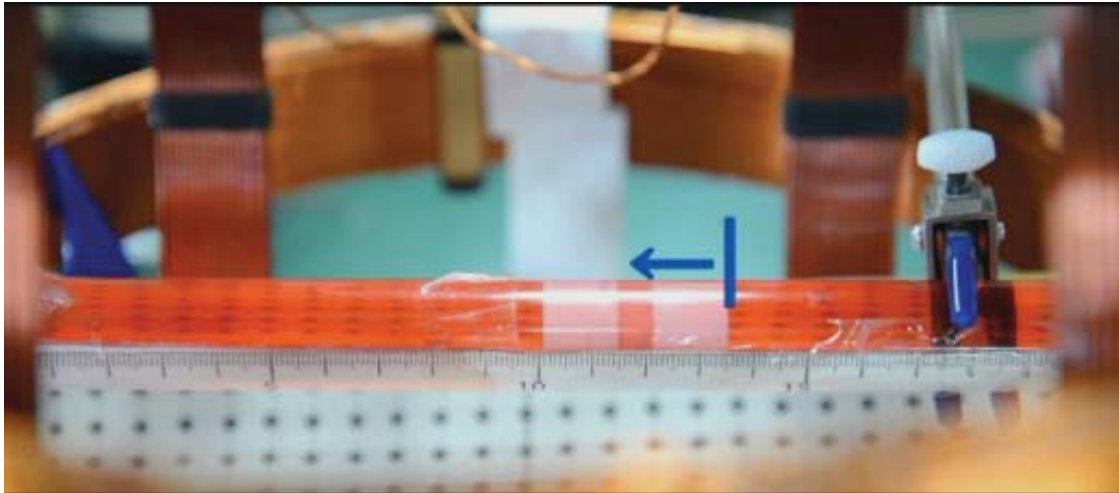
(a) t=0s (forward motion)
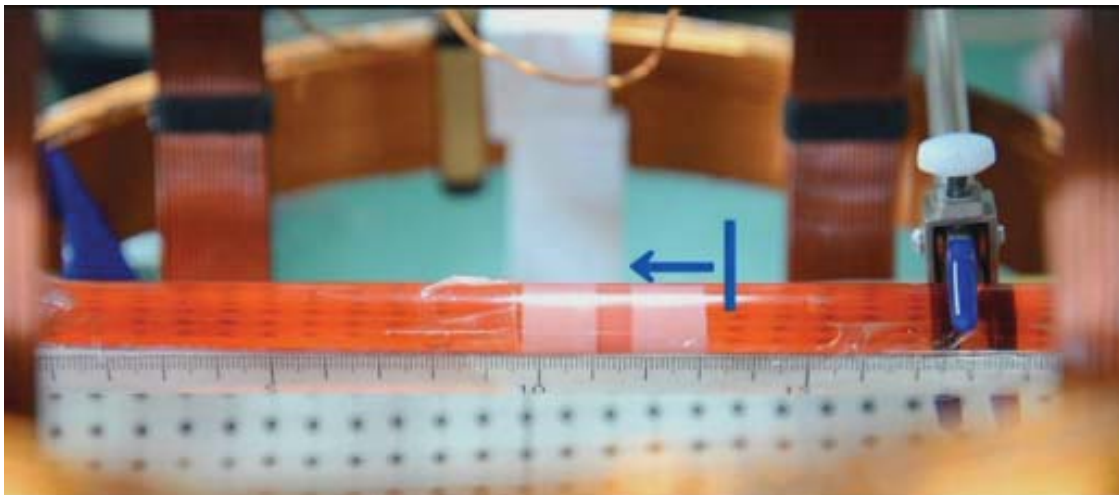
(b) t=5s (forward motion)
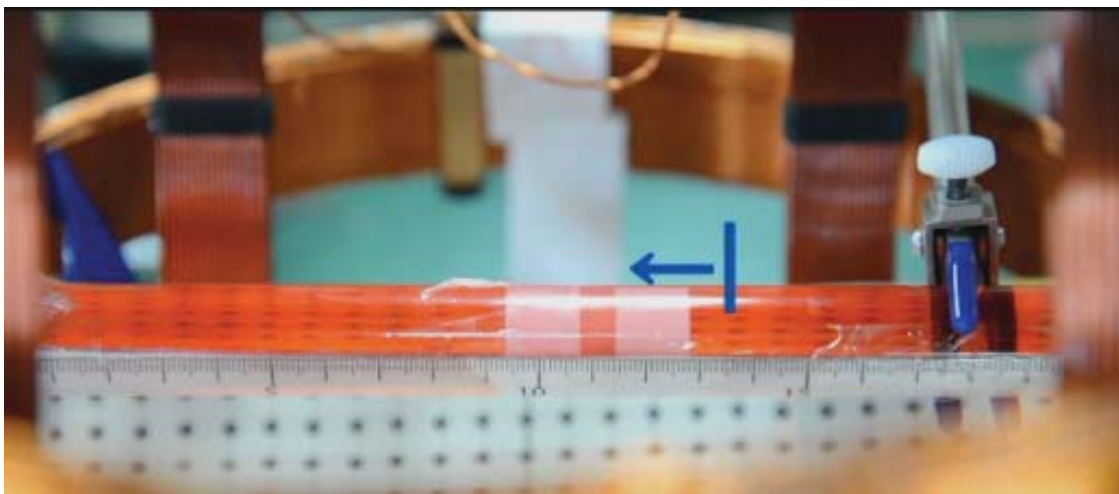
(c) t=10s (forward motion)
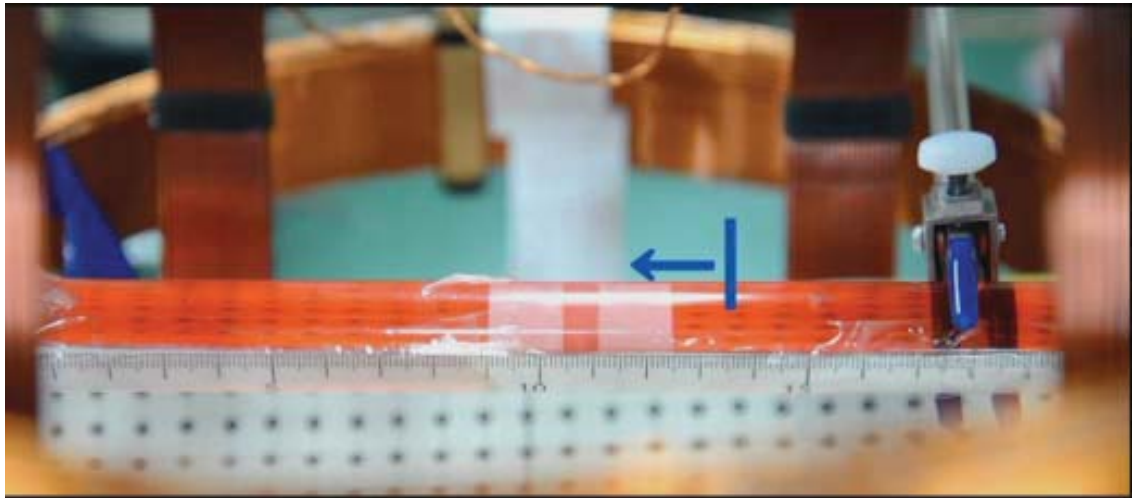
(d) t=15s (forward motion)
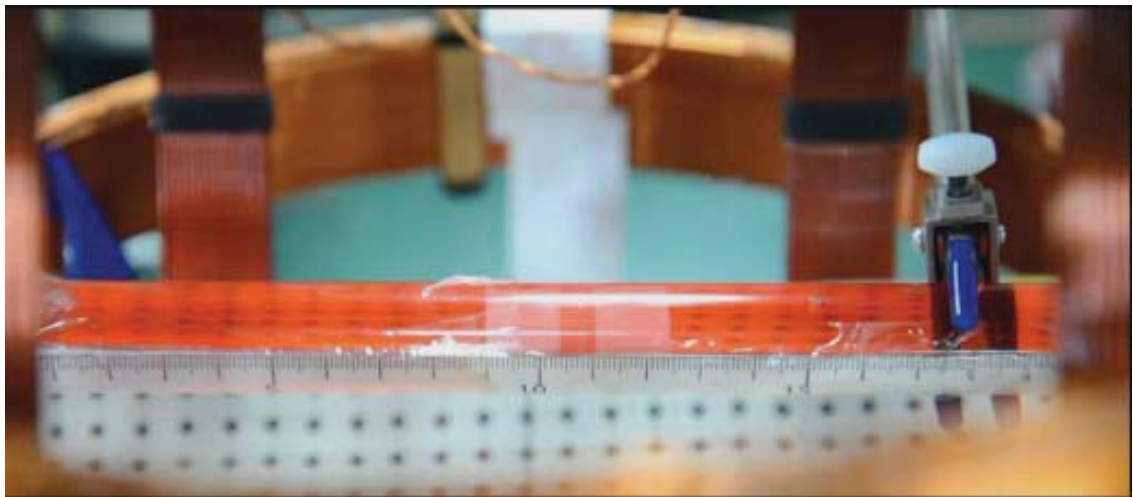
(e) t=20s (stop at a point)
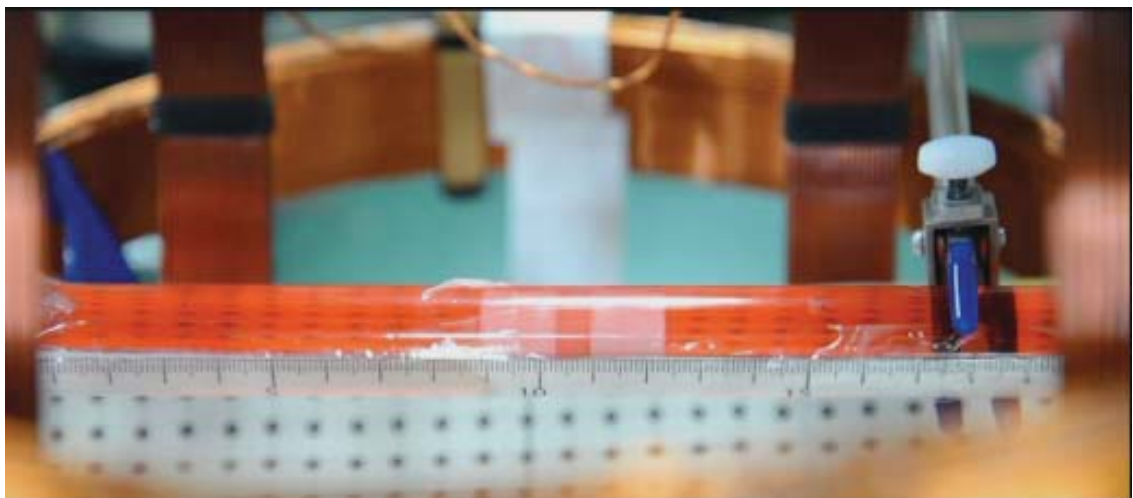
(f) t=25s (stop at a point)
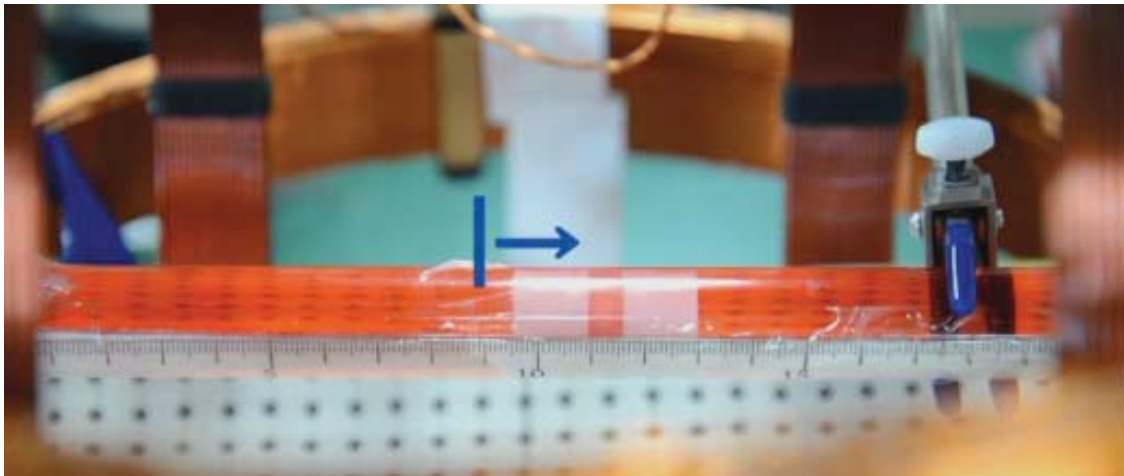
(g) t=30s (backward motion)
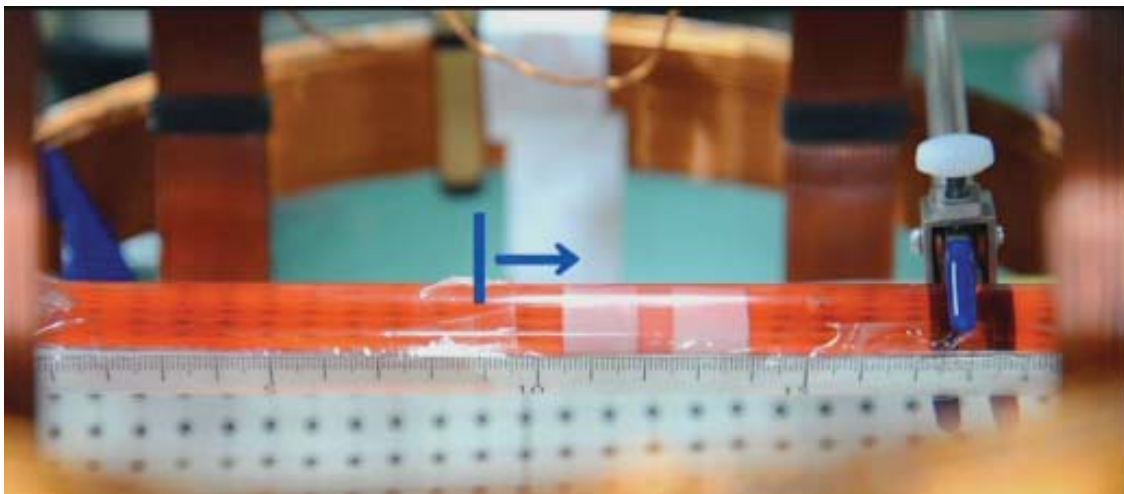
(h) t=35s (backward motion)
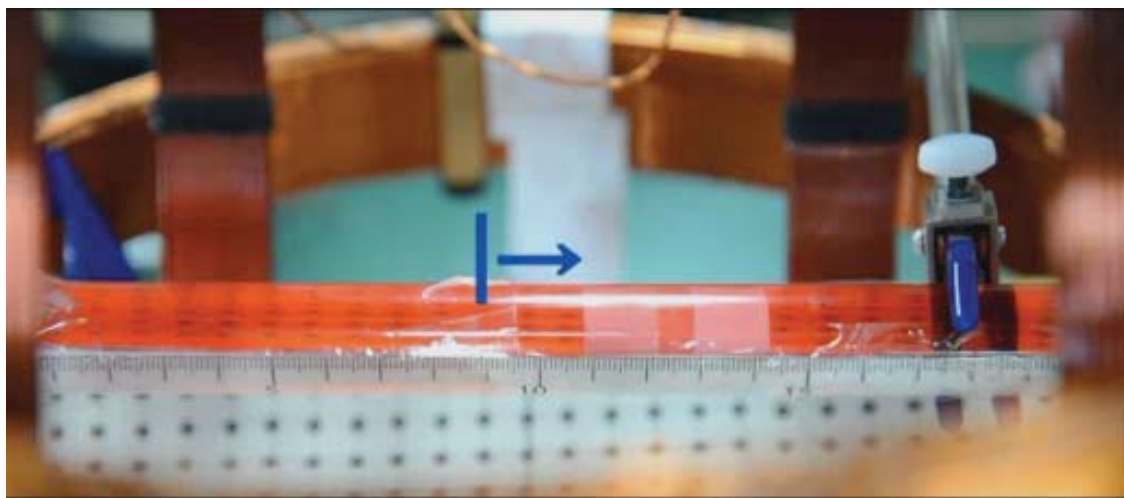
(i) t=39s (backward motion)

Figure 5.13 Forward-stop-backward motion.

5.5 Summary

In this chapter, we improved the control system with Phantom Omni, which can realize real time control the wireless microrobot in the pipe. And an experimental system for evaluating the characteristics of wireless microrobot is developed. Firstly, the principle of the system is introduced. And then, based on the control system, we set the experimental system for motion in horizontal plane. By adjusting the rotational angle of the handle of the Phantom Omni, the wireless microrobot achieves accelerated motion, retarded motion and stop in the pipe. At last, a tele-operation control system has been developed.

Chapter 6　　Characteristic Evaluation of Magnetic Actuated Microrobotic Systems

6.1 Experimental setup

The experimental setup and the schematic diagram are shown in Figure 6.1. The hybrid microrobot is placed in a transparent pipe with diameter 26mm. The transparent is filled with water (water density: 998.203 kg/m^3) at temperature 22°C and inserted 3 axes Helmholtz coils. The web camera will monitor inside of pipe and generate a visual image on the display. Meanwhile, the operator operates the Phantom Omni device to control the position and posture of the hybrid microrobot while viewing the display. The display shows the data to obtain the real-time position of the robot. The drive signals are generated by Phantom Omni device and sent to the 3 axes Helmholtz coils to control the hybrid microrobot. The magnetic flux density changing frequency is shown by oscilloscope.

As the first step for programming, the programming flow chart has been drawn as shown in Figure 6.2. Based on the flow chart, the Microsoft® Virtual Studio® VC++ is used to develop the program of the control system.

In this research, the PCI-3329 DA board has been used as the interface for the developed control system. So, we must study on the application program interface (API) for this interface board before starting a program. Here, we list out the useful API for this DA board.

The PCI-3329 board is 12-bit DA board. Their resolution is 0 ~ 4096 and output voltages are -5 ~ +5 V. They will be used to generate the voltages for power supplies and obtain the waveform. The device name of the PCI-3329 is "FbiDa1".

There are many programming API functions for controlling the PCI-3329 board as given in Interface® product development kite. Here, the useful API functions which used for the complex macro/micro mechanism have been listed as followings.

- HANDLE DaOpen (LPCTSTR lpszName)
- int * DaSetSmplConfig (Handle hDeviceHandle, PDASMPLREQ pSmplConfig)
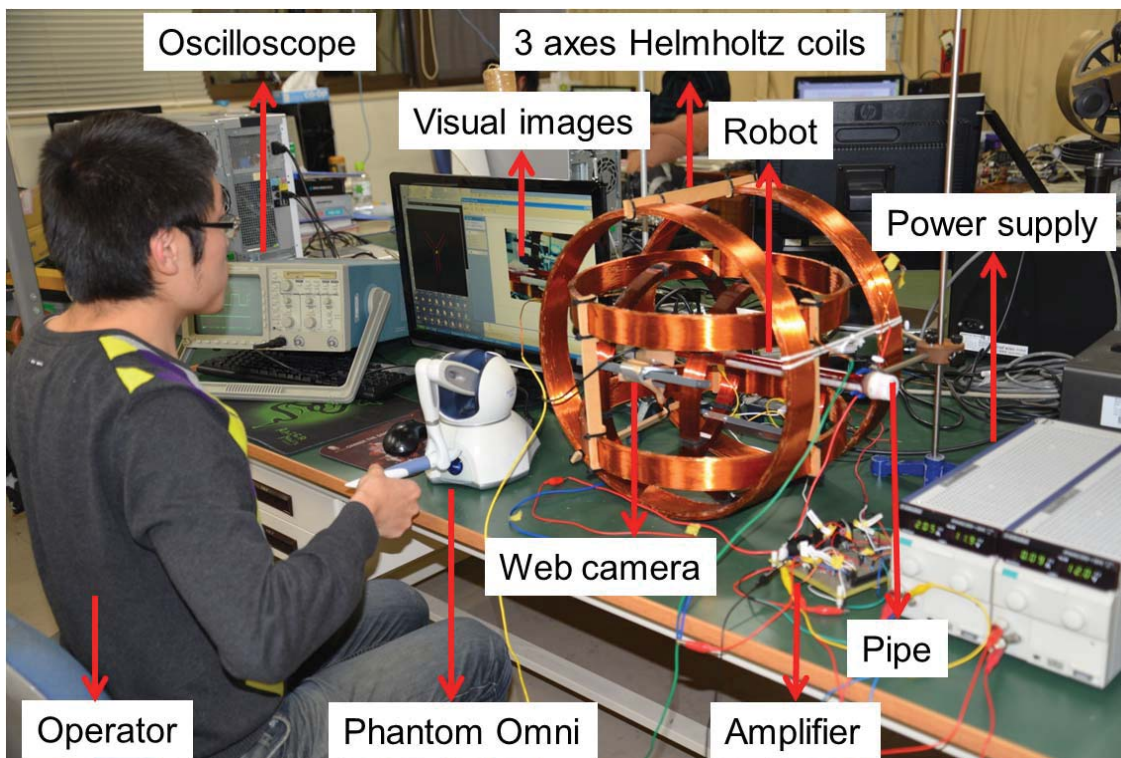
Figure 6.1 Experimental setup
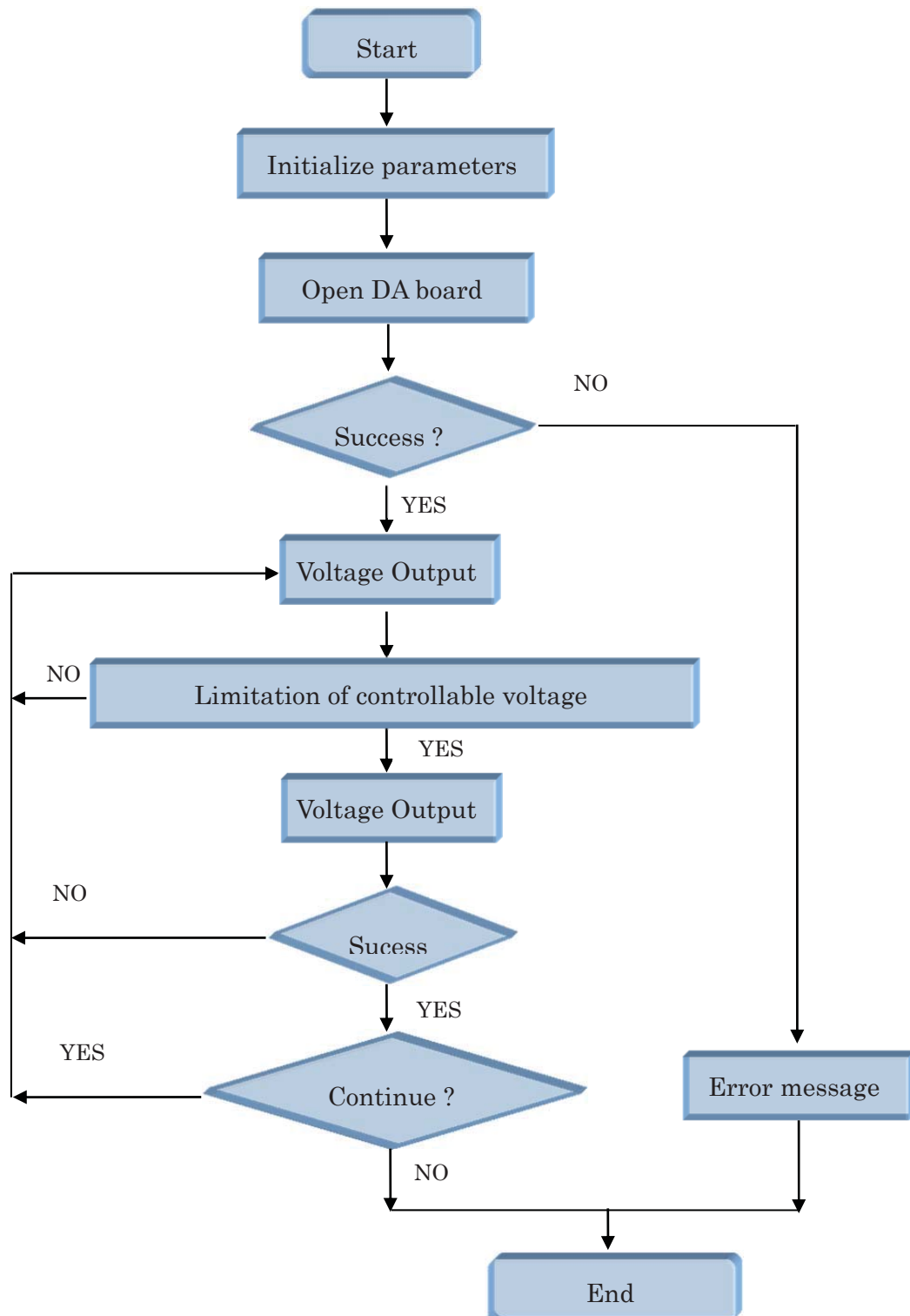
Figure 6.2 Flow chart of data processing

6.2 Multi-DOF locomotion of the hybrid microrobot

Using the experimental setup, the multi-DOF locomotion of the hybrid microrobot is to be tested in the pipe. The microrobot realized multi-DOFs locomotion by this spiral jet motion and fin motion. The microrobot moves forward-backward and stops by changing the rotational uniform magnetic field. Additionally, it is confirmed the microrobot has equivalent moving speed even backward by experiment. Experimental results of the hybrid motion in a horizontal direction are shown in Figure 6.3. Experimental results of the moving state of the microrobot in vertical direction are shown in Figure 6.4. Based on experimental results, the hybrid microrobot realized the movement in the horizontal plane and vertical plane by adjusting rotational magnetic field.
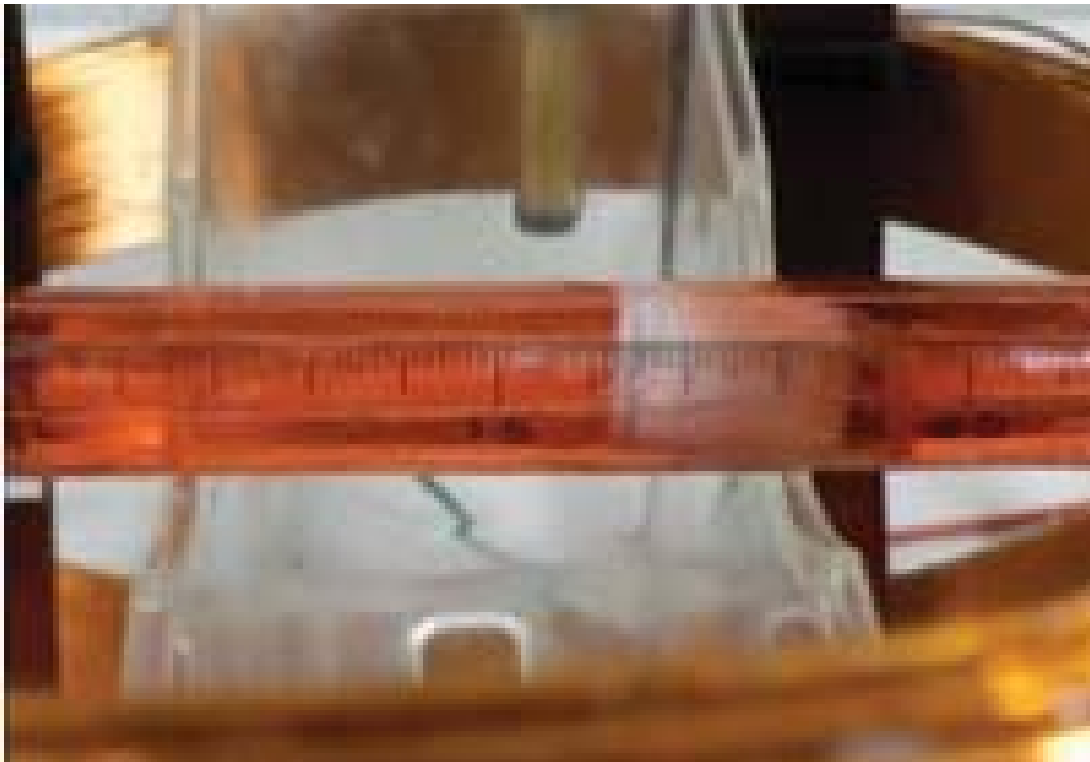
Figure 6.3 Moving state in horizontal direction.
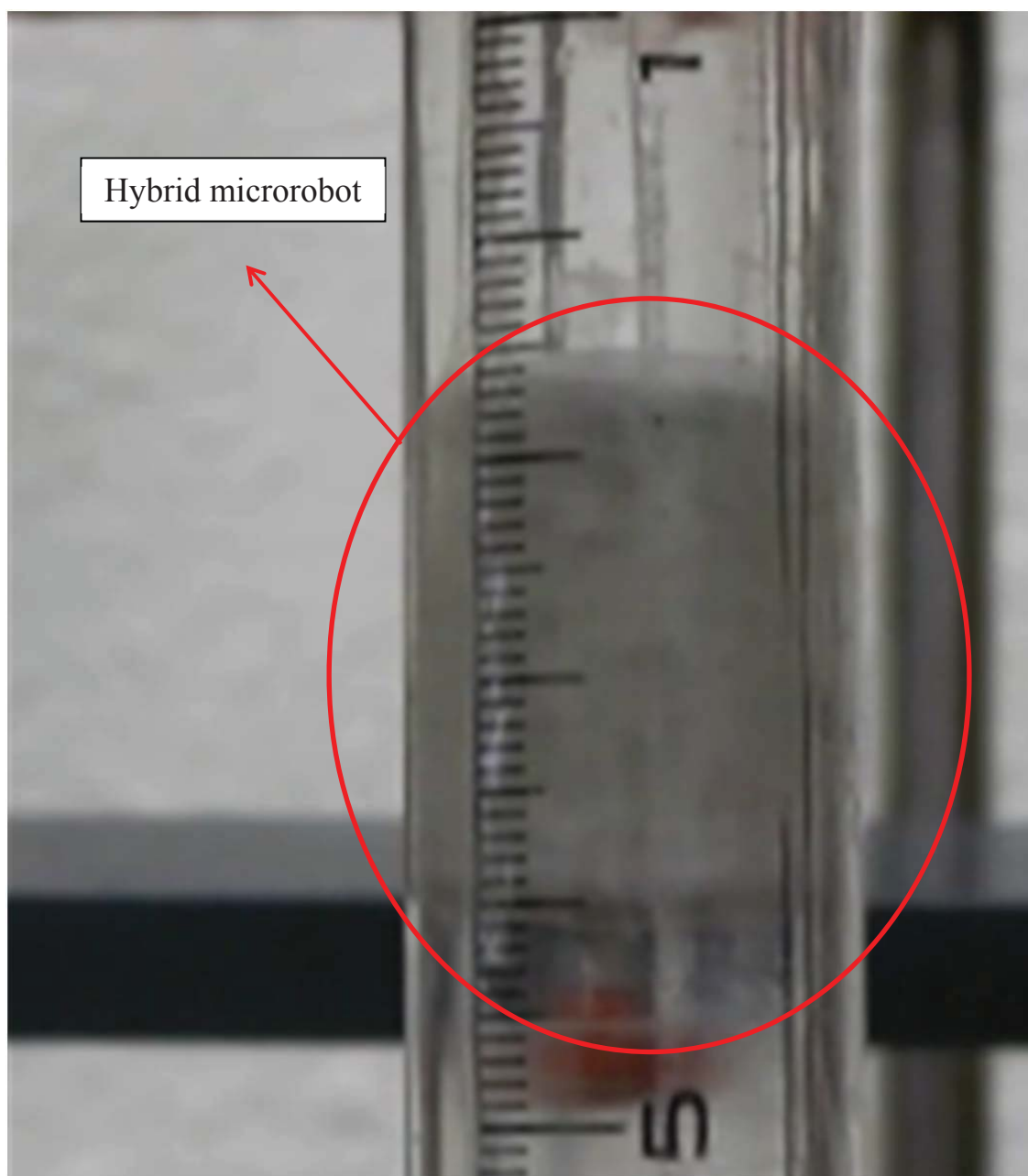
Figure 6.4 Moving state in vertical direction

Experiment of forward-turning-forward locomotion is realized and evaluated, as shown in Figure 6.5. Experimental states of the microrobot which is turning left are shown in Figure 6.5(a). The microrobot moves forward along X axis toward the center by rotating motion or fin motion, as shown in Figure 6.5(b). Secondly, the plane of rotational magnetic field is

rotated by counter-clockwise (CCW), the microrobot turns left at branch point, as shown in Figure 6.5(c). Finally, the microrobot moves forward along Y axis as shown in Figure 6.5(d). In the same way, the plane of rotational magnetic field is rotated by clockwise (CW), the microrobot turns right at branch point. Experiment of backward-turning-forward locomotion is also conducted and evaluated.

Experiment of backward-turning-forward locomotion is also conducted and evaluated, as shown in Figure 6.6. Experimental states of the microrobot are shown in Figure 6.6(a). Firstly, the microrobot moves backward along X axis toward the center by rotating motion, as shown in Figure 6.6(b). Secondly, the plane of the rotational magnetic field is rotated by clockwise (CW), the microrobot turns right at branch point, as shown in Figure 6.6(c). Finally, the microrobot moves forward along Y axis as shown in Figure 6.6(d). In the same way, the plane of rotational magnetic field is rotated by counter-clockwise (CCW), the microrobot turns left at a branch point.
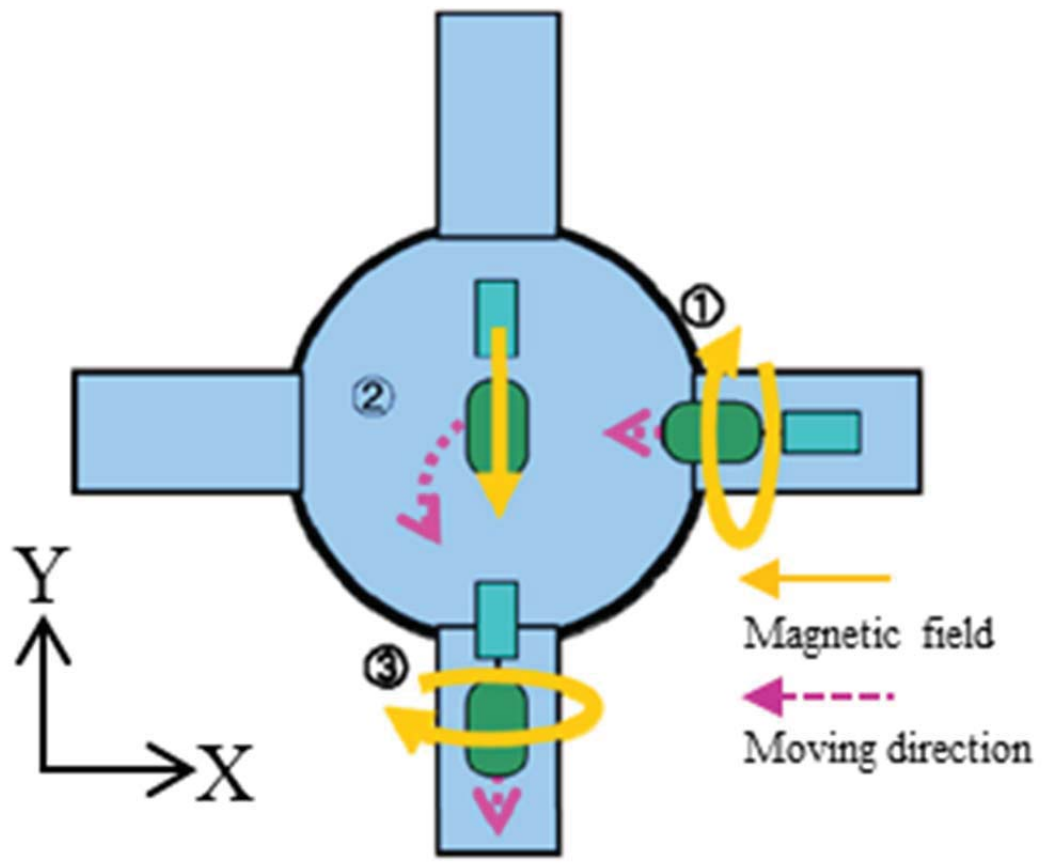
(a)

(b)
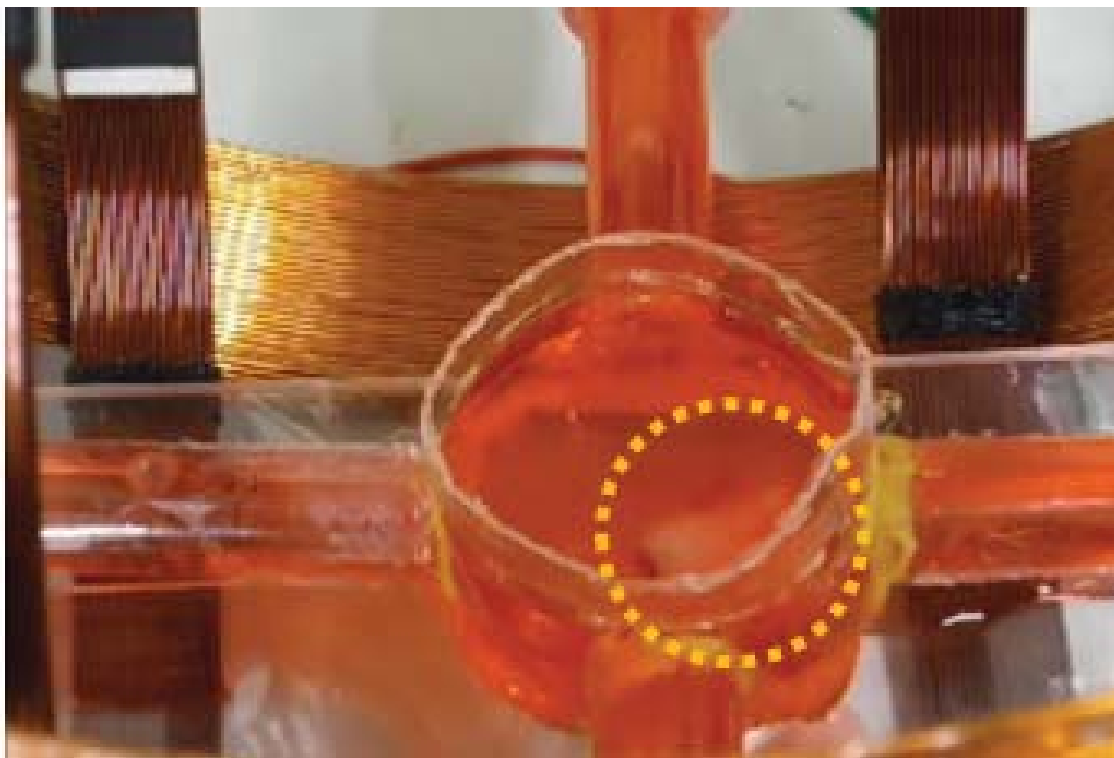
(c)
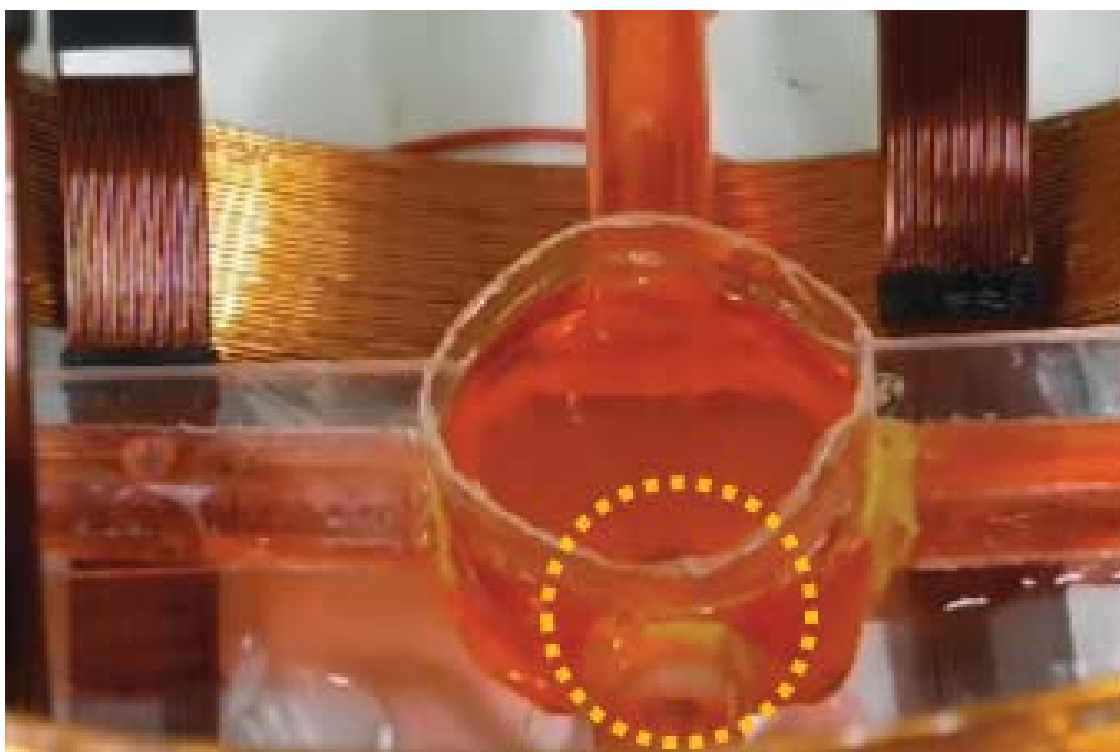
(d)

Figure 6.5 Forward-turning-forward locomotion
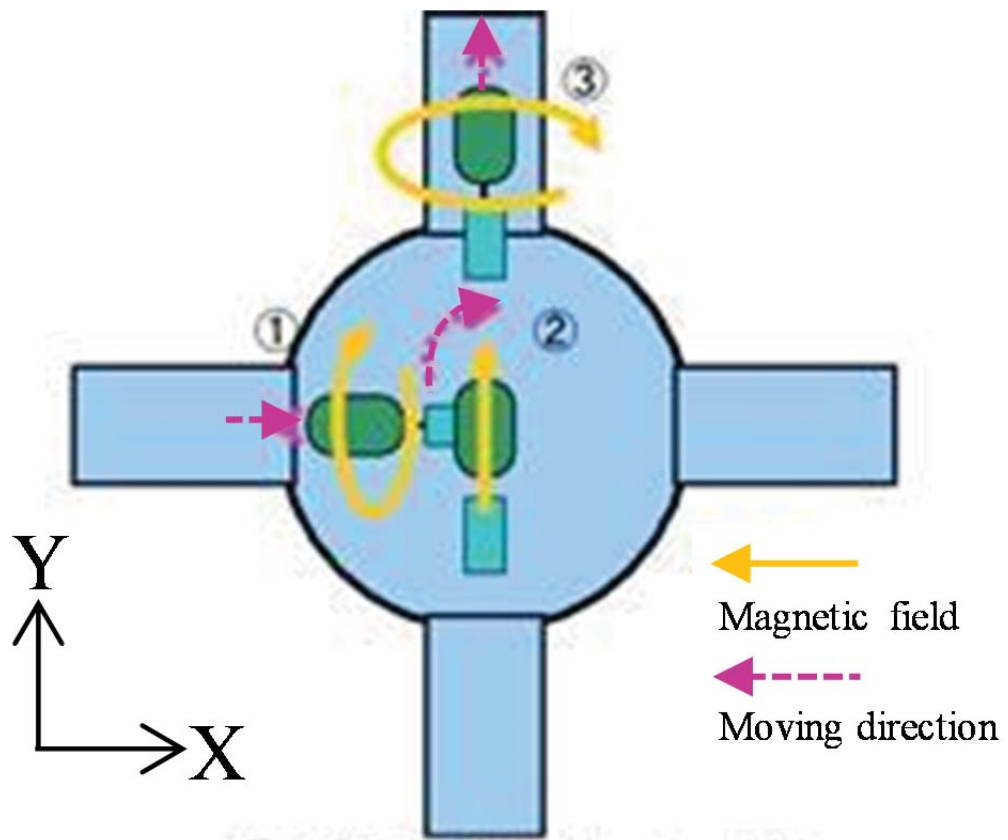
(a)

(b)
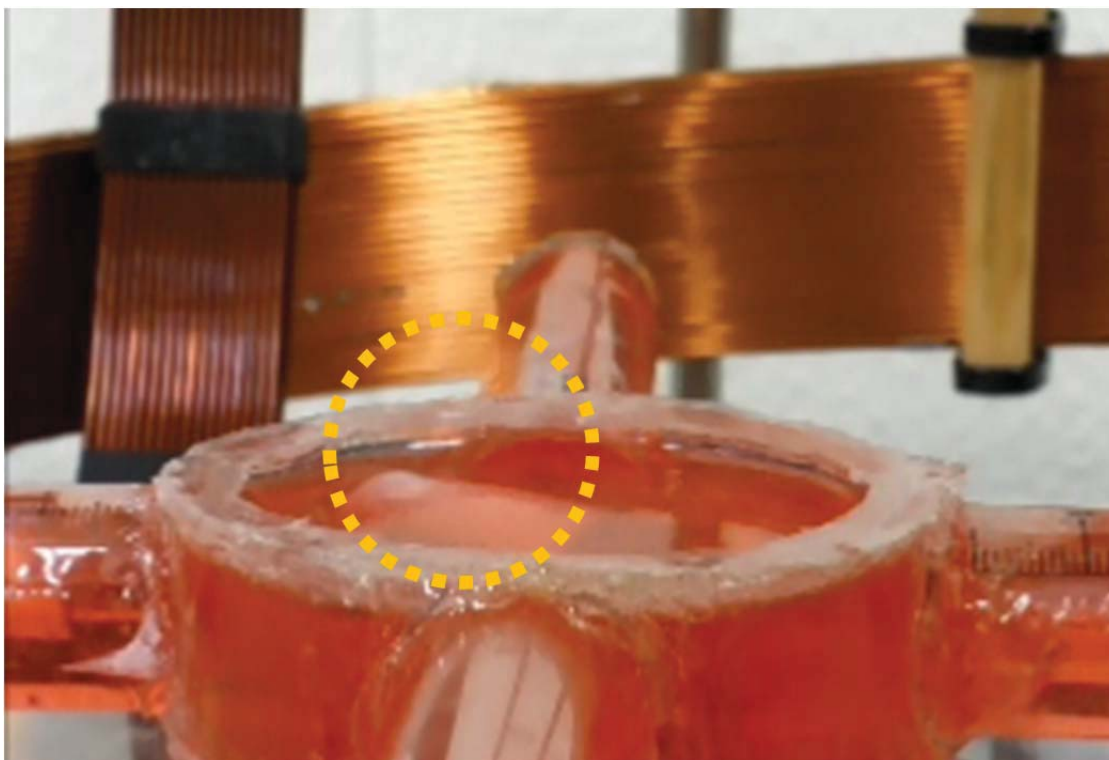
(c)
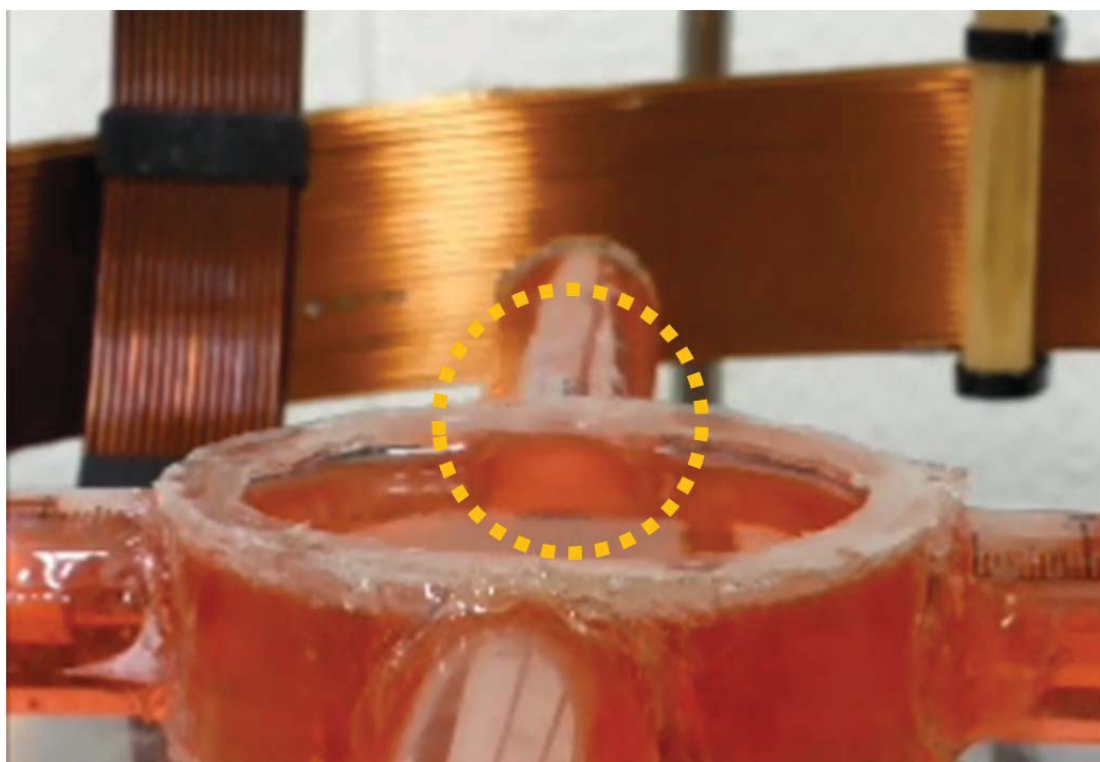
(d)

Figure 6.6 Backward-turning-forward locomotion

6.3 Experimental results and discussions

The relationships between the propulsive force, moving speed and frequency are indicated in Figure 6.7. The experimental results implied that when the hybrid microrobot with spiral jet motion move from 10Hz to 40Hz, the moving speed is increasing with the propulsive force increasing. The maximum propulsive force is 5.4mN. The performance of hybrid motion microrobot in water is evaluated in water. The experimental results show the fin motion and the spiral jet motion work in different frequency, as shown in Figure 6.8. The hybrid microrobot can move using the fin motion below 10Hz. The maximum moving speed is 4.74 mm/s. And it can move using the fin motion or spiral jet motion from 10 Hz to 25 Hz by controlling the rotational magnetic field. The maximum speed of the fin motion is 7 mm/s at 14 Hz. While the frequency is above 25Hz, the hybrid microrobot moves using the spiral jet motion. Additionally, the performance is evaluated in oil to prove the microrobot is able to move in a high viscosity liquid, and the result is shown in Figure 6.9. The maximum moving speed is 0.22 mm/s in oil. According to these results, we did an experiment of hybrid motion by adjusting the rotational magnetic field. The experimental results of forward with fin motion (FF), stop motion (S), forward with spiral jet motion (FS) and backward with spiral jet motion (BS) are shown in Figure 6.10.

There are two phenomena of interest. One is the initial frequency (10Hz). It means that the hybrid microrobot generates enough propulsion to overcome resistance of fluid at this frequency. The other one is step out

frequency (40Hz) that means the frequency above which the microrobot can no longer rotate continuously in synchronous with the rotational magnetic fields. Step-out frequency is well understood for magnetic helical microrobots in uniform fields, it is discussed in our previous researches. The experimental results of the spiral jet motion indicated the linearity between magnetic field changing frequency and the moving speed from 10Hz to 40Hz. The approximate numerical formula of spiral jet motion and Fin motion are shown in equation (6-1) and (6-2).

$$v_{screw}(f) = 0.08921f - 0.4737 \qquad (6-1)$$

$$v_{fin}(f) = -0.03279f^2 + 0.8229f \qquad (6-2)$$
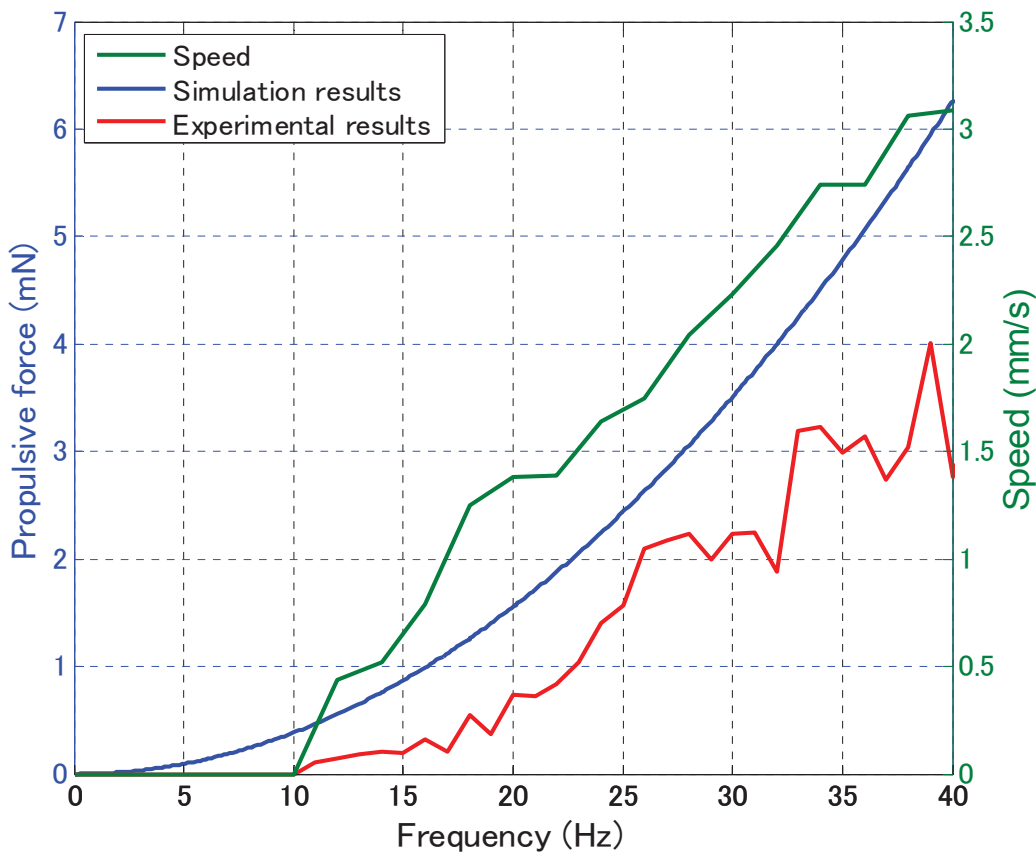
Figure 6.7 Relationships between propulsive force, moving speed and frequency
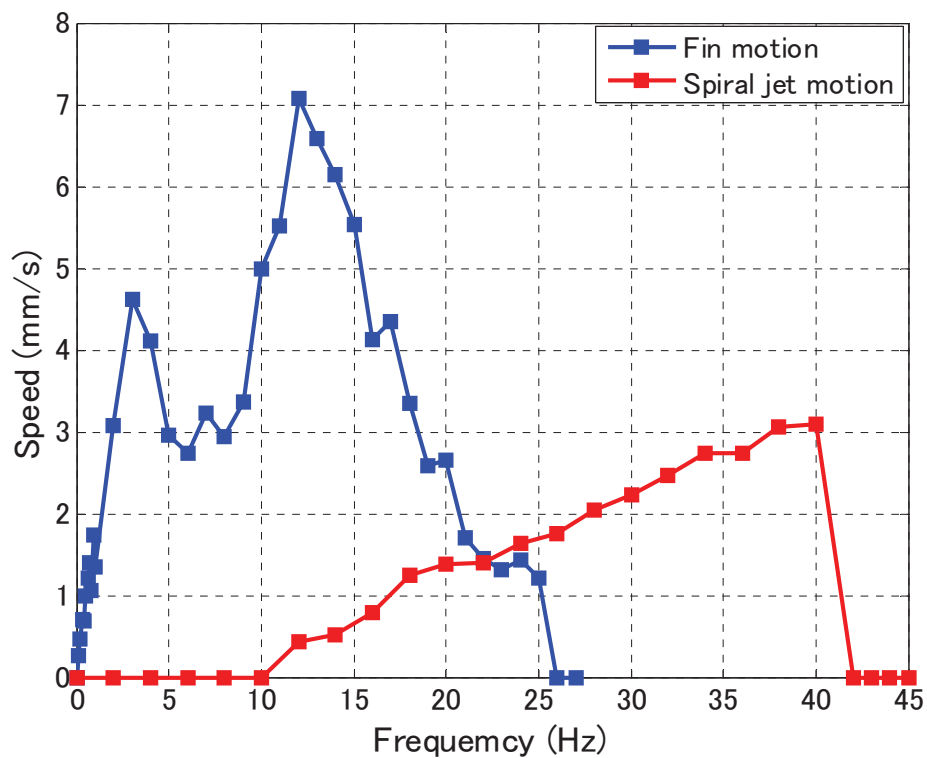
Figure 6.8 Hybrid motion in water
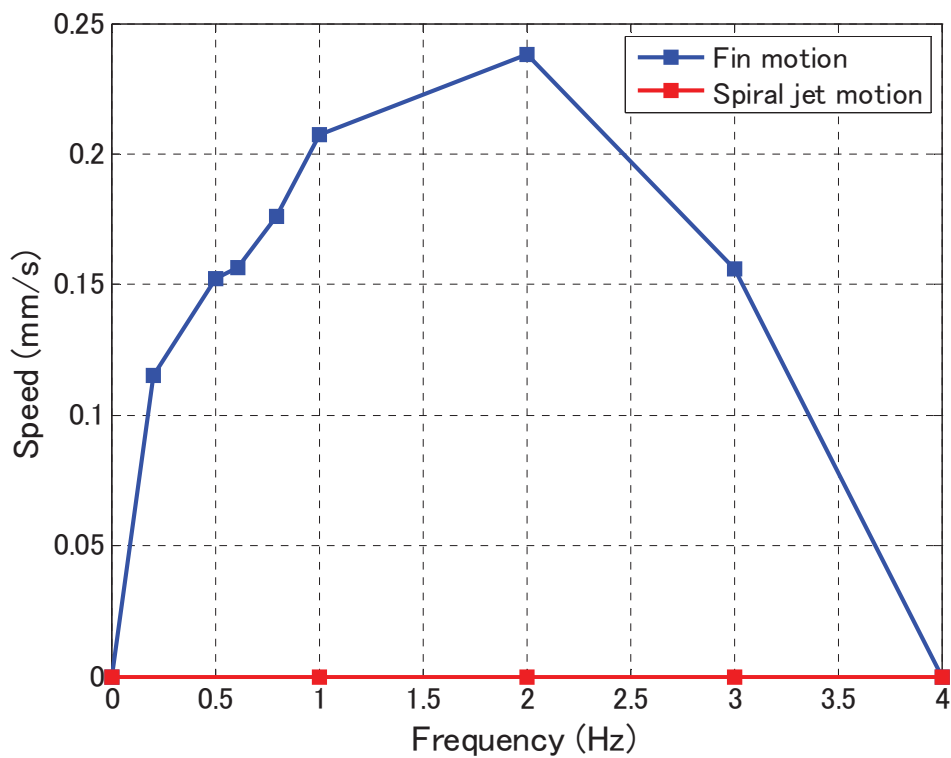
Figure 6.9 Hybrid motion in oil
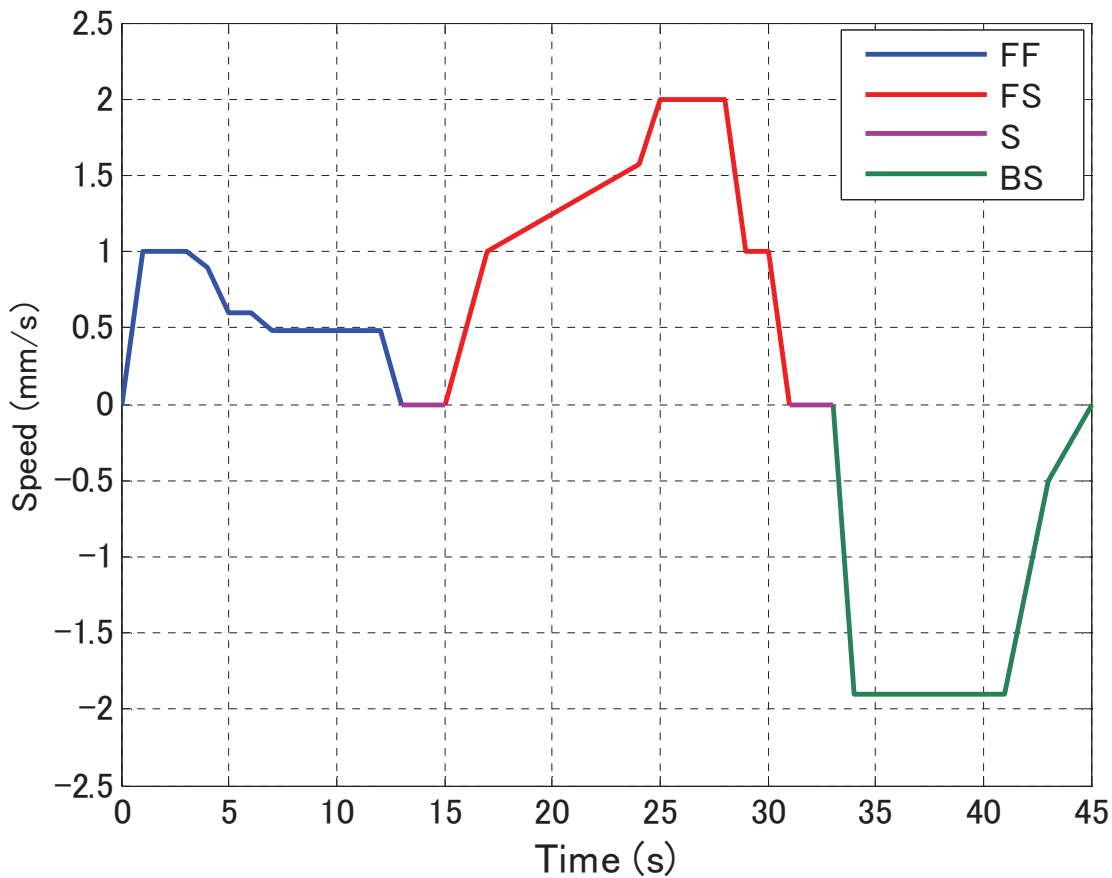
Figure 6.10 Forward-stop-backward motion

6.4 Summary

In this chapter, we evaluated the performance of the multi-module magnetic actuated microrobotic system. The microrobot realized the flexible motion in horizontal plane and vertical plane, such as, forward motion, backward motion, stop motion and turning motion. The moving speed is measured with the laser sensor. The results of the experiments show that the microrobot can moved in the low-frequency, through changing the direction of current which is flowing through Helmholtz coil pairs.

Chapter 7   Concluding Remarks

7.1 Thesis summary

Microrobots have become employed in minimally invasive procedures due to their reliability and flexibility. They are safe and can perform tasks in small or narrow areas deep within the human body. Microrobots have many potential applications in the field of medical engineering. With advances in precision processing technology, various microrobots with biomimetic locomotion have been developed, and further progress in the biomedical field is expected. As a tool for diagnosis and treatment, microrobots can be used for tasks such as drug delivery and complex surgical operation. Microrobots driven by an electromagnetic actuation system have recently been proposed. These combined coils generally generate a gradient magnetic field that provides a propulsive force to the microrobot. The speed of the microrobot varies with the strength of the magnetic field (a larger magnetic field strength leads to higher speed). There are some limitations for clinical examination due to the relatively large volume and high energy consumption of such microrobots.

Previously, we proposed a conceptual hybrid microrobot to reduce patient pain and discomfort. However, further clinical application is needed in order to produce a robot that is capable of treating disease, diagnosing intestinal problems and conducting minimal invasive surgery. As well, the robot needs to be able to install actuating elements (e.g. drug delivery

mechanism), a camera (e.g. endoscope) and sensing elements for achieving medical tasks. Therefore, medical safety, loading abilities and an effective propulsive performance is extremely important and challenging. This paper presents a new locomotive mechanism, named the shrouded propeller mechanism to improve medical safety and propulsive performance.

Therefore, we proposed a multi-module magnetic actuated microrobotic system. The microrobot can be separated into smaller module. First the penitents swallow these smaller modules, one by one, when the all the module are swallowed or pass the narrow space, and then these module groups a whole microrobot and move to the target, finish the functional.

Our proposed magnetic actuated microrobots include two kinds module. One is the magnetic microrobot, it has a capability to the loading the multi-module microrobot. Another is the multi-module microrobot. It has some functions, as a tool or as a module, such as CCD camera, to realize the diagnosis and treatment in human body. In medical application, we can realize the remote control or local control to our proposed magnetic actuated microrobot. It can reach to the target to achieve the medical produce, for example, drug deliver, endoscopy and minimally invasive surgery, and so on.

7.2 Research achievement

1) A new locomotive mechanism, named the shrouded propeller mechanism was proposed to achieve a high level of medical safety as well as effective propulsive performance in our study. The shrouded propeller mechanism consists of a bare spiral propeller and a

non-rotating nozzle. To obtain a high effective propulsive performance, two types of screw grooves with different shapes including the cylindrical screw groove and the rectangular screw groove with different parameters were analyzed using the shrouded model. Based on experimental results, the propulsive force of the proposed magnetic actuated microrobot with a shrouded propeller was larger than the magnetic actuated microrobot with a bare spiral propeller under the same parameters. Additionally, the shrouded propeller mechanism as an actuator can be used for other medical microrobots for flexible locomotion.

2) A novel type of magnetically actuated hybrid microrobot (MAHM) based on a rotational magnetic field is proposed. The hybrid microrobot with spiral jet motion and fin motion has a small scale with a wireless power supply, can be propelled by low voltage, and has a quick response. And also the hybrid microrobot can work for a long time in human. It can convert its two motions through the proposed structure of the microrobot with rotational magnetic field, so that it realizes the movement in the different environment. The body of the microrobot with a spiral jet motion can obtain a stable motion and high propulsive force than the spiral motion. The fin motion can improve the dynamic characteristic and reduce the shake which caused by the axial propulsive force of the spiral jet motion. Spiral motion and fin motion can be controlled separated without any interference, due to the hybrid microrobot has only use one actuator to realize the spiral jet motion and

fin motion.

3) A tele-operation system provides telepresence by allowing a doctor to remotely control a wireless capsule microrobot through a master device. This causes less pain to the patients and there will be less tissue trauma. Thus reducing hospitalization time and enhancing recovery. On the master side, the doctor views a monitor which is produced by a CT-scan and operates the wireless microrobot to detect or treat the disease with an unknown and dynamic environment. The control instructions are transmitted to the slave side. On receiving instructions, the slave mechanisms control the wireless capsule microrobot. The monitor can also show the data calculated from the magnetic sensor array for obtaining the real-time position of the robot. The positioning system helps us to realize the close-loop control and ensure the robot achieves the task. Consequently, the doctor appears to accurately control the position and posture of the wireless microrobot in human body.

7.3 Recommendations for the future

Future work of this research will focus on optimizing the structure to increase propulsive force. In addition, the propulsive force can be limited at high frequency due to the dynamics of the 3 axes Helmholtz coils system and natural frequency, the actuation frequency also should be improved. And also, the real time image should be feedback to operators for an accurate control about moving speed and direction of hybrid microrobot. It has a potential capability to satisfy the requirements for medical applications.

References

[1] Rentschler M.E and Oleynikov D., "Recent in vivo surgical robot and mechanism developments," *Surgical Endoscopy and other International Techniques*, Vol. 21, No. 9 pp. 1477-1481, 2007.

[2] J. Guo, S. Guo, X. Wei, Y. Wang "Development of a Wireless Endoscope with Symmetrical Motion Characteristics" *International Journal of Advanced Robotic Systems*, Vol. 11, pp. 1-13, 2014

[3] G. Ciuti, A. Menciassi, and P. Dario, "Capsule endoscopy: From current achievements to open challenges," *IEEE Reviews in Biomedical Engineering*, vol. 4, pp. 59 –72, 2011.

[4] Day, Nicholas J., Patrick Fultz, and Danielle Marino. "Recurrent Small-Bowel Obstruction Caused by a Meckel's Diverticulum Diagnosed on Video Capsule Endoscopy." *Clinical Gastroenterology and Hepatology,* Vol.14, No. 6, pp.A21-A22, 2016.

[5] Jing, Wuming, Nicholas Pagano, and David J. Cappelleri. "A novel micro-scale magnetic tumbling microrobot," *Journal of Micro-Bio Robotics*, Vol. 8, No. 1 pp.1-12, 2013

[6] X. Wang and M. Q-H. Meng, "Perspective of active capsule endoscope: actuation and localization," *International Journal of Mechatronics and Automation*, Vol.1, No.1, pp.38-45, 2011.

[7] Zhou W., Hui A.P., Li W.J., Xi N., Development of a force-reflection controlled micro underwater actuator. I*n Proceedings of IEEE/RSJ*

International Conference on Intelligent Robots and Systems, Maui, Hawaii, USA. Oct., pp. 363-368, 2001.

[8] Alexanderowicz A., Katchalsky A., "Colligative properties of polyelectrolyte solutions in excess of salt." *Journal of Polymer Science*, Vol.1A, pp.3231-3260, 1963.

[9] Chigasaki S., Mori M., Yamada H. and Hirose S., "Design and control of amphibious snake-like robot "CM-R5" (in Japanese)." *In Proceedings of 2005 JSME Conference on Robotics and Mechatronics*, pp. ALL-N-020, 2005.

[10] Clark J.E., Cham J.G., Bailey S.A., Froehlich EM, et al. "Biomimetic design and fabrication of a hexapedal running robot." *In Proceedings of IEEE International Conference on Robotics and Automation*, Vol. 4, pp. 3643-3649, 2001.

[11] Altendorfer R., Moore N., Komsuoglu H., Buehler M., Brown Jr HB, McMordie D., Saranli U., Full R.J., Koditschek D.E. RHex: "A Biologically Inspired Hexapod Runner." *Autonomous Robots*, Vol.11, pp.207-213, 2001.

[12] Anton M., Punning A., Aabloo A. and Kruusmaa M., "Towards a biomimetic EAP robot." *In Proceedings of Towards the Autonomous Mobile Robots (TAROS'04)*, pp. 1-7, 2004.

[13] Asaka K., Oguro K., Nishimura Y., Mizuhata M. and Takenaka H., "Bending of polyelectrolyte membrane-platinum composites by electric stimuli, I. response characteristics to various waveforms." *Polymer Journal*, Vol.27, No.4, pp.436-440, 1995.

[14] Ayers J., "Underwater walking." *Arthropod Structure and Development*, Vol.33, Issue 3, pp. 347-360, 2004.

[15] Barrett D. S., Triantafyllou M. S., Yue D. K. P., Grosenbaugh M.A. and Wolfgang M. J., "Drag reduction in fish-like locomotion", *Journal of Fluid Mechanics*, 392, 183-212, 1999.

[16] Hirose Y., Shiga T., Okada A., Kurauchi T., "Gel actuators driven by an electric field." *In Proceedings of the 3rd International Symposium on Micro Machine and Human Science*, pp. 21-26, 1992.

[17] Hollar S., Flynn A., Bellew C., Pister K.S.J., "Solar powered 10mg silicon robot." *In MEMS 2003*, Kyoto, Japan, January 19-23, 2003.

[18] Inagaki S., Yuasa H., Arai T., "Cpg model for autonomous decentralized multi-legged robot system-generation and transition of oscillation pattern and dynamics of oscillators." *Robotics and Autonomous Systems*, 44: 171-179, 2003.

[19] Ishimaru K., Hyakawa K., Ishiguro A., Kawakatsu T., "Toward a 'well-balanced' design." *In Proceedings of the 2nd International Symposium on Adaptive Motion of Animals and Machines*, Kyoto, 2003.

[20] Zhang W., Guo S., Asaka K., "A tripodic biomimetic underwater microrobots utilizing ICPF actuators." *In Proceedings of IEEE/RSJ International Conference on Intelligent Robots and Systems*. Oct. 9-15. Beijing, China. pp. 2418-2423, 2006.

[21] Fukuda T., Kawamoto A., Arai F., Matsuura H., "Steering mechanism of underwater micro mobile robot." *In Proceedings of IEEE*

International Conference on Robotics and Automation, Vol.1, pp.363-368, 1995.

[22] Behkam B. and Sitti M., "Modeling and testing of a biomimetic flagellar propulsion method for microscale biomedical swimming robots." *In Proceedings of 2005 IEEE/ASME International Conference on Advanced Intelligent Mechatronics*, 37-42, 2005.

[23] Berk K., Vollmers K. and Nelson B., "Modeling and control of untethered biomicrorobots in a fluidic environment using electrmagnetic fields." *International Journal of Robotics Research*, 25(5-6), 527-536, 2006.

[24] Cruse H., "Which parameters control the leg movement of a walking insect? i. velocity control during the stance phase." *The Journal of Experimental Biology*, 116: 343-355, 1985.

[25] De Rossi D., Domenici C., Chiareli P.,. "Analog of biological tissues for mechanoelectrical transduction: Tactile sensors and muscle-like actuators." NATo-ASI Series, *Sensors and Sensory Systems for Advanced Robots*, Vol.F43, pp.201-218, 1988.

[26] Durr V., Konig Y., Kittmann R., "The antennal motor system of the stick insect Carausius morosus: anatomy and antennal movement pattern during walking." *Journal of Comparative physiology*, 187: 131-144, 2001.

[27] Durr V., Krause A.F., Schmitz J., Cruse H., Neuroethological concepts and their transfer to walking machines. *The International Journal of Robotics Research*, 22(3-4):151-167, 2003.

[28] Eisen G.M., Eliakim R., Zaman A., et al. "The accuracy of PillCam ESO capsule endoscopy versus conventional upper endoscopy for the diagnosis of esophageal varices: a prospective three-center pilot study." *Endoscopy*, 38:31–35, 2006.

[29] http://rfsystemlab.com/sayaka/norika/system/001.html

[30] Moglia, A., Menciassi, A., Schurr, M. O. and Dario, P. "Wireless capsule endoscopy: from diagnostic devices to multipurpose robotic systems." *Biomedical microdevices*, Vol. 9 No.2, pp. 235-243, 2007

[31] Basar, M. R., Malek, F., Juni, K. M., Idris, M. S. and Saleh, M. I. M., "Ingestible wireless capsule technology: A review of development and future indication." I*nternational Journal of Antennas and Propagation*, 2012.

[32] X. Wang and M. Q-H. Meng, "Perspective of active capsule endoscope: actuation and localization," *International Journal of Mechatronics and Automation*, Vol.1, No.1, pp.38-45, 2011.

[33] B. S. Lewis, "Small intestinal bleeding," *Gastroenterology Clinics of North America*, vol. 29, no. 1, pp. 67–95, 2000.

[34] G. D. Meron, "The development of the swallowable video capsule (M2A)," *Gastrointestinal Endoscopy*, vol. 52, no. 6, pp. 817–819, 2000.

[35] M.arcia Yu, BSN, RN, "M2A™ capsule endoscopy- a breakthrough diagnostic tool for small intestine imaging" *Gastroenterol Nursing*, Vol. 25, No. 1, pp. 24-27, 2002.

[36] Pan Q.; Guo S.; Okada T. "A Novel Hybrid Wireless Microrobot" *International Journal of Mechatronics and Automation*, Vol.1 pp.60-69, 2011.

[37] Desai J.P.; Pillarisetti A. and Brooks A.D. "Engineering approaches to biomanipulation". *Annual Review of Biomedical Engineering*, Vol. 9, pp. 35-53, 2007.

[38] Zarrouk D. and Shoham M. "Analysis and Design of One Degree of Freedom Worm Robots for Locomotion on Rigid and Compliant Terrain". *Journal of Mechanical Design*, Vol. 134, pp.1-9, 2012.

[39] Robot, E. M. A. "Design of Micro Robot for Minimally Invasive Surgery". *International Journal of Robotics and Automation (IJRA)*, Vol. 2 No.1, pp. 35-44, 2013.

[40] Gao B.; Guo S. and Ye X. "Motion-control analysis of ICPF-actuated underwater biomimetic microrobots," *International Journal of Mechatronics and Automation*, Vol.1, pp.79-89, 2011.

[41] Honda T., Sakashita T., Narahashi K. and Yamasaki J., "Swimming properties of bending-type magnetic micro-machine," *Journal of Magnetics Society of Japan*, 25(4-2), 1175-1178, 2001.

[42] C. Yu, J. Kim, H.l Choi, J. Choi, S. Jeong, K. Cha, J. Park and S. Park "Novel electromagnetic actuation system for three-dimensional locomotion and drilling of intravascular microrobot," *Sensors and Actuators A Physical*, Vol.161, No. 1–2, pp.297–304, 2010.

[43] Yesin, k. B., Vollmers, K. and Nelson, B. J., "Modeling and control of untethered biomicrorobots in a fluidic environment using

electromagnetic fields," *International Journal of Robotics Research*, Vol.25, No. 5–6, pp.527-536, 2006.

[44] B. Behkam and M. Sitti, "Modeling and testing of a biomimetic flagellar propulsion method for microscale biomedical swimming robots," *Proceedings of 2005 IEEE/ASME International Conference on Advanced Intelligent Mechatronics*, pp. 37-42, 2005.

[45] T. Mei, Y. Chen, G. Fu and D. Kong, "Wireless drive and control of a swimming microrobot," *Proceedings of 2002 IEEE International Conference on Robotics and Automation*, pp.1131-1136, 2002.

[46] Li, Junyang, Weicheng Ma, Fuzhou Niu, Yu Ting Chow, Shuxun Chen, Bo Ouyang, Haibo Ji, Jie Yang, and Dong Sun. "Development of biocompatible magnetic microrobot transporter using 3D laser lithography," *In Advanced Intelligent Mechatronics (AIM)*, 2*016 IEEE International Conference on*, pp. 739-744, 2016.

[47] Guo S., Pan Q. and M. B. Khamesee, "Development of a novel type of microrobot for biomedical application", *Journal of Microsystem Technologies*, 14(3), 307-314, 2008.

[48] Mathieu J., Martel S., Yahia L., Soulez G. and Beaudoin G., "Preliminary studies for using magnetic resonance imaging systems as a mean of propulsion for microrobots in blood vessels and evaluation of ferromagnetic artefacts," *In Proceedings of IEEE CCECE 2003*, Vol. 2, 835-838, 2003.

[49] Pan Q. and Guo S., "A Paddling Type of Microrobot in Pipe," *In Proceedings of 2009 IEEE International Conference on Robotics and Automation (ICRA2009)*, Kobe, Japan, pp. 2995-3000, 2009.

[50] Pan Q., Guo S., Li D., "Mechanism and Control of a Spiral Type of Microrobot in Pipe," *In Proceedings of the 2008 IEEE International Conference on Robotics and Biomimetics (ROBIO 2008)*, Bankok, Thailand, pp. 43-48, 2009.

[51] Pan Q. And Guo S., "Development of a Spiral Type of Wireless Microrobot," *In Proceedings of the 2008 IEEE/ASME International Conference on Advanced Intelligent Mechatronics (AIM2008)*, pp. 813-818, 2008.

[52] Pan Q. and Guo S., "A novel type of microrobot moving in the vertical pipe," *24th Annual Conference of the Robotics Society of Japan*, 2G22, 2006.

[53] Pan Q. and Guo S., "Development of the novel types of biomimetic microrobots driven by external magnetic field," *In Proceedings of 2007 IEEE International Conference on Robotics and Biomimetics*, 256-261, 2007.

[54] Pan Q. and Guo S., "Development of a spiral type of wireless microrobot in pipe," *The 26th Annual Conference of the Robotics Society of Japan*, Japan, 3F2, 2008.

[55] Pan Q. and Guo S., "Development of multifuncional wireless microrobot for biomimedical application," I*n Proceedings of 2007*

IEEE/ICME International Conference on Complex Medical Engineering, pp.1867-1872, 2007.

[56] Pan Q. and Guo S., "Mechanism and control of a novel type of microrobot for biomedical application," *In Proceedings of IEEE International Conference on Robotics and Automation (ICRA'07)*, 187-192, 2007.

[57] Yesin K. Berk, Vollmers Karl and Nelson Bradley J., "Modeling and Control of Untethered Biomicrorobots in a Fluidic Environment Using Electromagnetic Fields," *The International Journal of Robotics Research*, Vol. 25, No. 5-6, pp.527-536, 2006.

[58] Ye, Zhou, Collin Edington, Alan J. Russell, and Metin Sitti. "Versatile non-contact micro-manipulation method using rotational flows locally induced by magnetic microrobots." *In 2014 IEEE/ASME International Conference on Advanced Intelligent Mechatronics*, pp. 26-31, 2014.

[59] Ye, Z. and Sitti, M, "Dynamic trapping and two-dimensional transport of swimming microorganisms using a rotating magnetic microrobot," *Lab on a Chip*, Vol. 14, No.13, pp.2177-2182, 2014.

[60] Arcese, Laurent, Matthieu Fruchard, and Antoine Ferreira. "Adaptive controller and observer for a magnetic microrobot." *IEEE Transactions on Robotics*, Vol. 29, No. 4, pp. 1060-1067, 2013.

[61] Steager, Edward B., Blaine Zern, Mahmut Selman Sakar, Vladimir Muzykantov, and Vijay Kumar. "Assessment of protein binding with magnetic microrobots in fluid." *In Robotics and Automation (ICRA), 2013 IEEE International Conference on*, pp. 5502-5507, 2013.

[62] Thomas W. R. Fountain, Prem V. Kailat, and Jake J. Abbott, "Wireless Control of Magnetic Helical Microrobots using a Rotating-Permanent-Magnet Manipulator," *Proceedings of 2010 IEEE International Conference on Robotics and Automation*, pp. 576-581, 2010.

[63] Sehyuk Yim and Metin Sitti, "Design and Rolling Locomotion of a Magnetically Actuated Soft Capsule Endoscope," *Transactions on Robotics*, Vol. 28, No.1, pp. 183-193, 2012.

[64] Hyunchul Choi, Jongho Choi, Gunhee Jang, Jong-oh Park and Sukho Park, "Two-dimensional actuation of a microrobot with a stationary using two-pair coil system," *Smart Materials and Structures*, Vol. 18, No. 5, pp.1-8, 2010

[65] Qiang Fu, Shuxiang Guo, Qiang Huang, Hideyuki Hirata and Hidenori Ishihara, "Development and Evaluation of Novel Magnetic Actuated Microrobot with Spiral Motion using Electromagnetic Actuation System", *Journal of Medical and Biological Engineering* , Vol.36, No. 4, pp.506-514, 2016.

[66] Shuxiang Guo, Qiang Fu, Yasuhiro Yamauchi, Chunfeng Yue, "Characteristic Evaluation of a Wireless Capsule Microrobotic System", *Proceedings of 2013 IEEE International Conference on Mechatronics and Automation*, pp. 831-836, August 4-7, Takamatsu, Japan, 2013.

[67] Takuya Okada, Shuxiang Guo, Fu Qiang, Yasuhiro Yamauchi, "A Wireless micro-robot with Two Motions for Medical Applications",

Proceedings of the 2012 ICME International Conference on Complex Medical Engineering, pp. 306-311, July 1 - 4, Kobe, Japan, 2012.

[68] Takuya Okada, Shuxiang Guo, Nan Xiao, Fu Qiang, Yasuhiro Yamauchi, "Control of the Wireless micro-robot with Multi-DOFs Locomotion for Medical Applications", *Proceedings of 2012 IEEE International Conference on Mechatronics and Automation*, pp. 2405-2410, August 5-8, Chengdu, China, 2012.

[69] Qiang Fu, Shuxiang Guo, Songyuan Zhang, Hideyuki Hirata and Hidenori Ishihara, "Characteristic Evaluation of a Shrouded Propeller Mechanism for a Magnetic Actuated Microrobot", *Micromachines*, VOL.6, No.9, pp. 1272-1288, 2015.

[70] Qiang Fu, Shuxiang Guo, Songyuan Zhang and Yasuhiro Yamauchi, "Performance Evaluation of a Magnetic Microrobot Driven by Rotational Magnetic Field", *Proceedings of 2015 IEEE International Conference on Mechatronics and Automation*, pp.876-880, August 2-5,Beijing, China, 2015.

[71] Qiang Fu, Shuxiang Guo, Yasuhiro Yamauchi, "A Control System of the Wireless Microrobots in Pipe", *Proceedings of 2014 IEEE International Conference on Mechatronics and Automation*, pp. 1995-2000, August 2-5, Tianjin, China, 2014.

[72] Keller, Henrik, Aleksandar Juloski, Hironao Kawano, Mario Bechtold, Atsushi Kimura, Hironobu Takizawa, and Rainer Kuth. "Method for navigation and control of a magnetically guided capsule endoscope in the human stomach." *In 2012 4th IEEE RAS & EMBS International*

Conference on Biomedical Robotics and Biomechatronics (BioRob), pp. 859-865, 2012.

[73] Qiang Fu and Shuxiang Guo, "Design and Performance Evaluation of a Novel Mechanism with Screw Jet Motion for a Hybrid Microrobot Driven by Rotational Magnetic Field", *Proceedings of 2016 IEEE International Conference on Mechatronics and Automation*, pp.2376-2380, 2016.

[74] Arfelli, F., M. Assante, V. Bonvicini, A. Bravin, G. Cantatore, E. Castelli, L. Dalla Palma et al. "Low-dose phase contrast x-ray medical imaging." *Physics in medicine and biology*, Vol.43, No.10 pp.2845, 1998.

[75] Pfeiffer, Franz, Martin Bech, Oliver Bunk, Philipp Kraft, Eric F. Eikenberry, Ch Brönnimann, Christian Grünzweig, and Christian David. "Hard-X-ray dark-field imaging using a grating interferometer." *Nature materials*, Vol.7, No. 2, pp.134-137, 2008.

[76] Iversen, Daniel Høyer, Frank Lindseth, Geirmund Unsgaard, Hans Torp, and Lasse Lovstakken. "Model-based correction of velocity measurements in navigated 3-D ultrasound imaging during neurosurgical interventions." *IEEE transactions on medical imaging*, Vol. 32, No. 9, pp.1622-1631, 2013.

[77] Chin, Patrick TK, Mick M. Welling, Stefan CJ Meskers, Renato A. Valdes Olmos, Hans Tanke, and Fijs WB van Leeuwen. "Optical imaging as an expansion of nuclear medicine: Cerenkov-based luminescence vs fluorescence-based luminescence." *European journal*

of nuclear medicine and molecular imaging, Vol. 40, No. 8, pp.1283-1291, 2013

[78] Yuan, Lin, Weiying Lin, Kaibo Zheng, Longwei He, and Weimin Huang. "Far-red to near infrared analyte-responsive fluorescent probes based on organic fluorophore platforms for fluorescence imaging." *Chemical Society Reviews*, Vol. 42, No. 2, pp.622-661, 2013

[79] Popek, Katie M., Arthur W. Mahoney, and Jake J. Abbott. "Localization method for a magnetic capsule endoscope propelled by a rotating magnetic dipole field." *In Robotics and Automation (ICRA), 2013 IEEE International Conference on*, pp. 5348-5353, 2013.

[80] Yu, Zhenwei, Jason A. Mix, Soji Sajuyigbe, Kevin P. Slattery, and Jun Fan. "An improved dipole-moment model based on near-field scanning for characterizing near-field coupling and far-field radiation from an IC." *IEEE Transactions on Electromagnetic Compatibility*, Vol. 55, No. 1, pp.97-108, 2013.

[81] Petruska, Andrew J., Arthur W. Mahoney, and Jake J. Abbott. "Remote manipulation with a stationary computer-controlled magnetic dipole source." *IEEE Transactions on Robotics*, Vol. 30, No. 5, pp.1222-1227, 2014.

[82] Song, Shuang, Chao Hu, Baopu Li, Xiaoxiao Li, and Max Q-H. Meng. "An electromagnetic localization and orientation method based on rotating magnetic dipole." *IEEE Transactions on Magnetics*, Vol. 49, No. 3, pp.1274-1277, 2013.

[83] Wahlström, Niklas, and Fredrik Gustafsson. "Magnetometer modeling and validation for tracking metallic targets." *IEEE Transactions on Signal Processing*, Vol. 62, No. 3, pp.545-556, 2014.

[84] Wang, Junqiao, Chunzhen Fan, Jinna He, Pei Ding, Erjun Liang, and Qianzhong Xue. "Double Fano resonances due to interplay of electric and magnetic plasmon modes in planar plasmonic structure with high sensing sensitivity." *Optics express*, Vol. 21, No. 2, pp.2236-2244, 2013.

[85] Espenschied K.S., Quinn R.D., Beer R.D., Chiel HJ., "Biologically based distributed control and local reflexes improve rough terrain locomotion in a hexapod robot." *Robotics and autonomous systems*, Vol. 18, pp.59-64, 1996.

[86] Waters, Shaun, and George A. Aggidis. "Over 2000 years in review: revival of the archimedes screw from pump to turbine." *Renewable and Sustainable Energy Reviews*, Vol. 51 pp.497-505, 2015

[87] Delghavi, Mohammad B., and Amirnaser Yazdani. "A simple passive voltage-balancing scheme for three-phase induction generators interfaced with single-phase grids in micro hydroelectric systems." *International Journal of Electrical Power & Energy Systems*, Vol.74 pp.42-48, 2016.

[88] Lin, Chih-Lang, Guy Vitrant, Michel Bouriau, Roger Casalegno, and Patrice L. Baldeck. "Optically driven Archimedes micro-screws for micropump application." *Optics express*, Vol.19, No.9, pp.8267-8276, 2011

[89] Abbott, Jake J., Marco Cosentino Lagomarsino, Li Zhang, Lixin Dong, and Bradley J. Nelson. "How should microrobots swim?" *The International Journal of Robotics Research*, Vol.28, pp.1434-1447, 2009.

[90] E. M. Purcell. "Life at low Reynolds number," *Am. J. Phys.*, Vol. 45, No.1, pp.3-11, 1977.

[91] Brennen, Christopher, and Howard Winet. "Fluid mechanics of propulsion by cilia and flagella." *Annual Review of Fluid Mechanics*, Vol.9, No. 1, pp.339-398, 1977.

[92] Q. Fu, S. Guo, Y. Yamauchi, H. Hirata, and H. Ishihara, "A Novel Hybrid Microrobot using Rotational Magnetic Field for Medical Applications" *Biomedical Microdevices*, Vol.17, No.2, pp.1-12, 2015.

[93] Rorres C.; "The turn of the screw: Optimal design of an Archimedes screw." *Journal of Hydraulic Engineering*, Vol. 126, pp.72-80, 2000.

[94] Guo S.; Fukuda T.; Asaka K. "Fish-like underwater microrobot with 3 DOF." *Proceedings of IEEE International Conference on Robotics and Automation*, Vol.1, pp.738-743, 2002.

[95] Guo S., Fukuda T. and Asaka K., "A new type of fish-like underwater microrobot." *IEEE/ASME Transactions on Mechatronics*, Vol.8, No.1, pp.35-40, 2003.

[96] Fukuda T., Hosokai, et al., "Distributed type of actuator by shape memory alloy and its application to underwater mobile robotic mechanism." *In Proceedings of IEEE International Conference on Robotics and Automation*, Vol.2, pp.1316-1332, Nara, Japan, 1991.

[97] Fukuda T., Kawamoto A., Arai F., Matsuura H., "Mechanism and swimming experiment of micro mobile robot in water." *In Proceedings of IEEE International Conference on Robotics and Automation*, vol.1, pp. 814-819, 1994.

[98] Guo S., Okuda Y. Zhang W., Ye X. and Asaka K., "The development of a hybrid type of underwater micro biped robot." *Applied Bionics and Biomechanics, Woodhead Publishing Limited*, Cambridge UK, Vol. 3, No. 3, pp. 143-150, 2006.

[99] Guo S., Sasaki Y. and Fukuda T., "A new kind of microrobot in pipe using driving fin." *In Proceedings of IEEE/ASME International Conference on Advanced Intelligent Mechatronics (AIM 2003)*, 667-702, 2003.

[100] Van Oene, Maarten M., Laura E. Dickinson, Francesco Pedaci, Mariana Köber, David Dulin, Jan Lipfert, and Nynke H. Dekker. "Biological Magnetometry: Torque on Superparamagnetic Beads in Magnetic Fields." *Physical review letters*, Vol. 114, No. 21, pp.218301, 2015.

[101] Munoz, Fredy, Gursel Alici, Hao Zhou, Weihua Li, and Metin Sitti. "Analysis of the magnetic torque on a tilted permanent magnet for drug delivery in capsule robots." *In Advanced Intelligent Mechatronics (AIM), 2016 IEEE International Conference on*, pp.1386-1391, 2016.

Publication List

International Journal Papers

1. **Qiang Fu**, Shuxiang Guo, Yasuhiro Yamauchi, Hideyuki Hirata and Hidenori Ishihara, "A Novel Hybrid Microrobot using Rotational Magnetic Field for Medical Applications", *Biomedical Microdevices*, VOL.17, No.2, pp.1-12, 2015. Impact Factor (IF): 2.227.

2. **Qiang Fu**, Shuxiang Guo, Songyuan Zhang, Hideyuki Hirata and Hidenori Ishihara, "Characteristic Evaluation of a Shrouded Propeller Mechanism for a Magnetic Actuated Microrobot", *Micromachines*, VOL.6, No.9, pp. 1272-1288, 2015. Impact Factor (IF): 1.295.

3. **Qiang Fu**, Shuxiang Guo, Qiang Huang, Hideyuki Hirata and Hidenori Ishihara, "Development and Evaluation of Novel Magnetic Actuated Microrobot with Spiral Motion using Electromagnetic Actuation System", *Journal of Medical and Biological Engineering* , Vol.36, No. 4, pp.506-514, 2016. Impact Factor (IF): 1.018.

International Conference Papers

1. **Qiang Fu** and Shuxiang Guo, "Design and Performance Evaluation of a Novel Mechanism with Screw Jet Motion for a Hybrid Microrobot Driven by Rotational Magnetic Field", *Proceedings of 2016 IEEE International Conference on Mechatronics and Automation,* pp.2376-2380, 2016.

2. **Qiang Fu,** Shuxiang Guo, Songyuan Zhang and Yasuhiro Yamauchi,

"Performance Evaluation of a Magnetic Microrobot Driven by Rotational Magnetic Field", *Proceedings of 2015 IEEE International Conference on Mechatronics and Automation*, pp.876-880, August 2-5,Beijing, China, 2015.

3. **Qiang Fu**, Shuxiang Guo, Yasuhiro Yamauchi, "A Control System of the Wireless Microrobots in Pipe", *Proceedings of 2014 IEEE International Conference on Mechatronics and Automation*, pp. 1995-2000, August 2-5, Tianjin, China, 2014.

4. Shuxiang Guo, **Qiang Fu**, Yasuhiro Yamauchi, Chunfeng Yue, "Characteristic Evaluation of a Wireless Capsule Microrobotic System", *Proceedings of 2013 IEEE International Conference on Mechatronics and Automation*, pp. 831-836, August 4-7, Takamatsu, Japan, 2013.

5. Takuya Okada, Shuxiang Guo, **Fu Qiang**, Yasuhiro Yamauchi, "A Wireless micro-robot with Two Motions for Medical Applications", *Proceedings of the 2012 ICME International Conference on Complex Medical Engineering*, pp. 306-311, July 1 - 4, Kobe, Japan, 2012.

6. Takuya Okada, Shuxiang Guo, Nan Xiao, **Fu Qiang**, Yasuhiro Yamauchi, "Control of the Wireless micro-robot with Multi-DOFs Locomotion for Medical Applications", *Proceedings of 2012 IEEE International Conference on Mechatronics and Automation*, pp. 2405-2410, August 5-8, Chengdu, China, 2012.

Biographic Sketch

Qiang Fu received his B.Sc. degree from Harbin University of Science and Technology, Harbin, Heilongjiang, China in 2010. He received his M.Sc. degree from Kagawa University, Kagawa, Takamatsu, Japan in 2014. Currently, he is a Ph.D. candidate in Kagawa University, Japan. He researches on development of multi-module magnetic actuated microrobotic systems.

He has published 9 refereed journal and conference papers in recent 5 years.